UNIVERSIDADE ESTADUAL DE CAMPINAS
Faculdade de Engenharia Agrícola

Artur Fernando de Vito Júnior

Otimização Topológica de Estruturas de Madeira Laminada Colada

Topological Optimization of Glued Laminated Timber Structures

Campinas
2023

Artur Fernando de Vito Júnior

Topological Optimization of Glued Laminated Timber Structures

Otimização Topológica de Estruturas de Madeira Laminada Colada

Tese apresentada à Faculdade de Engenharia Agrícola da Universidade Estadual de Campinas como parte dos requisitos exigidos para a obtenção do título de Doutor em Engenharia Agrícola, na Àrea de Máquinas Agrícolas

Thesis presented to the School of Agricultural Engineering of the University of Campinas in partial fulfillment of the requirements for the degree of Doctor in Agricultural Engineer the area of Agricultural Machinery.

Supervisor/Orientador: Prof. Dr. William Martins Vicente

Este trabalho corresponde à versão final da Tese defendida por Artur Fernando de Vito Júnior e orientada pelo Prof. Dr. William Martins Vicente.

Campinas
2023

Ficha catalográfica
Universidade Estadual de Campinas
Biblioteca da Área de Engenharia e Arquitetura
Rose Meire da Silva - CRB 8/5974

V833t

Vito Júnior, Artur Fernando de, 1991-
Topological optimization of glued laminated timber structures / Artur Fernando de Vito Júnior. – Campinas, SP : [s.n.], 2023.

Orientador: William Martins Vicente.
Tese (doutorado) – Universidade Estadual de Campinas, Faculdade de Engenharia Agrícola.

1. Otimização topológica. 2. Madeira Produtos. 3. Modelagem computacional. I. Vicente, William Martins, 1980-. II. Universidade Estadual de Campinas. Faculdade de Engenharia Agrícola. III. Título.

Informações Complementares

Título em outro idioma: Otimização topológica de estruturas de madeira laminada colada
Palavras-chave em inglês:
Topological optimization
Engineered wood
Computational modeling
Área de concentração: Máquinas Agrícolas
Titulação: Doutor em Engenharia Agrícola
Banca examinadora:
William Martins Vicente [Orientador]
Julio Soriano
Renato Pavanello
Renato Picelli Sanches
Sandro Luis Vatanabe
Data de defesa: 28-08-2023
Programa de Pós-Graduação: Engenharia Agrícola

Identificação e informações acadêmicas do(a) aluno(a)
- ORCID do autor: https://orcid.org/0000-0003-2451-2740
- Currículo Lattes do autor: http://lattes.cnpq.br/0771202622629992

Este exemplar corresponde à redação final da **Tese de Doutorado** defendida por **Artur Fernando de Vito Júnior**, aprovada pela Comissão Julgadora em 28 de agosto de 2023, na Faculdade de Engenharia Agrícola da Universidade Estadual de Campinas.

Prof. Dr. William Martins Vicente – Presidente e Orientador

Prof. Dr. Julio Soriano – Membro Titular

Prof. Dr. Renato Pavanello – Membro Titular

Prof. Dr. Renato Picelli Sanches – Membro Titular

Prof. Dr. Sandro Luis Vatanabe – Membro Titular

A Ata da defesa com as respectivas assinaturas dos membros encontra-se no SIGA/Sistema de Fluxo de Dissertação/Tese e na Secretaria do Programa da Unidade.

A Mara e Artur, meus exemplos de dedicação; A Agda, minha esposa e paciente companheira; Pipoca, minha adorável companheira canina; e à minha querida filha Alice, que está para vir neste mundo, carregando em seu futuro a inspiração para cada passo dado. A todos vocês, meu amor e gratidão, tornaram esta tese possível.

Last but not least, I wanna thank me
I wanna thank me for believing in me
I wanna thank me for doing all this hard work
I wanna thank me for having no days off
I wanna thank me for, for never quitting
I wanna thank me for always being a giver
And tryna give more than I recieve
I wanna thank me for tryna do more right than wrong
I wanna thank me for just being me at all times.

(Snoop Dogg)

Agradecimentos

Gostaria de expressar minha profunda gratidão a todas as pessoas que tornaram esta tese possível. Sem o apoio inestimável da minha esposa, família, orientador e, é claro, a companhia constante da pipoca, nada disso teria sido alcançado.

Em primeiro lugar, quero dedicar um agradecimento especial aos meus pais, Mara e Artur, que me apoiaram incondicionalmente em todas as etapas da minha jornada acadêmica.

À minha esposa, Agda, agradeço por ouvir pacientemente minhas reclamações e monólogos sobre meus códigos, por me apoiar nos momentos difíceis e compartilhar comigo a alegria das conquistas.

Ao meu orientador, sou imensamente grato pelo apoio técnico ao longo de todo o doutorado. Suas orientações foram esclarecedoras e inspiradoras, transformando muitas de nossas conversas em ideias para artigos e trabalhos futuros. Espero sinceramente ter a oportunidade de trabalhar com o senhor novamente no futuro.

Também quero agradecer ao professor Yi Min 'Mike' Xie. Mesmo sem tê-lo conhecido pessoalmente, sua participação em nosso trabalho foi de extrema importância, com respostas rápidas e precisas que enriqueceram nossos resultados.

Aos professores que compuseram a banca de qualificação e defesa, meu sincero agradecimento. Suas contribuições foram fundamentais para o aprimoramento técnico desta tese, e os conselhos valiosos que ofereceram certamente influenciarão positivamente minha trajetória acadêmica e profissional.

Agradeço a todos os amigos e colegas que estiveram presentes durante esta jornada, oferecendo suporte e encorajamento durante todo o doutorado.

O presente trabalho foi realizado com apoio do Conselho Nacional de Desenvolvimento Científico e Tecnológico (CNPq), bolsa processo nº 140498/2020-6.

Resumo

A madeira engenheirada é um produto fabricado pela união de camadas de madeira através de colagem ou pregos. Os dois tipos proeminentes de produtos de madeira engenheirada são a Madeira Laminada Colada (MLC) e a Madeira Laminada Colada Cruzada (MLCC). Esses produtos são amplamente utilizados na construção civil, pois são produzidos principalmente com madeira de reflorestamento e possuem a capacidade de armazenar carbono ao longo de seu ciclo de vida. Esta tese aborda a tendência crescente de utilizar madeira como material de construção e explora duas abordagens para aplicar métodos de otimização topológica em produtos de madeira engenheirada. Inicialmente, a tese aborda a otimização topológica de estruturas de MLC e MLCC. A função objetivo é a minimização de deslocamento, com restrição de volume. Durante o processo de otimização, diferentes topologias otimizadas foram identificadas para diferentes camadas, evidenciando diferenças estruturais na importância de cada camada. Para possibilitar a fabricação de estruturas otimizadas, mesmo com o avanço da fabricação digital, a aplicação de restrições de periodicidade mostrou-se essencial. Posteriormente, a tese aborda a utilização do método de otimização topológica para o posicionamento de vigas de reforço na estrutura de MLC. Além do posicionamento, o método permite a identificação de quantidades economicamente viáveis de vigas de reforço e a determinação da posição otimizada delas na estrutura.

Palavras-chaves: Otimização Topológica, Madeira Engenheirada, Modelagem Computacional.

Abstract

Engineered wood, also known as mass timber, is a manufactured product made by bonding of wood together. Two prominent types of engineered wood products are glued laminated timber (GLULAM) and cross-laminated timber (CLT). These products are widely used in the construction industry due to their environmental appeal, as they are mainly produced from reforested wood and have the ability to store carbon during their lifecycle. This thesis addresses the growing trend of using wood as a construction material and explores two approaches to applying topology optimization methods in engineered wood products. Initially, the thesis focuses on topology optimization of GLULAM and CLT structures with the objective of minimizing displacement and volume restriction. During the optimization process, various optimized topologies were discovered for different layers, highlighting structural variations in layer importance. To facilitate the fabrication of optimized structures, despite advances in digital fabrication, applying periodicity constraints proved essential. Subsequently, the thesis discusses the utilization of topology optimization methods for the placement of reinforcing beams in GLULAM structures. In addition to positioning, the method allows for the iterative identification of the strength attributed to each added or removed reinforcing beam. This enables the identification of economically viable quantities of reinforcing beams and their optimized placement in the structure.

Keywords: Topological Optimization, Engineered Wood, Computational Modeling.

List of Figures

List of Tables

List of Symbols

$\nabla \cdot \sigma_{\mathbf{s}}$	Cauchy stress tensor
ρ	Mass density
$\mathbf{f}$	Prescribed external load
$\mathbf{u}$	Structural displacement
$\mathbf{N}$	Shape function
$\mathbf{w}$	Weight functions
Ω	Structural domain
Γ_n	Neumann boundary condition
Γ_d	Dirichlet boundary condition
D	Orthotropic constitutive matrix
E_L	Longitudinal Young's modulus
E_R	Radial Young's modulus
E_R	Tangencial Young's modulus
v_{LT}	Poisson rate in LT plane
v_{LR}	Poisson rate in LR plane
v_{RT}	Poisson rate in LR plane
G_{LT}	Shear modulus in LT plane
G_{LR}	Shear modulus in LR plane
G_{RT}	Shear modulus in LR plane
$\mathbf{x}$	Design variable vector
x_{min}	Minimum relative density for void value
p	Penalty factor
$\mathbf{K}$	Stiffness matrix
$\mathbf{M}$	Mass matrix
$\mathbf{U}^k$	Displacement of the degree or degrees of freedom of interest
$\mathbf{Q}$	Unit load vector to the degree (or degrees) of freedom of intereset
$\mathbf{U}^p$	Response of the structure to the load Q on the node of interest
V^*	Prescribed optimization value
V_i	Element volume
α	Sensitivity value
$\overline{\alpha}$	Filtered sensitivity value

r_{min}	Filter radius
Ψ	Sub-domain defined by filter radius
$\tilde{\alpha}_i$	Averaged sensitivity value
τ	Convergence error
N	Number of iterations of stable compliance
ER	Evolutionary volume ratio
AR	Admission volume ratio

List of Acronyms

BESO	Bi-directional Evolutionary Structural Optimization
CFRP	Carbon Fiber Reinforced Polymer
CLT	Cross-Laminated Timber
CW	Compressed Wood
ESO	Evolutionary Structural Optimization
EWP	Engineered Wood Products
FRP	Fiber-Reinforced Polymer
GFRP	Glass Fiber Reinforced Polymer
GLULAM	Glued-Laminated Timber
GWP	Global Warming Potential
HC-CLT	Hollow-Core Cross-Laminated Timber
HC-GLULAM	Hollow-Core Glued-Laminated Timber
MLC	Madeira Laminada Colada
MLCC	Madeira Laminada Colada Cruzada
SIA	Sustainability Impact Assessment
SIMP	Solid Isotropic Material with Penalisation
TCC	Timber-Concrete Composite
TO	Topology Optimization

Contents

Works Published in Connection with this thesis

- A. F. de Vito Jr., W. M. Vicente and Y. M. Xie, "**Topology optimization applied to the core of structural engineered wood product**", Structures Journal, 2023, https://doi.org/10.1016/j.istruc.2023.01.036.

- A. F. de Vito Jr. and W. M. Vicente, "**Application of Multi-material Topology Optimization Method for Positioning Reinforcements in Glued laminated Timber Structures**", In: International Symposium on Solid Mechanics - MECSOL, 2022, Campinas.

- A. F. de Vito Jr. and W. M. Vicente, "**Innovative Approach for Enhancing GLULAM Performance with Reinforcing Steel Bars: A BESO-based Study**", In: Latin American Journal of Solids and Structures, 2023, https://doi.org/10.1590/1679-78257558

Chapter 1

Introduction

The first chapter provides a overview of the key driving factors behind the investigation of topology optimization as it applies to Glued-Laminated Timber (GLULAM) and Cross-Laminated Timber (CLT). By delving into the central reasons for this study, readers will gain a understanding of the critical issues and challenges that topology optimization can address in the context of these types of timber structures. This section aims to lay the foundation for the subsequent literature review and analysis, highlighting the critical role that topology optimization plays in achieving structural efficiency and sustainability in modern timber building design.

1.1 Opportunities in structural timber design

The utilization of timber in construction has been found to be inefficient [1, 2], as highlighted in Figure 1.1. This inefficiency arises because the structural material in standard timber elements is not maximally utilized for strength potential. In most cases, simple CLT- or GLULAM-elements are designed based on the highest demand location, such as the maximum bending moment at the element's center, resulting in overdesigned sections for a significant portion of the element's length [3]. With the loading considered in the in Figure 1.1, to maximize the strength in section, the material should be placed as far as possible from the section's center. However, in current structural engineered wood products, a significant proportion of the material remains underutilized. Moreover, the distribution of internal loads, such as bending moment and shear force, varies longitudinally and is a fixed condition imposed by the structural system. While the strength of the element is constant throughout its length, this presents

a missed opportunity to reduce the amount of structural material to what is strictly necessary. One solution to this problem is to adapt the element's shape in response to changes in demand, both in section and along its length, to optimize the governing form-giving internal demand [2, 4]

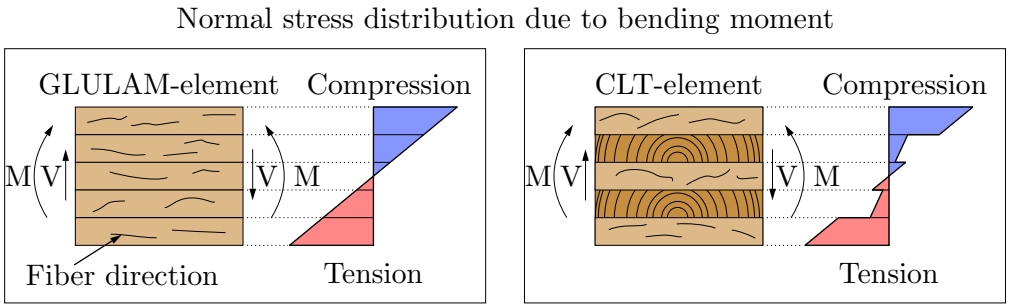

Figure 1.1: Free-body diagram illustrating regions of a GLULAM- and CLT-element where the material is not optimally utilized, adapted from [1, 2].

The emerging research agendas aim to make society more sustainable, with a specific focus on the construction industry [5]. Conducting research is crucial in the process of change as it will deliver better and more efficient solutions to tackle global warming, structural integrity, and material efficiency issues. CLT is an excellent choice for multi-storey urban infill buildings due to their versatility and many outlined advantages when compared to concrete and steel. A low-carbon, zero-waste construction system with a focus on waste avoidance in construction will develop low-carbon-lifecycle building construction components for inner-city housing by applying 'design for disassembly' and modular prefabrication principles. More research in sustainable construction materials and systems will lead to greener supply chains, less environmental impact over their entire lifecycle, lightweight construction to reduce embodied energy, fully recyclable/reusable materials, and off-site prefabrication and prototyping [6].

1.2 Research questions, hypothesis and main objectives

This thesis is dedicated to the comprehensive investigation of two vital research questions:

- How can the implementation of topology optimization be effectively utilized to optimize the distribution of materials in engineered wood products, with a specific emphasis on

CLT and GLULAM, for the purpose of enhancing structural efficiency and reducing the overall construction mass?

- How can topology optimization techniques be applied with precision to determine the optimal placement of steel beams within GLULAM structures, aiming to maximize structural efficiency, minimize material consumption, and ensure the structural integrity and satisfactory performance of the construction?

By delving into these research questions, this thesis endeavors to contribute to the existing knowledge and understanding surrounding the practical application of topology optimization methods within the field of engineered wood products. The outcomes of this research endeavor hold potential to generate insights and recommendations, facilitating the enhancement of efficiency, cost-effectiveness, and reliability of structural systems involving CLT, GLULAM, and steel bars.

For each of these research questions, a hypothesis has been formulated:

- The first hypothesis assumes that the application of topology optimization techniques in engineered wood products, including CLT and GLULAM, will yield an optimized distribution of materials. Consequently, this optimization will enable a reduction in the overall construction mass without compromising the integrity and performance of the structure.

- The second hypothesis assumes that by utilizing topology optimization, it is possible to determine the optimal positioning of steel bars within GLULAM structures. This approach will lead to a distribution that maximizes structural efficiency, minimizes material consumption, and satisfactory performance of the construction.

Therefore, the principal objectives of this thesis are presented as follows:

- Apply topology optimization techniques to engineered wood products, particularly CLT and GLULAM, with the aim of optimizing material distribution. This optimization will facilitate the reduction of the total construction mass while ensuring a satisfactory performance of the structure.

- Apply topology optimization methods to accurately determine the optimal placement of steel beams within GLULAM structures. The aiming is to achieve maximum structural

efficiency, minimize material consumption, and guarantee the structural integrity and satisfactory performance of the construction.

To address these research questions, hypotheses, and main objectives, the ensuing chapters will draw upon classical literature and recent scientific articles.

1.3 Thesis structure

This thesis focuses on the application of topology optimization methodology in structures made of glued laminated timber, with the aim of contributing to the development of more efficient and sustainable structural solutions in the field of engineering and architecture. The thesis presents an bibliography and literature review to gain a better understanding of glued laminated timber as a material and to explore the properties of its main derivatives such as GLULAM and CLT described in Chapter 2. Chapter 3 presents the methodology used in this thesis to achieve the objectives. Chapter 4 examines the direct application of the topology optimization method in the glued laminated timber core. Chapter 5 delves into the use of topology optimization for the placement of steel reinforcement bars in glued laminated timber. Finally, chapter 6 provides an overall conclusion of the thesis, including the limitations encountered during the project, and suggestions for future research.

Chapter 2

Literature Review

2.1 Contextualizing glue laminated timber structure

Wood in general possesses a range of properties that are intricately linked to its vital functions in supporting the requirements of the living tree. The underlying biological processes that govern the formation and growth of wood cells dictate the physical, mechanical, chemical, biological, and technological properties of wood [7, 8]. Wood cells must be arranged in a manner that meets the specific requirements of the tree and enables it to carry out critical functions such as structural support, water and nutrient transport, and defense against pathogens and pests. This has resulted in the evolution of over 20,000 distinct species of woody plants, each with unique properties, uses, and capabilities that are relevant in both plant and human contexts [7, 8].

In a living tree, there are two primary domains: the shoot and the roots. Roots, which are located underground, are responsible for the absorption of water and mineral nutrients, mechanical support of the shoot, and storage of biochemicals. On the other hand, the shoot comprises the trunk or bole, branches, and leaves.

Upon examining the stump of a tree, several distinct features can be observed. The trunk is composed of various materials arranged in concentric bands, with outer bark, inner bark, vascular cambium, sapwood, heartwood, and pith arranged in order from the outside of the tree to the inside, represented in Figure 2.1. The outer bark provides mechanical protection to the inner bark, while also restricting evaporative water loss. The inner bark serves as the medium through which sugars produced via photosynthesis are transported from the leaves to the roots or growing areas of the tree. The vascular cambium, the tissue layer situated between

the bark and the wood, is responsible for producing both of these tissues on a yearly basis. The sapwood, or living wood, is responsible for actively conducting water (or sap) from the roots to the leaves. Unlike heartwood, which is a core of darker-colored wood typically located at the center of most trees, sapwood has not yet accumulated the often-colored chemicals that differentiate non-conductive heartwood. Finally, the pith located at the very center of the trunk is the vestige of the trunk's early growth, prior to the formation of wood [8–10].

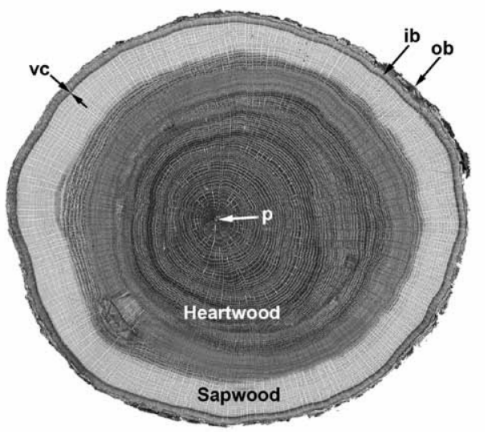

Figure 2.1: Figure extracted from [9] illustrates the cross-sectional anatomy of a Quercus alba tree trunk. The image provides a macroscopic view starting from the outer bark (ob) and proceeding inward to show the inner bark (ib), the narrow vascular cambium (vc), the sapwood, the heartwood, and finally, the pith (p) at the center. The sapwood is easily distinguishable from the heartwood, and the pith is barely visible within the heartwood.

Although this topic will be addressed further, it is important to mention that both glued laminated timber (GLULAM) and cross-lamianted timber (CLT) are formed by layers of sawn timber. Sawn timber is created by cutting logs into planks or boards using a sawmill or a similar tool. Specifically, softwood sawn timber refers to timber cut from coniferous trees, including pine, spruce, or fir. Softwood trees are known for their lighter, less dense wood, which makes them ideal for use in construction, furniture, and packaging due to their durability, strength, and versatility. The sawing process allows for flexibility in the shapes and sizes of the timber, making it suitable for different applications.

In contrast, sawn hardwood is timber cut or sawn from the logs of hardwood trees such as oak, maple, mahogany, or cherry. Hardwood is popular for its strength, durability, and attractive appearance, making it suitable for use in flooring, cabinetry, furniture, and decorative trim applications. The thickness and width of sawn hardwood can vary based on the intended use, and the quality of the wood can also vary depending on factors such as tree species, age, and specific requirements of the intended use.

Although the name and typical applications may suggest that softwood has lower mechanical characteristics than hardwood, there are exceptions to this generalization. In fact, there are certain softwood species that can be harder than some hardwoods, and vice versa. For example, Douglas-fir is a popular softwood used in wood products that possesses stronger characteristics than certain hardwoods like basswood or aspen [9, 10]. Therefore, understanding the anatomy and botanical classification of each species is necessary to accurately classify them as either hardwood or softwood. Botanically, hardwoods are angiosperms with seeds enclosed in the flower's ovary, while softwoods are gymnosperms or conifers with seeds that are not enclosed in the flower's ovary. Anatomically, hardwoods have pores that form a continuous tube, which serves to transport water, while softwoods do not contain pores [8–10].

Softwoods and hardwoods have different microstructures, with softwoods being mainly composed of tracheids and rays. Tracheids are long and slender cells that account for about 90% of the softwood volume. They store water and provide the mechanical strength of softwood. In contrast, rays are small brick-shaped cells that perform storage, synthesis, and transportation of biochemistry and water [9, 11]. Hardwoods, on the other hand, have a more intricate microstructure with a variety of fibrous elements and diverse cells such as rays, but in different forms. Fibers are the primary component of hardwood, and they function mainly as mechanical supporting cells. Although shorter than tracheids, the width of the fibers is responsible for the density and mechanical capacity of the wood. Overall, the presence of tracheids and fibers makes wood an orthotropic material, which is a crucial aspect of its versatility and suitability for various applications [9, 11].

An orthotropic structure exhibits unique and independent mechanical properties along its three main axes: the longitudinal, radial, and tangential axes. These axes are conventionally defined in wood. The longitudinal axis runs parallel to the wood fibers or grain, while the radial axis is perpendicular to the fibers and normal to the growth rings, as highlighted in Figure 2.1. The tangential axis is perpendicular to the fibers and tangential to the growth rings. Together, these three axes create a complex network of mechanical properties that contribute to the exceptional strength, durability, and versatility of wood. Figure 2.2 provides a clear visualization of the three main axes of wood and their relationships

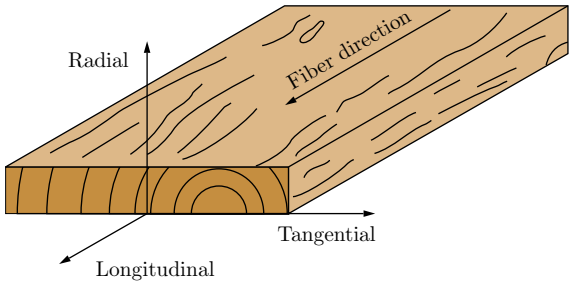

Figure 2.2: Main axes adopted as a reference in relation to the fibers and growth rings, adapted from [9].

2.1.1 Types of glued laminated structures

GLULAM is an Engineered Wood Products (EWP) used for structural purposes, has its roots in the early 1900s, when the German Otto Karl Freidrich Hetzer, obtained his first patent for this method of construction. In 1901, Hetzer was granted a patent in Switzerland for a straight beam made of several laminations bonded with adhesive. The technology continued to advance, and in 1906, Hetzer was granted a German patent for curved glued laminated construction, which marked the beginning of clear span timber arch construction. Hetzer's method quickly gained popularity, with patents being sought and granted in several European industrialized nations Today, GLULAM is commonly used to create massive beams or curved arches in construction projects [12, 13].

GLULAM combines finger-jointing and lamination of timber boards to create a highly versatile and strong material. Finger-jointing is an effective technique for joining GLULAM longitudinally, particularly when the glued surfaces are perpendicular to the main grain direction, as depicted in Figure 2.3. By increasing the surface area of the lumber pieces to be glued with the grain running in parallel, finger-jointing produces higher strength values and enables the creation of lumber pieces of any length. However, natural anomalies and defects of wood, such as knots, shakes, and cracks, make it challenging to create longer timber boards, which is why finger joints are often necessary to join two or more boards to achieve certain length spans. Despite the interlocking sides of finger joints providing maximum contact area for the adhesive, they are frequently viewed as weak points and a common source of failure for GLULAM beams that are subject to bending. This is because small voids between finger joints and the thickness of the lamination can make the material more brittle and susceptible to failure [14, 15].

(a)

(b)

Figure 2.3: **(a)** Finger joint in a wood piece, image available in `https://www.swedishwood.com/wood-facts/about-wood/wood-grades/` **(b)** GLULAM beam made by Kal Snikoff `https://kalesnikoff.com/products/mass-timber-glulam-beams/`

CLT is another popular EWP in timber construction. It is created by gluing layers of lumber together perpendicular to each other, forming a panel with wood fibers running in two directions as shown in Figure 2.4. These panels are used for floor systems or walls, and can efficiently transfer loads in two directions when used in out-of-plane bending. The cross lamination enhances the dimensional stability of the panels, as the deformation of the grain in one direction is constrained by the grain running in the perpendicular direction. CLT panels typically have a strong direction and a weak direction, with the strong direction having the highest resistance and the largest dimension.

GLULAM and CLT owes much of its success to the development of adhesives. Prior to the advancements in adhesive technology, the dimensions of a tree would limit the size and scope of timber structures. However, with modern adhesives, larger elements can now be assembled and glued together from standardized lumber pieces, thus enabling the creation of larger sections. This innovation has allowed for the construction of modern wood structures that are no longer restricted by the size of the tree. Additionally, finger-jointing techniques have allowed the creation of structural elements with virtually unlimited length, providing even more flexibility in the design of mass timber buildings.

GLULAM and CLT are two of the most commonly used engineered wood products, particularly in civil construction in various European countries, Canada, and the USA. The dimensions of GLULAM and CLT can be customized according to specific requirements, mak-

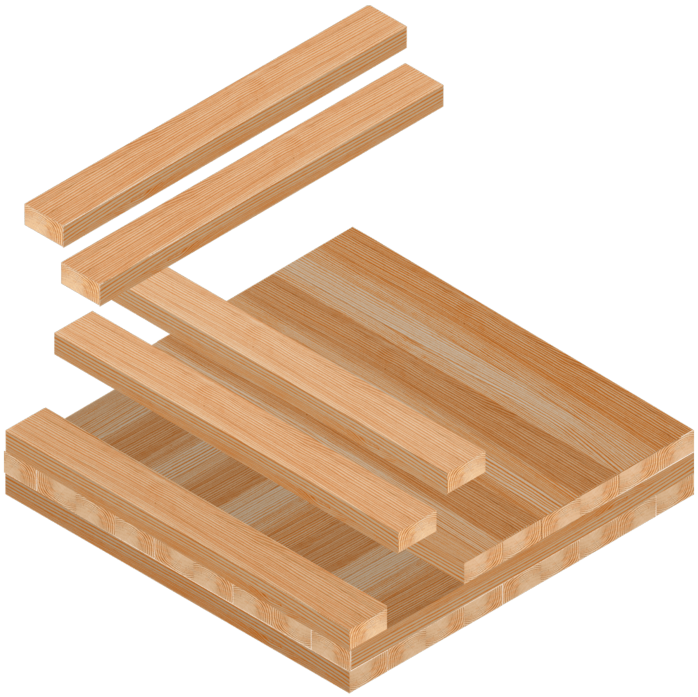

Figure 2.4: Cross laminated timber construction scheme, image available in `https://www.thinkwood.com/mass-timber/cross-laminated-timber-clt`

ing them versatile and widely used in the construction industry as walls, ceilings, and floors [135–137].

In construction, concrete and steel are the primary materials used globally due to their mechanical properties, affordability, and ability to be molded into various shapes [138]. Engineered wood products, on the other hand, have inferior mechanical properties, higher prices per volume, and are more challenging to manufacture than steel and concrete. Nevertheless, they offer several advantages, including low density, sustainability, ease of transportation, reduced foundation size due to their low density, and high accessibility from growing forests [139]. Moreover, they have the ability to absorb carbon from the atmosphere [9, 136].

GLULAM and CLT play a crucial role in the current economies of several countries worldwide, including Europe, North America, and Asia. Furthermore, even in countries where wood is not commonly used, such as Brazil, these products have been gaining market traction. The scientific community has been actively researching these materials, as evidenced by Table 2.1, which displays the number of scientific articles published in the Web of Science database from 01/01/2018 to 9/12/2023 and the keywords used in the research. The data indicates that CLT has received more attention in the research community, while topological optimization techniques have been relatively underexplored in the context of EWP applications.

Table 2.1: Keywords and number of scientific article publications in the Web of Science database from 01/01/2018 to 9/12/2023.

Keywords	Number of publications
"Cross-Laminated Timber"	1330
"Glued Laminated Timber"	442
"Cross Laminated Timber" and "Optimization"	44
"Glued Laminated Timber" and "Optimization"	20
"Glued Laminated Timber" and "Topology Optimization"	2 [16, 17]

The two papers that appear in the Web of Science database between 01/01/2018 and 9/12/2023 with the keyword filters "Glued Laminated Timber" and "Topology Optimization" are addressed in this thesis. In [16], a technique is proposed for the topology optimization of truss structures using two materials, taking into account objectives and constraints, including embodied carbon. This framework enables the automatic generation of topology-optimized truss designs that incorporate elements of two different materials, such as timber and steel. The framework determines both the material composition and cross-sectional area of all truss members using a ground structure approach. Meanwhile, the work in [17] was published with results from this thesis.

2.1.2 In- and out-of-plane loading and properties

Although GLULAM and CLT are used in different construction scenarios, they are both subject to two common types of loading: out-of-plane loading and in-plane loading. Out-of-plane loading occurs when a force or load is applied perpendicular or transverse to the plane of the material or structure. In contrast, in-plane loading refers to a type of loading where the force or load is applied parallel or tangential to the plane of the material or structure, causing tension, compression, or shear within the plane of the material. Examples of in-plane loading on a CLT or GLULAM structure include wind or seismic loads [18–20].

Li et al. [20] compared the bending and shear characteristics CLT and GLULAM beams under out-of-plane and in-plane loading. Results showed that the CLT beams had lower mechanical properties than the GLULAM beams due to the orthogonality of the fibers between

adjacent layers, which dispersed the stiffness and strength to the minor strength direction. For out-of-plane loading, the rolling shear failure of the CLT transverse layer was the main difference from the GLULAM beam, while for in-plane loading, delamination caused by shear stress of the transverse and parallel layers was observed in the CLT beams. The CLT beams had lower bending deflection results under out-of-plane loading but higher results under in-plane loading compared to GLULAM beams.

In addition to the evaluation of in-plane and out-of-plane loads, Wei et al. [21] investigated the axial compression behavior of CLT and GLULAM columns. The authors conducted experiments on two lengths of column specimens and determined that the compression strength values of GLULAM column specimens were significantly higher than those of CLT column specimens. However, the CLT columns exhibited enhanced ductility and energy absorption properties due to cross-lamination, indicating potential advantages in certain applications that require better connection performance. The study also found that the length of the column did not significantly affect the compression modulus of elasticity of the specimens, suggesting that the compression modulus of elasticity obtained from the experiments is objective and can be used for comparative analyses of stress-strain models. The CLT columns exhibited more complicated failure modes, such as longitudinal cracking, which the authors suggest calls for circumferential reinforcement.

Still in the context of in-plane and out-of-plane properties, Zhou et al. [22] proposes a non-destructive technique that utilizes modal testing and genetic algorithm to determine the effective elastic constants of CLT panels. The study includes sensitivity analysis which is the contribution of each elastic constant to each vibration mode varies depending on aspect ratio and the orthotropic ratios (E_L/E_T, E_L/G_{LT}, E_L/G_{LR}, and E_T/G_{TR}); specimen design; and genetic algorithm execution strategies to ensure reliable measurements. The study demonstrate that the proposed method is capable of determining the effective bending and shear stiffness values of three symmetric CLT panels. The effective bending and shear stiffness values in the major strength direction were found to agree well with reference values based on the shear analogy method. However, there was a discrepancy between the determined and predicted effective shear stiffness values in the minor strength direction.

In the context of timber construction, the suitability of GLULAM and CLT should be evaluated based on their respective advantages and limitations, as there is no definitive answer as to which material is superior. The decision to use either GLULAM or CLT must be tailored

to the particular application and project specifications. For instance, while GLULAM columns demonstrate higher compression strength values than CLT columns, CLT columns exhibit better ductility and energy absorption properties due to cross-lamination, making them ideal for applications that necessitate better connection performance. Additionally, CLT panels can be manufactured in larger sizes than GLULAM, rendering them more appropriate for larger structures. However, GLULAM may be more fitting for curved and intricate shapes since it can be curved during production. Ultimately, the selection of GLULAM or CLT should be determined on a case-by-case basis, taking into account factors such as structural requirements, aesthetics, cost, and environmental impact.

The use of computational and numerical simulations has become increasingly prevalent in recent research focusing on GLULAM and CLT. For instance, simulations have been employed to evaluate fire resistance in CLT [23–27], assess the performance of CLT and GLULAM structures in combination with steel bars [28–30], study their behavior under seismic loads [31–34], and investigate the stress distribution in these materials [35–37], GLULAM beams reinforced with CFRP [38], among other topics. This thesis aims to leverage the power of computational simulations and topology optimization to generate innovative designs and improvements in GLULAM and CLT structures. The proposed strategies may involve changes in geometry or the addition of new materials to the existing structure.

2.1.3 Innovative designs and enhancement

The field of laminated timber has been the subject of extensive research, owing to its importance in the construction industry. This thesis aims to contribute to this area by focusing on enhancing the mechanical capacity and reducing production input costs of two types of laminated timber, namely glued GLULAM and CLT. The study explores innovative techniques, such as topology modification and reinforcing material incorporation, to achieve these goals. Consequently, the thesis presents a systematic review of scientific studies that have investigated these approaches.

Anshari et al. [39] presented a novel approach to enhance the mechanical properties of GLULAM beams by using Compressed Wood (CW) made of lower grade wood through densification as a reinforcing material. The results of destructive bending tests on short and long GLULAM beams reinforced by CW blocks and a CW lamina demonstrated a significant increase in bending capacity and initial stiffness. For instance, the bending stiffness of short

beams increased by 19-22% and the load-carrying capacity increased by 14-19% with only 1.2-1.8% of the total beam volume being reinforced with CW. Similarly, for the long beams, the bending stiffness increased by 37.1-45.8% and the load-carrying capacity increased by 11%. The study also showed that the controlled moisture-dependent swelling of compressed wood is crucial in pre-stressing the GLULAM beams and producing pre-camber and initial stresses. The approach developed is economically and environmentally friendly as only a small amount of compressed wood is required, and no bonding between the CW and the beam is necessary.

As previously mentioned, GLULAM is typically crafted from hardwood, but numerous studies are exploring alternative raw materials like bamboo. Several scientific articles are dedicated to understanding the potential limitations, mechanical properties, and environmental impact of using bamboo in the same construction configuration as GLULAM. The rising demand for carbon reduction [70, 165] and the advantages of engineered wood products have spurred research aimed at enhancing their structural capacity [147–149, 166]. The integration of engineered wood products with other materials is being investigated as a strategy to decarbonize new buildings [70]. This can be achieved by combining wood with materials such as concrete [143], aluminum [144], bamboo [45], and steel [49, 142, 145, 146, 166]. The following paragraphs present relevant work in the area of combining wood with various other materials.

One of the main advantages of using bamboo is that it is a readily available and rapidly renewable material that can be used in various construction applications. To manufacture engineered bamboo products, the raw bamboo undergoes processing and is transformed into a laminated composite material, similar to the manufacturing process of EWP products [23, 40–45]. Although this thesis does not discuss the use of bamboo as a raw material and topology optimization, Sharma et al. [44] argues that optimizing the beam section of laminated bamboo to take advantage of its high flexural strength-to-density ratio and investigating the influence of the orientation of the original board on stiffness will provide further application opportunities. This indicates a potential area of study related to EWP.

Engineered wood composites that are made up of layers of concrete and wood are product variations that aim to strike a balance between weight, vibration reduction, and sound transmission under various loads, connections, and conditions [141–143], presented in Figure 2.5a. Apart from the concrete combination, combinations of aluminum-wood [144], presented in Figure 2.5b, and steel-wood [49, 145, 146], presented in Figure 2.5c.

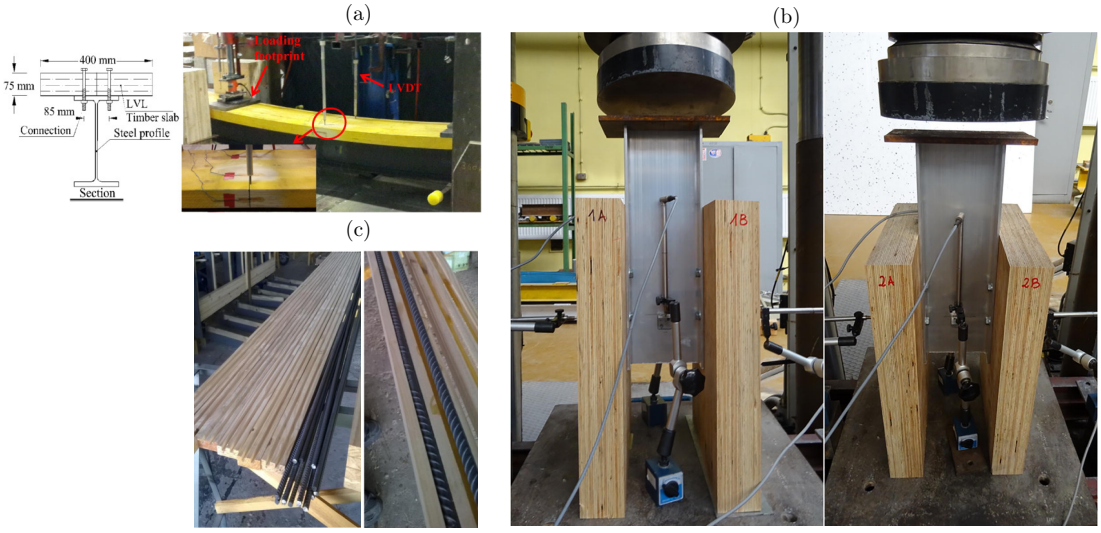

Figure 2.5: (**a**) The geometric shape and specific features of four-point bending experiments conducted on composite beams made of steel and timber [142]. (**b**) Both specimens subjected to testing were made of a combination of aluminum and wood [144]. (**c**) the two-step process for manufacturing reinforced glulam involves creating laminates with grooves and steel bars first, followed by the application of adhesive [49].

Sinha, Way, and Mlasko [46] found that laminated bamboo beam had higher allowable and average strength values in tension and bending than Select Structural Douglas fir members. However, there were differences in properties between the radial and tangential directions of bamboo, which affect stiffness and failure patterns in compression-based applications, as shown in Figure 2.6. This suggests that specific engineering is needed to position and dimension the slats of laminated bamboo beam for targeted end use. The study also showed that the bonding between two pieces of laminated bamboo beam to make GLULAM was not a concern, but the adhesive used or other process parameters limited the GLULAM strength.

The preceding discussion presented the use of CW technology in GLULAM beams and the incorporation of other materials, such as bamboo, in their construction. However, ongoing research is investigating a wide range of materials for reinforcement in EWP, including steel, concrete, FRP, carbon fiber, and others. This signifies that the EWP field is continuously evolving, with new innovations being explored to enhance the products' capabilities and performance. Further literature discussion in this area is expected to provide additional insights into the latest developments, which could potentially open up new avenues for research and application of EWP in various fields.

One of the main ways to reinforce laminated wood is with the use of steel, and this topic will be addressed in chapter 5 through the application of topological optimization in wood

Figure 2.6: This figure, extracted from the research by Sinha, Way, and Mlasko [46], depicts the various types of failure modes encountered during flexure testing of bamboo GLULAM beams. The figure showcases four different failure modes, including **(a)** interlaminar shear failure in the tension zone, **(b)** interlaminar shear failure in the compression zone, **(c)** interlaminar shear failure in the middle of the beam, and **(d)** tensile failure.

structures reinforced with steel bars. The use of steel as a reinforcement material is known in concrete and gained traction in many studies for its application in GLULAM. De Luca and Marano [47] in 2012 studied GLULAM beams and the effects of simple reinforcements as well as a combination of reinforcements and prestressing. According to De Luca and Marano [47], the use of steel bars at both the top and bottom of the beams for reinforcement resulted in a 48.1% increase in the maximum load-carrying capacity and a 25.9% increase in stiffness. Reinforcing the beams with both steel bars and prestressing led to a 40.2% increase in the maximum load-carrying capacity and a 37.9% increase in stiffness. The results are depicted in Figure 2.7 and compared to a previous study conducted by De Luca and Marano [48] in 2011, which employed steel bars without prestressing.

In their research, De Luca and Marano [47] observed that the strains experienced by both simply reinforced and reinforced-prestressed beams were roughly 50% lower compared to the

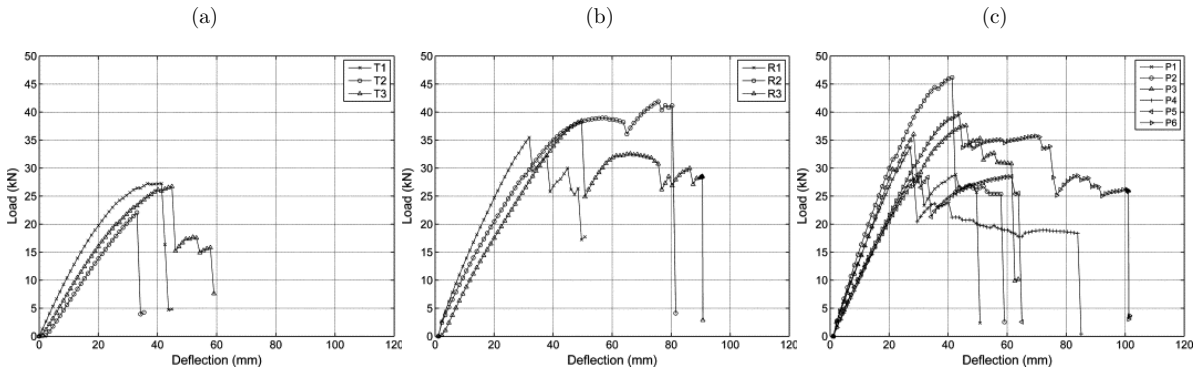

Figure 2.7: **(a)** Load-deflection curve showing the behavior of unstrengthened beams (T series), as presented in [48]. **(b)** Load-deflection curve showing the behavior of simply strengthened beams (R series), reinforced with 10 mm diameter steel bars, as presented in [48]. **(c)** Load-deflection curve showing the behavior of strengthened-prestressed beams (P series), reinforced with 10 mm diameter steel bars and prestressing, as presented in [47].

unreinforced beams. The failure mode of the unreinforced timber beams exhibited brittle traction due to broken fibers, while the reinforced beams displayed a compression-initiated flexural failure mode characterized by increased ductility. As for the reinforced-prestressed beams, they failed in bending with a compression failure mode, also characterized by increased ductility. The presence of steel bars served to decrease the opening of cracks and confined the rupture within a narrow zone, thereby increasing the failure tensile strain in the reinforced and reinforced-prestressed beams. Moreover, the study revealed that the strength of the GLULAM-steel material was mostly utilized, except for some specimens where debonding or delamination occurred between the two bonded materials. Suggesting that the strength of the glulam-steel composite was not entirely utilized.

In addition to the positioning of the reinforcement beams at the ends as previously presented, Soriano, Pellis, and Mascia [49] propose the use of steel reinforcement beams within the GLULAM structure formed by two types of wood layers. At the end, four layers of a material called "higher category" are used, and in the center, three layers called "lower category" are used. The difference in mechanical capacity between the two categories is approximately 60%. For evaluation, three configurations were built, which are presented in Figure 2.8, the first without steel reinforcement, the second with two equidistant steel bars from the neutral axis with a diameter of 10 mm, and the third with four steel bars positioned in pairs vertically equidistant from the neutral axis. Also shown in Figure 2.8 are the grooves made in the laminates for the insertion of the reinforcement bars before the gluing process.

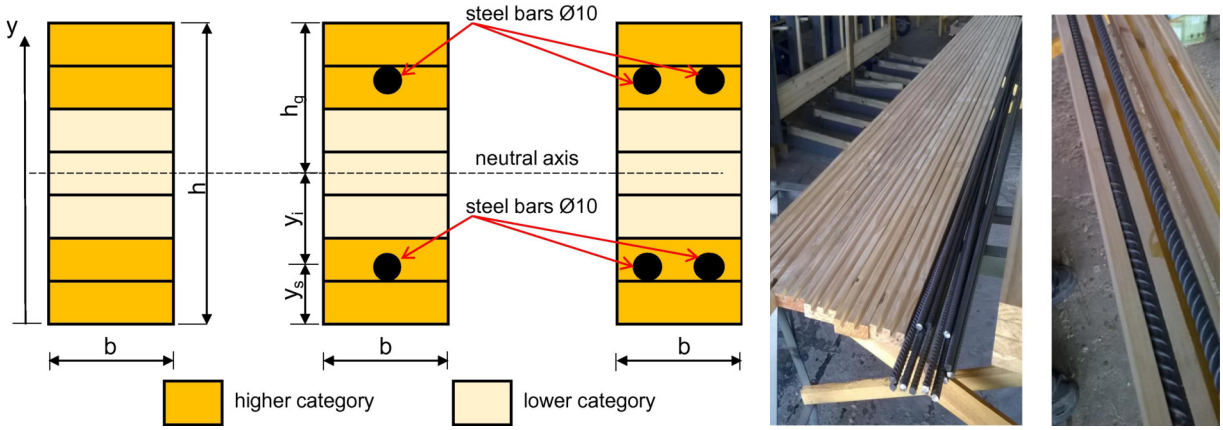

Figure 2.8: Figure extracted from the work presented by Soriano, Pellis, and Mascia [49] containing the three evaluated beam configurations, the first without steel reinforcement, the second with two equidistant steel bars from the neutral axis with a diameter of 10 mm, and the third with four steel bars positioned in pairs vertically equidistant from the neutral axis. And the grooves made in the layers for the application of steel reinforcement.

Based on the experimental results from bending tests and the transformed cross-section method, the study found that the insertion of symmetrical steel bars increased the beam capability from 53.1% to 79.2% considering the serviceability limit states. However, the transformed cross-section method has restrictions with regard to accuracy for high reinforcement ratios. The study also found that the reinforcing effect for GLULAM beams indicates the importance of a high modular ratio and that using higher reinforcement ratios can lead to the ultimate limit state characterized by lateral instability. Based on these conclusions, the study suggests additional research on other dimensions of beams and other reinforcement ratios, as well as the optimization of reinforcement as a function of the variation of bending moment along the length of the beam.

In the same vein of using steel for reinforcement in wooden structures, Wei et al. [50] proposes a novel steel-reinforced bamboo scrimber beam in which steel bars or prestressed steel bars are embedded in a bamboo composite material. The flexural performance of the reinforced bamboo beam with different reinforcement ratios and different levels of prestressing forces was investigated. The results show that the ultimate bearing capacity of the reinforced beams increases with an increasing reinforcement ratio and prestressing, and the influence of the prestressing is inferior to that of the diameter of the reinforced bars. The flexural stiffness at the serviceability limit state of the reinforced beams increases linearly with an increasing reinforcement ratio and can be enhanced by up to 36.80% compared with that of control

beams. Calculation methods for the flexural rigidity and bearing capacity are presented, which can accurately predict both reinforced and prestressed reinforced bamboo beams. The study suggests that steel-reinforced bamboo scrimber beams can be used for long-span, heavy-load bamboo structural engineering.

Another important material used as reinforcement in EWP structures is Fiber-Reinforced Polymer (FRP), which, along with steel, FRP-wood composite has been evaluated by several researchers. Just like in steel, the main concern in using other materials to improve EWPs is the adhesive. Given this concern, Raftery, Harte, and Rodd [51] demonstrates that high-quality, durable bonds can be formed when specific FRP reinforcement is bonded with certain conventional wood laminating adhesives using a vacuum-pressure, soaking-drying cyclic procedure and the block shear test. The study found that moisture-cycled FRP-wood specimens showed mechanical performance that compared extremely well with non-moisture-cycled FRP-wood bonded specimens, wood-wood bonded specimens, and solid control specimens taken from the same board.

Strategically adding reasonable percentages of FRP reinforcement in the tension zone of the beam can lead to moderate stiffness improvements and significant increases in ultimate moment capacity. The placement of the FRP reinforcing material in the highly stressed tensile region of the beam can enhance ductility and facilitate a more efficient use of timber in the compression laminations. The use of FRP plates can also help to mitigate weak local defects in the timber, resulting in less variability in the results for the FRP reinforced beams. Additionally, FRP plates show potential as both a substitute for high-quality wood laminations and as flexural reinforcement for low-grade GLULAM beams [52].

In addition to FRP, Glass Fiber Reinforced Polymer (GFRP) and Carbon Fiber Reinforced Polymer (CFRP) were also evaluated as reinforcement materials in EWP [53–56]. Li et al. [54] proposed a method to strengthen hollow-sectioned wood beams using GFRP rods and CFRP composite sheets. Five groups of specimens were tested using the four-point bending test to obtain force-displacement relationships of the wood beams, with and without FRP reinforcement. The results were compared, and a sectional analysis method was proposed to predict the force-displacement relationships of the wood beams strengthened by GFRP rod and CFRP sheets. The study found that the proposed method of using GFRP rods and CFRP composite materials effectively strengthens wood beams in heritage buildings that have decayed in the middle of the section, resulting in an increased average strength. The bending moments of the

reinforced specimens were also higher than those of the unreinforced specimens, with the on average strengths 3.5% to 9.5% more than the control group.

Another experimental study conducted by [55] investigated the effectiveness of U-shaped steel sections and CFRP in reinforcing composite timber beams. The specimens were subjected to three-point bending tests, and various strengthening configurations were evaluated, including steel-only reinforcement, CFRP-only reinforcement, and a combination of both materials. The study focused on failure behavior, displacement, strain response, ductility, bending capacity, and structural efficiency. The results revealed that plain timber specimens exhibited abrupt failure, while the inclusion of steel sections or epoxy reinforcement delayed or prevented brittle failure. The most effective configuration involved a composite beam element with a combination of compressive stress from the timber and steel in the top half and tensile stress from CFRP on the bottom. This configuration consisted of 2 mm thick steel reinforcement, CFRP reinforcement, and an epoxy connection, resulting in the highest bending resistance. Additionally, the U-shaped steel sections not only enhanced the tensile capacity of the timber beams but also significantly increased their overall capacity. The reinforcement offered substantial benefits for each configuration, highlighting its potential as a lightweight structural element in resisting bending.

Furthermore, in the comparison between CFRP and steel reinforcement in EWPs Yang et al. [57] studied the effect of reinforcement materials on the flexural behavior of GLULAM beams, using both FRP and steel materials. The study carried out a series of four-point bending tests on both reinforced and unreinforced Douglas fir GLULAM beams to evaluate the effects of reinforcement ratio and arrangement on flexural capacity, flexural stiffness, and timber tensile strain at failure. The results showed a significant improvement in these factors for reinforced timber beams compared to the control group, with an average improvement of 56%, 28%, and 49%, respectively. Additionally, the same study proposed a theoretical model to predict the flexural capacity and stiffness of reinforced timber beams. The proposed model showed differences between theoretical and experimental results of on average about 10%. A parametric analysis was then conducted to investigate the effects of influential factors on flexural capacity and stiffness, including the axial stiffness ratio of reinforcement to timber, the relative location of tensile reinforcement, and the strength ratio of reinforced timber between flexural tension and compression.

Full-scale testing provides a realistic representation of the structural behavior and performance of the system being studied. It allows for the assessment of the actual response of the materials and components under real-life conditions, capturing complex interactions and behaviors that may not be accurately replicated in small-scale or laboratory tests. Vahedian, Shrestha, and Crews [58] investigates the feasibility of using CFRP composites to strengthen GLULAM beams and explores the effects of different bond geometries on their flexural capacity, stiffness, deflection, and failure mode. Eight timber beams were tested under four-point bending, with some beams reinforced with CFRP sheets and others serving as controls, as presented in Figure 2.9. The results indicate that reinforcing GLULAM beams with CFRP sheets significantly improves their ultimate flexural strength and stiffness. The stiffness of the strengthened timber beams increased between 31% and 64% based on the results. Increasing the bond length and width led to a noticeable decrease in shear stress at failure, resulting in a more ductile collapse. The presence of natural defects like knots initially caused some samples to fail, but the FRP strips helped control the cracks and delay their growth.

The application of Vectran-FRP reinforcement to GLULAM beams resulted in significant improvements. Donadon et al. [59] investigated the use of Vectran-FRP reinforcement in timber beams, specifically glue-laminated timber beams made from reforested Pinus Elliottii wood. Vectran, a high-performance synthetic fiber, was explored as a reinforcement material, despite its limited application in this context. Bending tests were conducted on the reinforced beams, and a numerical procedure based on the finite element method was developed to compare with experimental results.The reinforced beams exhibited an increase in both initial stiffness and ultimate load compared to unreinforced beams. The stiffness enhancement ranged from 19.5% to 35.0% in the 10% to 50% of the ultimate load interval. However, beyond 50% of the ultimate load, a decrease in stiffness was observed.

The findings revealed significant enhancements in the reinforced beams compared to the unreinforced ones. Notably, the application of Vectran-FRP reinforcement resulted in increased initial stiffness and ultimate load capacity. The improvement in stiffness ranged from 19.5% to 35.0% within the load interval of 10% to 50% of the ultimate load. However, beyond 50% of the ultimate load, a decrease in stiffness was observed [59].

The results of the study demonstrated notable improvements when FRP sheets were utilized. Specifically, the average enhancement in initial stiffness for FRP-confined CLT and GLULAM specimens was 29% and 24%, respectively, compared to specimens without rein-

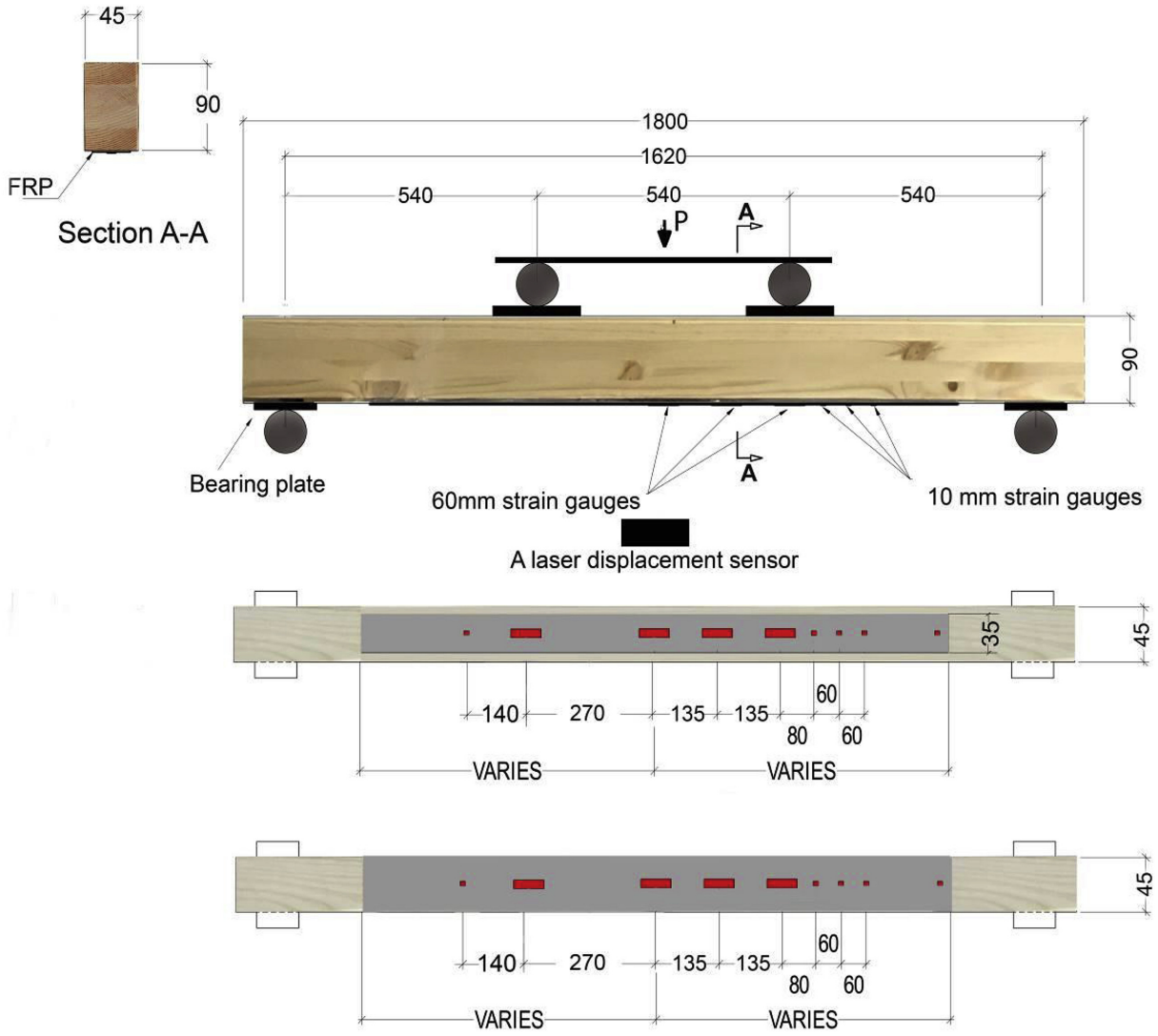

Figure 2.9: Figure extracted from the work presented by Vahedian, Shrestha, and Crews [58] representing a a schematic view of the experimental evaluation and the position of the CFRP reinforcement.

forcement. Furthermore, the energy dissipation capacity of the CLT and GLULAM specimens significantly increased by 358% and 266%, respectively, with the incorporation of FRP sheets. Through an analysis of hysteresis loop curves, three failure modes were observed in the FRP-confined specimens: timber crushing failure, FRP cracking failure, and longitudinal buckling failure [60].

In addition to the evaluation of the mechanical capacity of the CFRP and wood combination, it is essential to consider the interface between CFRP and wood. Vahedian, Shrestha, and Crews [56] emphasize the complexity associated with externally bonding CFRP to timber and the limited research conducted to understand the bond behavior between FRP and timber interfaces. To address this knowledge gap, the researchers conducted pull-out tests on 136

FRP-to-timber joints. The experimental results served as the basis for establishing a new analytical model that accurately determines the strain distribution profile, slip profile, and shear stress along the interface of the FRP-to-timber joint. By comparing the predicted parameters obtained from the analytical model with the measured parameters from the experimental tests, a satisfactory correlation was observed. This finding underscores the effectiveness of the proposed analytical model in accurately predicting the behavior of FRP-to-timber joints. The research by Vahedian et al. contributes valuable insights into understanding the bond behavior between CFRP and timber interfaces, further enhancing our knowledge of this important aspect in composite structural elements.

In addition to the use of metallic materials and FRP as reinforcement for EWP, concrete is also being studied as a form of reinforcement and as a supplementary material to reduce costs and enhance efficiency in the work. Lukaszewska, Johnsson, and Fragiacomo [61] conducted a study on connectors embedded into prefabricated concrete slabs for timber-concrete composite structures. The primary objective of this research was to investigate the feasibility of achieving a high degree of prefabrication to reduce construction costs and facilitate the widespread utilization of timber-concrete systems in the market. To accomplish this, direct shear tests were performed on small blocks consisting of a GLULAM segment connected with a prefabricated concrete slab. The shear force-relative slip relationships were measured, and various mechanical properties such as slip moduli and shear strengths were subsequently calculated.

According to the same authors, this structure offers notable cost savings when compared to conventional cast-in-situ (or cast-in-place) concrete methods. Additionally, the use of prefabricated elements allows for an acceleration in the construction process. Moreover, the composite system is less susceptible to the effects of concrete shrinkage in comparison to cast-in-situ concrete. These findings strongly support the notion that achieving a high level of prefabrication and employing "dry" connections can significantly contribute to cost reduction in construction and facilitate the broader adoption of timber-concrete composite structures in the market. [61]

Martins et al. [62] proposed a novel approach in the field of structural flooring by introducing Timber-Concrete Composite (TCC) panel. The primary objective of this panel is to provide an environmentally friendly and cost-effective solution through the utilization of natural resources with low commercial value and industry sub-products. To evaluate its per-

formance, nine TCC beams were fabricated, each employing a different type of fastener, and subsequently subjected to a four-point bending test after a curing period of 28 days. By adjusting the spacing between the connectors, comparable mechanical performances were achieved for all three configurations. The study consistently revealed that the failure of the TCC beams was primarily influenced by the bending strength of the logs. Importantly, the experimental results confirmed that the TCC panel not only met the stringent mechanical requirements for multi-storey building slabs but also satisfied the acoustic and dynamic criteria.

Another innovation using TCC panel was presented by Estévez-Cimadevila et al. [63] introduced an innovative TCC panel for structural flooring. This system offers a unique combination of high stiffness, strength, and lightweight properties. By employing perforated boards, an efficient timber-concrete connection is established, further reinforced by strategically placed reinforcement bars. Compared to conventional wood-only or concrete-only solutions, this TCC panel demonstrates several advantages. These include simplified construction processes, monolithic structural integrity, reduced overall weight, and improved resistance against horizontal forces. This research contributes to the advancement of TCC technology and its potential applications in modern construction practices.

In addition to material combinations, changes in the geometry of traditionally manufactured timber structures are also a constant topic of study. For instance, using computer models, Franzoni et al. [147] evaluated the loss of mechanical strength in CLT structures in the presence of small gaps. Intentionally including gaps in CLT can encourage the creation of new designs by filling the gap with other materials, thus improving the acoustic and thermal properties of the structure. For example, in the case of CLT, the greater the gap between the layers, the smaller the bending stiffness in the same proportion of volume change [148, 149]. This knowledge can aid in developing improved CLT designs.

Structural optimization is another approach to improving design characteristics. It involves seeking the optimal solution for a project while adhering to the limitations defined during the project planning stage. Topology optimization, a form of structural optimization, has been widely employed to seek the optimal material distribution within a design domain, all while considering the system's peculiarities and constraints imposed by users. This topic is discussed in more detail in Section 2.2.

There are few studies on structural engineered wood and topology optimization. In this context, Ching and Carstensen [16] proposed a truss topology optimization framework in-

volving two materials: timber and steel. Within this framework, it is possible to minimize compliance, which can be interpreted as the inverse of stiffness, while subject to volume and Global Warming Potential (GWP) constraints. Another option proposed was the minimization of GWP with restrictions on stress.

In this vein, Mayencourt and Mueller [3] introduced a methodology for optimizing the shape of CLT structures. The study argues that up to 70% of the material used can be saved. Concerning the minimization of material usage in CLT manufacturing, Mayencourt and Mueller [4] addressed the improvement of CLT structures from an optimization standpoint. They worked with the possibility of optimizing the density of the intermediate layers in one-way slab CLT. The intermediate layers were modified by adding voids to achieve the optimal density value. According to the proposed methodology, in a CLT composed of five layers, the optimal relative density for layers two and four was 0.41. Consequently, removing material from these layers resulted in an 18% reduction in material consumption, reflecting a cost reduction of up to 14% with acceptable capacity loss.

Hollow-Core Cross-Laminated Timber (HC-CLT) is the term used to describe CLT structures with intentionally created voids in the core. In hollow-core designs, the primary objective is to reduce mass and material usage during manufacturing. However, in addition to these advantages, Huang et al. [160] investigated the acoustic performance of HC-CLT when used for flooring and its response to human-generated sound pressure. The authors found that the acoustic performance did not deteriorate in any situation and, in some cases, was the best acoustic insulator.

Similar to HC-CLT, Perković, Rajčić, and Pranjić [161] experimentally evaluated multiple designs of Hollow-Core Glued-Laminated Timber (HC-GLULAM) structures with elliptical and circular voids. However, in contrast to HC-CLT, the HC-GLULAM structures with hollow cores exhibited up to a 40

2.1.4 Sustainability and environmental considerations of using engineered wood products in construction

Building construction is a global industry that demands extensive resources, leading to significant environmental impacts. The urgency to mitigate carbon emissions, particularly in construction activities, has intensified. Among the primary building materials, namely wood, concrete, and steel, wood construction stands out as a viable solution for reducing greenhouse

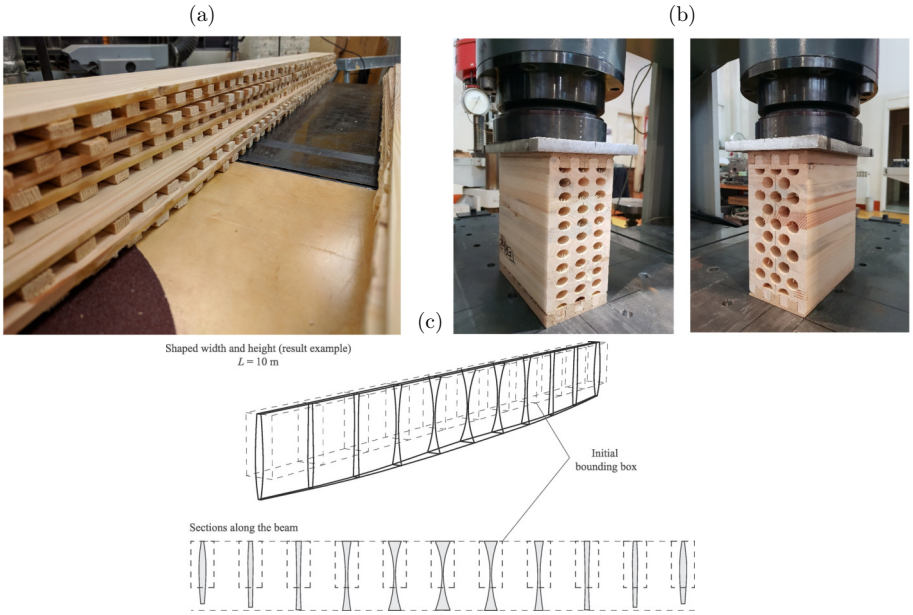

Figure 2.10: (**a**) Hollow-core CLT before the glue application [4]. (**b**) experimental validation of hollow-core GLULAM [161]. (**c**) sections of a optimized section considering a beam with a span of 10 meters [3].

gas emissions. Wood is sourced from renewable and sustainable forests, making it an environmentally friendly choice [9, 42, 64, 65].

Replacing traditional construction materials with wooden structures can reduce up to 31% of the global CO_2 emissions [140], and in some regions, it can even avoid the emission of 50 Mt CO_2 by 2050 [70]. Therefore, there is a growing need to understand the behavior of structural engineered wood products and their combinations.

Wood as a building material offers several advantages in terms of sustainability and carbon footprint reduction, with the carbon-cycle presented in Figure 2.11 created by the United States Department of Agriculture. Firstly, wood is a renewable resource, meaning it can be replenished through responsible forestry practices. This sustainable sourcing ensures the long-term availability of wood for construction purposes. Additionally, wood has a lower embodied energy compared to concrete and steel, meaning it requires less energy during the manufacturing and construction processes.

Wood acts as a carbon sink, as it naturally absorbs and stores carbon dioxide from the atmosphere throughout its lifespan (Figure 2.11). This carbon sequestration capacity contributes to mitigating greenhouse gas emissions, making wood construction an effective strategy for combating climate change.

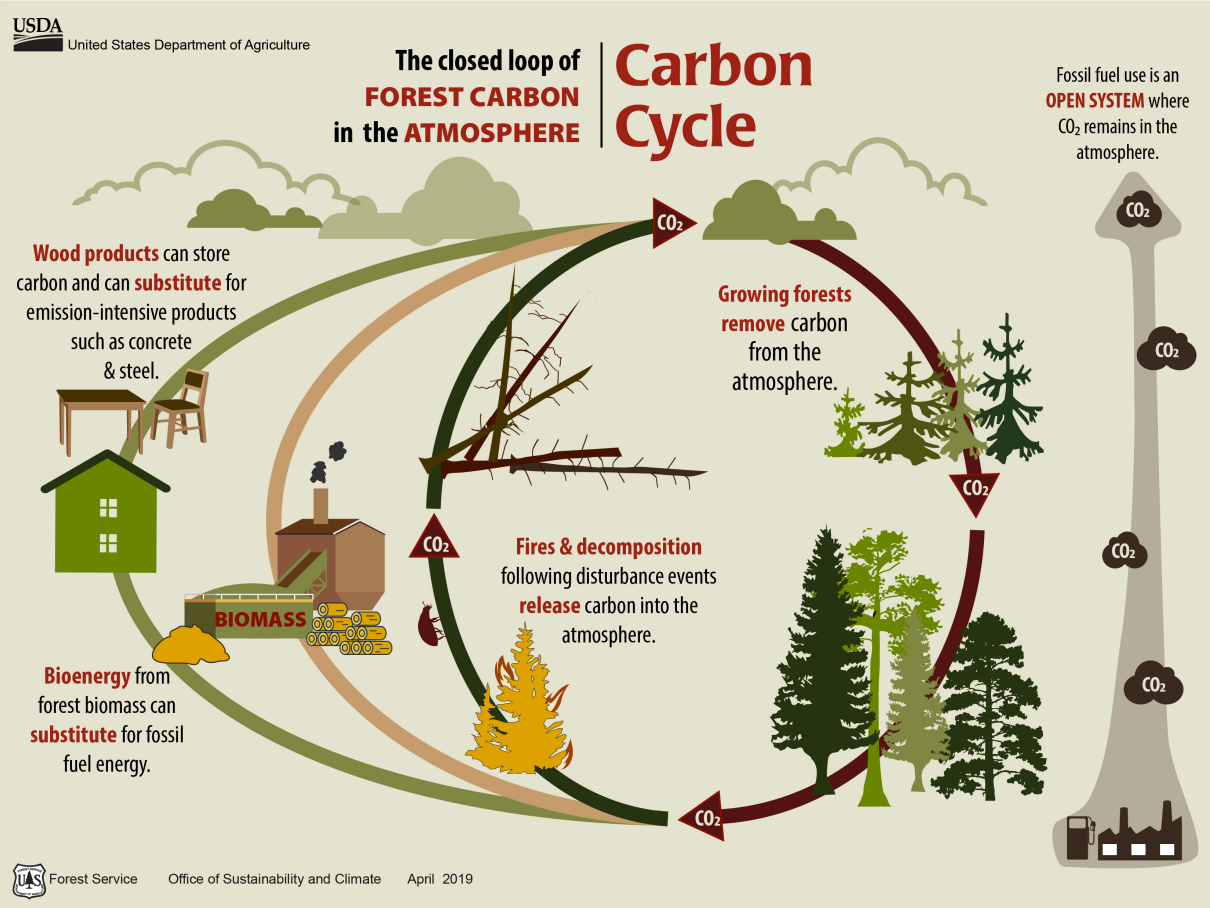

Figure 2.11: Carbon-cycle extracted from the United States Department of Agriculture [66].

In a study conducted by Hassan and Johansson [64], it was concluded that GLULAM beams offer superior environmental friendliness compared to steel beams due to the wood's carbon storage capacity. However, it should be noted that the use of GLULAM beams may necessitate larger dimensions, especially for longer spans. This study underscores the significance of investigating the environmental and economic implications of building elements in order to attain sustainability in construction engineering.

In a comparative study conducted by Hassan, Öberg, and Gezelius [65] the structural design, economic aspects, and environmental impact of CLT and concrete slab flooring were examined. The research findings strongly emphasized the environmental advantages of wood, particularly CLT, over concrete. Wood has the ability to store carbon throughout its lifespan, while concrete stores carbon dioxide through the carbonation process. The study highlighted the crucial role of forests in carbon storage and suggested that using wood in construction could contribute positively to reducing the greenhouse effect. However, it was noted that CLT material tends to be more expensive than concrete. Despite this cost difference, the study

revealed that the overall estimated costs of both floor types, when ready to assemble, were similar.

Additionally, the study investigated the influence of floor span on design values, costs, and carbon dioxide emissions. It concluded that CLT flooring can effectively compete with concrete slab flooring for spans up to 7 meters without compromising structural requirements. However, for larger spans, meeting the vibration requirements becomes more challenging for CLT flooring compared to concrete slabs [65].

Hassan, A.A., and Abdulahad [67] emphasizes the importance of integrating environmental and economic considerations into the technical design of buildings to enhance their sustainability. Concrete is better suited to resist greater axial forces without significant increases in cross-sectional dimensions. However, axial forces have a more pronounced impact on the cross-sectional area of GLULAM columns compared to concrete columns. In terms of environmental consequences, GLULAM columns are found to be the superior choice in greenhouse gas emissions. Wood's carbon storage capacity makes it more favorable as it stores more carbon dioxide than is emitted during the manufacture of GLULAM columns. Concrete production, on the other hand, generates significant greenhouse gas emissions. Although concrete stores some carbon dioxide, it does not possess the same storage capacity as wood. Even when GLULAM columns are demolished and the wood is used for energy recovery, releasing the stored carbon dioxide into the atmosphere, they still remain a more environmentally friendly alternative to concrete.[67].

When comparing a reinforced concrete building and a hybrid mid-rise commercial building using CLT, an average reduction of 26.5% in global warming potential for the hybrid CLT building compared to the concrete building, excluding biogenic carbon emissions. The substitution of concrete and steel with CLT in building structures offers substantial environmental advantages, including an average reduction of 26.5% in global warming potential, a 30% decrease in eutrophication potential, and a 25% reduction in depletion potential of the stratospheric ozone layer when considering the cradle-to-gate analysis. Furthermore, the hybrid CLT building exhibited a significantly higher proportion of renewable energy compared to non-renewable energy, with a net non-renewable energy consumption 8% lower than that of traditional reinforced concrete buildings [68].

Cordier et al. [69] conducted a case study at a regional scale in the province of Quebec, Canada, to examine the increasing use of wood structures in non-residential buildings. The

researchers aimed to assess the environmental implications of this trend and developed material substitution factors by comparing different structures. The study reveals that, on average, wood can replace steel and concrete by approximately 0.59 and 4.54 times their respective weight. However, the advantages of steel substitution outweigh those of concrete substitution. By comparing three substitution scenarios across four impact categories, the research identifies a favorable outcome for wood utilization in seven out of twelve combinations. Notably, the ecosystem quality indicator exhibits contrasting trends compared to climate change, human health, and resource indicators, making it the least favorable. These findings contribute to the growing evidence supporting wood as an environmentally friendly option in construction. As decision-makers increasingly consider large-scale timber usage, this study provides valuable insights into the regional-level environmental consequences of wood substitution. It underscores the importance of considering not only climate change but also human health, ecosystem quality, and resources in material substitution assessments. The research emphasizes the necessity for strategies and policies that address urgent climate challenges while safeguarding ecosystem quality.

The replacement of concrete floors with CLT panels in steel structural systems on a global scale is the focus of D'Amico, Pomponi, and Hart [70] study. The replacement offers a viable solution for immediate implementation without requiring technological advancements or changes in professional practice. The research combines Material Flow Analysis with Life Cycle Assessment, considering different levels of uptake of the hybrid construction system over the next 30 years. The results demonstrate that the potential for greenhouse gas emissions savings ranges from 20 to 80 Mt CO2e, with an average of approximately 50 Mt CO2e if the hybrid construction system is fully adopted by 2050. It is important to note that these estimates do not include the carbon sequestration potential of timber, which would further increase the savings. The urgent need for substantial reductions in anthropogenic greenhouse gas emissions to avoid a climate catastrophe. The projected growth of urban areas combined with increased material consumption in the construction sector reinforces the importance of finding alternative solutions to curb emissions. Despite improvements in operational energy efficiency, the manufacturing and construction phases of buildings have become significant sources of carbon emissions. Steel and concrete, the most widely used materials in construction, are particularly challenging to decarbonize due to their energy-intensive production processes.

According to Žemaitis et al. [71], Sustainability Impact Assessment (SIA) of building materials is crucial for decision-makers and can influence material choices. The study compared the sustainability impact assessment of wood- and concrete-based building material value chains using the decision support tool ToSIA. The results showed that the value chains for GLULAM and sawn timber have more positive sustainability impacts compared to those for site-cast concrete and precast reinforced concrete, especially in terms of environmental indicators such as greenhouse gas emissions, energy use, waste generation, and water use. The study also revealed that wood-based building materials have more positive socio-economic impacts that could increase regional competitiveness and promote sustainable development. While the study's results are specific to Lithuania, they may be applicable to other countries with comparable economic development levels. The study provides practical scientific knowledge that is valuable to policy experts, decision-makers, companies, and architects who wish to compare different building materials.

2.1.5 Notable engineered wood products structures

EWP have been increasingly used as an alternative to traditional building materials such as steel and concrete, due to their sustainability, cost-effectiveness, and versatility. These products are made from wood fibers, strands, or veneers that are bonded together with adhesives or other methods, resulting in a high-performance material with consistent strength and stiffness properties.

Malo, Abrahamsen, and Bjertnæs [72] presented the design and construction of "Treet," a 14-storey timber apartment building in Norway, which is one of the tallest timber buildings in the world. The building comprises load-carrying GLULAM trusses and prefabricated building modules stacked on top of a concrete garage and intermediate strengthened levels. The design and construction process, including investigations, considerations, and discussions, is discussed, along with the chosen structural solution and design verifications. The chosen structural solution results in insignificant vibrational effects caused by wind exposure. Overall, the chosen design provides a robust solution for the construction of "Treet" and demonstrates the potential of timber buildings in modern construction.

The Ascent MKE Building, standing at 25 stories high (86.6 m), is officially the tallest hybrid mass timber building in the world (Figure 2.12), surpassing Norway's Mjösa 18-story tower. The USDA Forest Service provided support for Ascent through the agency's Wood Innova-

tions program and Forest Products Laboratory fire testing. The project was granted a wood innovations grant that facilitated engineering and design work, and the lab conducted critical fire testing of GLULAM columns [73].

Figure 2.12: Picturs of the Ascent MKE Building, the tallest mass timber building in the world [74].

Lefebvre and Richard [75] discusses the design and construction of a new bridge spanning the Uupaachikus Pass in Mistissini, Quebec (Figure 2.13). The project was undertaken to provide access to a larger territory for the Cree community and to satisfy the growing demand for gravel used in construction projects. The bridge is 160 meters long, 9.25 meters wide, and has four spans of 37, 43, 43, and 37 meters. It was designed using semi-continuous arches made GLULAM girders. The article describes the challenges faced by engineers during the design and construction phases, including the need to use local materials due to the remote location of the project. The GLULAM solution was ultimately chosen for its affordability and sustainability, with the wood used on the project coming from sustainable forests in the surrounding area. The article also discusses the geometric design of the bridge, which uses connectors between GLULAM girder segments to transfer shear, compression, and bending forces. The use of GLULAM allowed for the elimination of expansion joints over the 160-meter bridge, increasing its durability.

Figure 2.13: Bridge in the the Uupaachikus Pass in Mistissini, Quebec [76].

The "Smile" (Figure 2.14) represents a significant achievement in the realm of structural engineering and architectural design. As one of the Festival's Landmark Projects, it serves as a public space that invites exploration and inhabitation. The structure itself is a curved, tubular beam measuring 3.5 meters in height, 4.5 meters in width, and 34 meters in length, crafted from CLT American tulipwood. Represents the first ever creation of a "mega-tube" constructed from construction-sized panels of hardwood CLT, showcasing the structural and spatial potential of this innovative material [77].

2.2 Contextualizing structural optimization

Topology Optimization (TO) is a numerical approach used in mechanical and structural engineering to optimize material structures based on a given set of design requirements. This

Figure 2.14: The "Smile" structure in Festival's Landmark Projects [77].

approach involves determining the optimal allocation of material within a specified region, subject to constraints and boundary conditions [78]. By using computer-aided software programs, many iterations are performed to reach the optimum design. Unlike shape optimization, which determines the optimum shape of a domain with a prescribed topology, the use of topology optimization in many industries is expanding, providing improved designs and benchmark optimal designs that can be used to evaluate more feasible designs. This field is a rapidly growing area of research, with numerous peer-reviewed articles being published every year. According to the Web of Science database, using the keyword "topology optimization" between the period of 2013 to May 2023, 26,687 results were found, including articles, proceeding papers, and review articles. Overall, topology optimization provides an answer to the fundamental engineering question of how to optimally allocate material within a given design domain to achieve the best possible structural performance. Therefore, this chapter aims to present the main research involving TO and current research on TO, as well as the validation of the methods used in this work.

Bendsøe and Kikuchi [78] in 1988 were the first to introduce the concept of TO, which involves optimizing the shape and topology of mechanical elements. This method utilizes a material distribution approach that utilizes an artificial composite material with microscopic voids. Structural performance is enhanced by redistributing the structural material within a

limited volume. The design domain is typically divided into finite elements, with each element's existence (whether it is a solid or a void) serving as the primary design variable. To make use of gradient-based optimization algorithms and find the local optimal solution, the discrete problem is relaxed, resulting in a continuous representation of the elemental volume fraction.

Long before classical mechanics theories and equations were developed, optimization was already a topic of interest for structural systems. In fact, the concept of optimization can be traced back to as early as 1638 when Galileo delved into the beam optimization problem. In his book *Discorsi e dimostrazioni matematiche, intorno à due nuove scienze* (Discourses and Mathematical Demonstrations Relating to Two New Sciences), Galileo presented a definition and a logical solution for the optimal shape of a simply supported beam under concentrated loading, as shown in Figure 2.15 [79].

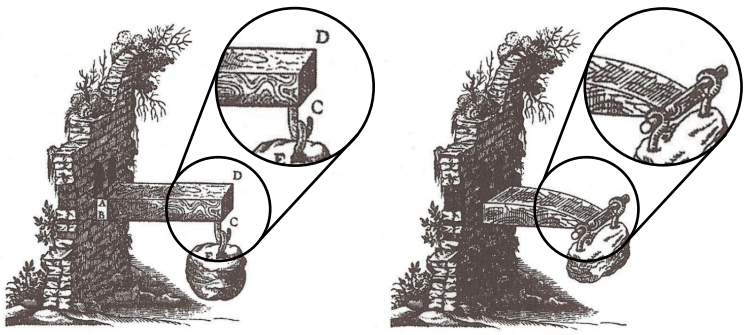

Figure 2.15: Optimization problem presented by Galileo in 1638, adapted from [79].

Despite being centuries old, Galileo's work on beam optimization still holds relevance today. His contributions to the field laid the foundation for subsequent research on optimization techniques for structural systems. Furthermore, his early recognition of the importance of optimization in structural engineering showcases the prescience of his scientific insights.

In 1904, Michell [80] authored one of the most influential works in the field of optimization titled "The limits of Economy of Material in Frame-Structures." This groundbreaking work focused on optimizing a centrally loaded simply supported structure (Figure 2.16). Michell's findings from 1904 continue to be subjects of ongoing research and discussions among scholars. Furthermore, his results serve as benchmark parameters for comparing and developing new optimization methodologies, as evidenced by numerous subsequent studies [81–86].

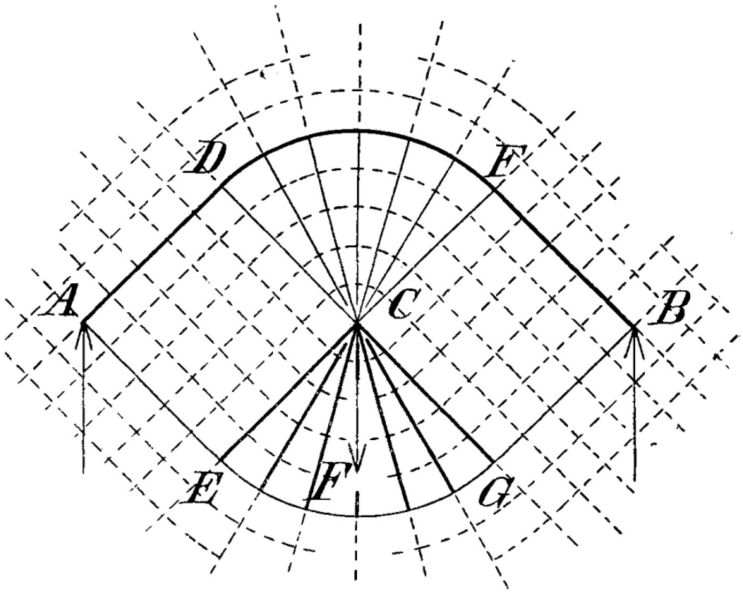

Figure 2.16: Structural optimization obtained by Michell [80]

2.2.1 Structural optimization

Structural optimization involves the systematic exploration of optimal structural configurations that can efficiently withstand specified load cases while satisfying relevant constraints. From a mathematical standpoint, an engineering optimization problem aims to determine the values of design variables ($\mathbf{x}$) that yield the highest performance or achieve desired objectives, as described in Eq. 2.1. These variables are carefully selected and manipulated to enhance the structural efficiency, strength, and stability, ultimately leading to the identification of an optimal solution within the given design space.

$$\begin{aligned} \min_{\mathbf{x}} \quad & f(x) \\ \text{s.t.} \quad & g(x) \leq 0 \\ & h(x) = 0 \end{aligned} \tag{2.1}$$

In the context of the general optimization problem presented, the design variables are denoted by the vector $\mathbf{x} = [x_1, x_2, x_3, \dots, x_n]$, while the objective function $f(x)$ quantifies the optimization goal. Incorporating the considerations of inequality constraints, the functions $g(x) = [g_1(x), g_2(x), g_3(x), \dots, g_m(x)]$ are introduced, which capture the conditions to be satisfied. Additionally, the equality constraints are accounted for through the functions $h(x) = [h_1(x), h_2(x), h_3(x), \dots, h_n(x)]$, thus defining the equalities that must hold within the optimization problem [87].

In structural optimization, the objective function $f(x)$ plays a crucial role in characterizing the structure and assessing its overall performance [88]. Various objective functions have been developed, each focusing on different aspects of the design. These include functions related to volume [88], local displacements [89], overall stresses [82, 90, 91], structural mean compliance [82, 84, 92, 93], vibration responses [94], heat conduction [95, 96], multi-objective optimization [97], and others. Constraints $g(x)$ and $h(x)$ are commonly employed to incorporate specific design requirements or limitations, such as structural mass, equilibrium conditions, maximum displacements, and more. The vector $\mathbf{x}$ represents the structural configuration and evolves throughout the optimization process. Each design variable x_n is defined based on the specific optimization problem at hand.

There exist three primary categories of structural optimization, namely size optimization, shape optimization, and topology optimization. Size optimization (Figure 2.17a) entails adjusting the dimensions or proportions of individual elements within a fixed topology and shape. By optimizing the sizes of these components, the overall structural behavior can be improved. Shape optimization (Figure 2.17b), on the other hand, involves modifying the geometry of an existing structure while maintaining its overall topology. This category allows for the refinement of specific regions or features to enhance performance. Lastly, topology optimization (Figure 2.17c) focuses on determining the optimal arrangement and interconnection of structural elements to achieve a desired objective. By exploring different topologies, this approach seeks to identify the most efficient distribution of material within a given design space. Each of these categories plays a vital role in tailoring the design to meet performance objectives and can be employed in various engineering disciplines [82].

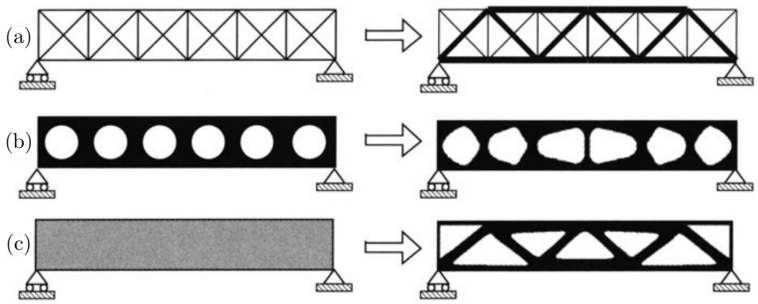

Figure 2.17: Three primary categories of structural optimization: (a) Sizing optimization of a truss structure, (b) Shape optimization, and (c) Topology optimization. The left-hand side displays the initial problems, while the right-hand side showcases the corresponding optimal solutions [82].

The field of structural design presents abundant opportunities for optimization in addressing diverse engineering problems. This thesis specifically concentrates on the domain of topology optimization for structures composed of orthotropic EWPs. The subsequent sections aim to delve into a comprehensive exploration of the historical context and the latest advancements in the field of structural topology optimization, offering valuable insights perspectives.

2.2.2 Topology optimization

TO is a valuable tool in engineering that aims to optimize the placement of material within a defined design domain to achieve optimal structural performance. Based on the classification presented by Sigmund and Maute [98], TO methods have evolved based on different concepts: density [99–101], level-set [102–104], topological derivative [105], evolutionary [106], and others.

In the field of TO, it is essential to recognize that there is no inherently "right" or "wrong" method. Each approach has its strengths, limitations, and specific application domains. The choice of TO method depends on various factors, including the problem at hand, available computational resources, design objectives, constraints, and material characteristics. Furthermore, considering the extensive experience of the advisor of this doctoral thesis [94, 107–111], and the fact that evolutionary methods are commonly used in multiphysics problems, the evolutionary method has been selected as the approach to be used in this doctoral thesis. Although this thesis does not specifically address multiphysics problems, future works will aim to expand the research into the field of multiphysics TO, with a particular focus on solving complex problems involving fluid-structure interaction and integrating additional physical phenomena.

2.2.3 Introduction to evolutionary optimization methods - ESO/BESO

In their work, Xie and Steven [106] in 1993 proposed the evolutionary method called Evolutionary Structural Optimization (ESO), which was further elaborated in Xie and Steven [112] in 1997. The initial procedure involved the gradual removal of less efficient material from the structure, utilizing finite element analysis. The fundamental concept is to conduct finite element analysis within the complete domain, known as the design domain, where the structure can exist. By evaluating the efficiency of each element based on the chosen objective function, the less efficient elements are progressively eliminated.

Through the continued development and refinement of the evolutionary method, significant progress has been made in addressing the initial limitations, particularly concerning convergence and process stability. As a result, the method has become highly versatile, capable of being applied to a wide range of optimization criteria. This evolution has enabled its successful adaptation across various fields, showcasing its effectiveness and adaptability in diverse applications [112–115].

The Bi-directional Evolutionary Structural Optimization (BESO) method, introduced by Querin, Steven, and Xie [115] in 1998 and Querin et al. [116] in 2000, extends the ESO approach by allowing the addition and removal of elements during the optimization process. This flexibility enables previously removed elements to be reintroduced in future iterations, enhancing the adaptability of the method. Furthermore, BESO incorporates the concept of adding new elements adjacent to regions with high stresses, enabling stiffness optimization based on the strain energy criterion, through the estimation of strain energy in void elements using displacement field extrapolation [84, 117].

The BESO method, initially introduced with some deficiencies, has undergone numerous algorithm modifications to enhance its robustness and efficiency. Significant advancements were made to render the method independent of mesh refinement, as demonstrated in the work of Huang and Xie [118]. Developments in the BESO method have shown stable convergence to optimal solutions with high computational efficiency. These solutions, obtained through BESO methods, align well with those obtained using the Solid Isotropic Material with Penalisation (SIMP) and continuation methods for stiffness optimization problems. Furthermore, the BESO method exhibits easy extension to accommodate other constraints, such as displacement [119]. Numerical experiments reveal that the so-called "non-optimal" solution identified by Zhou and Rozvany [120] in hard-kill optimization methods like ESO/BESO is actually a local optimum, which can also occur in various optimization methods. The occurrence of this local optimum is attributed to the artificial material penalty rather than the hard-killing of elements [119]. Dismissing the merit of ESO/BESO methods based solely on the Zhou and Rozvany [120] example is unjustified. Huang and Xie [119] Aims to showcase the effectiveness of the current BESO method and address critical comments raised by Rozvany [121] on the original ESO-type methods. While cautious removal of elements from the design domain is advisable, it is recommended to first develop a soft-kill BESO method for new topology optimization problems before considering the potential for hard-killing elements [119].

In recent years, the BESO methods have been investigated in the literature for their development and application in various engineering areas. Some of the relevant works to this doctoral thesis are cited as follows: Lin et al. [122] introduces an enhanced version of the BESO method called DER-BESO for structural topology optimization. The paper describes the implementation of DER-BESO using ANSYS APDL, including modules for finite element modeling, element sensitivity calculation, Lagrangian multiplier updating, and BESO elements updating with a dynamic evolution ratio strategy. Pereira, Lopes, and Pavanello [123] presents a multi-constrained BESO method applied to two different acoustic systems. The first system focuses on optimizing rigid-acoustic metasurfaces to reduce sound pressure levels while respecting constraints. The second system aims to optimize a coupled poro-acoustic absorptive system by maximizing the sound absorption coefficient of the porous material, employing virtual temperature method as a connectivity constraint. Gan and Wang [124] extends the mathematical framework for topology optimization, considering dynamic eigenfrequencies and static compliance in continuum structures with multiple materials. The method utilizes the advantages of the BESO method to obtain discrete topologies with clear boundaries and high convergence efficiency. Tian et al. [125] applies the BESO algorithm to topology optimization of jack-up platform leg structures. The optimization method is implemented on a case platform, resulting in a new leg structure with improved performance compared to traditional structures. Ching and Carstensen [16] proposes a technique for topology optimization of truss structures using two materials, considering objectives and constraints, including embodied carbon. The framework allows for automatic generation of topology-optimized truss designs that incorporate elements of two different materials, such as timber and steel. The framework determines both the material composition and cross-sectional area of all truss members using a ground structure approach.

It is important to note that the cited works represent a small subset of the extensive research conducted on BESO methods in the past five years. There are numerous other published works that explore and advance the BESO methodology in various engineering disciplines. These works contribute to the ongoing development and application of BESO methods, further expanding their capabilities and effectiveness in solving complex optimization problems.

As previously mentioned, wood is widely recognized as an orthotropic material, exhibiting distinct principal directions of strength. Despite its fundamental importance, the topic of structural orientation in anisotropic and orthotropic materials has received relatively limited

attention within the existing literature. Comprehensive investigations and thorough analyses in this domain are scarce, creating a notable research gap that demands further exploration. The consideration of anisotropic materials and their orientations during concurrent topology optimization is rare when compared with the isotropic structures, despite the potential benefits in improving structural performance, particularly in fiber-reinforced composites and hierarchical structures.

Bruyneel and Fleury [126] mixed monotonous/non-monotonous approximation belonging to the method of moving asymptotes and exhibited favorable convergence properties when optimizing laminates that consider both ply thickness and fiber orientations. These convex approximation schemes, combined with mathematical programming techniques, offer an effective approach for solving problems involving anisotropic materials. Similarly, Tong, Ge, and Zhang [127] proposed a design method that simultaneously optimizes fiber orientation and topology structures in compliant mechanisms.

Stegmann and Lund [128] introduces discrete material optimization as a gradient-based technique for maximizing structural stiffness by optimizing material choice and orientation. The method operates on a fixed domain and aims to select the material from a set of candidates that minimizes the objective for each element.

Gao and Ma [129] introduces a novel concurrent TO model that incorporates orientation variables for materials with microstructures. The model is tested by solving a compliance minimization problem under a volume constraint. To overcome local solutions and improve designs, an orientation adjustment strategy is developed using element strain energy values.

In 2019, the authors Yan et al. [130] introduced a concurrent multiscale topology design method with material orientation optimization, based on the BESO method. This method aims to achieve optimal designs for macrostructures, material microstructures, and material orientation distribution simultaneously. The authors proposed an analytical approach for determining material orientation, accommodating both "weak" and "strong" shear materials. The study showcased the profound interaction between structural and material designs. The concurrent optimization of macrostructures, material microstructures, and material orientation yields a substantial enhancement in structural performance.

The incorporation of material orientation into the design process results in an anisotropic material characterized by orthogonality and weak shear properties. This underscores the crit-

ical significance of considering material orientation in structures composed of anisotropic materials.

Later in 2020, Yan et al. [131] proposes a novel concurrent optimization method is introduced to maximize the natural frequency by considering macrostructures, material microstructures, and local material orientation. The BESO method is utilized for TO of macrostructures and material microstructures with a total weight constraint. Additionally, an analytical approach is developed to efficiently determine the optimal material orientation, which is then integrated into the two-scale topology optimization process.

Within the presented context, the current work aims to establish a significant contribution to the literature by narrowing the connection between two broad areas of knowledge: EWPs and topology optimization. This study not only seeks to fill a gap in existing knowledge, but also aims to pave new paths for the exploration of perspectives and strategies. By exploring the interconnections between the underlying principles of EWP and topological optimization, the research strives to advance not only the theoretical understanding of these domains, but also to provide practical insights for tackling complex real-world challenges.

Chapter 3

Framework Development for EWP-Based BESO Topology Optimization

In this doctoral thesis, the focus is solely on wood structures, more specifically, EWP structures, which can be accurately characterized by employing the differential equation of motion for a continuous body. To effectively model the structural behavior, certain assumptions are made regarding the structural domain. These assumptions include considering small deformations, as well as assuming the material to possess properties of homogeneity and orthotropy. By utilizing these assumptions, the analysis aligns with the principles of linear elasticity theory, ensuring a comprehensive understanding of the system's response.

As will be seen in this chapter, the procedure for the TO requires that the analysis/solution of the system be performed numerous times during the evolution of the topology. Therefore, the modeling of the system becomes crucial for the efficiency of the optimization procedure, since the system's solution represents the highest computational cost within the process. Given this, it was chosen to use the Ansys software to iteratively solve the finite element model. Therefore, the formulation of the finite element method will not be presented in this doctoral thesis.

While this thesis does not comprehensively present the finite element method's formulation, it is important to acknowledge the vital roles played by the stiffness matrix and the mass matrix within the context of the TO method. In light of the material's orthotropic character-

istics, Equation 3.1 defines the stiffness matrix. For an in-depth understanding of the finite element method, further information is available in [132].

$$\mathbf{K} = \int_{\Omega} (\mathbf{B})^T \, \mathbf{D} \, \mathbf{B} \, dV \tag{3.1}$$

where Ω is the structural domain; $\mathbf{B}$ is the strain-displacement matrix that is based on the element shape functions; $\mathbf{D}$ is the orthotropic elasticity matrix defined in Equation 3.2.

$$\mathbf{D} = \begin{bmatrix} E_L & -E_L/\nu_{LR} & -E_L/\nu_{LT} & 0 & 0 & 0 \\ -E_R/\nu_{RL} & E_R & -E_R/\nu_{RT} & 0 & 0 & 0 \\ -E_T/\nu_{TL} & -E_T/\nu_{TR} & E_T & 0 & 0 & 0 \\ 0 & 0 & 0 & G_{LR} & 0 & 0 \\ 0 & 0 & 0 & 0 & G_{RT} & 0 \\ 0 & 0 & 0 & 0 & 0 & G_{LT} \end{bmatrix} \tag{3.2}$$

where E_L, E_R, E_T are Young's moduli in the longitudinal, radial and tangencial directions, respectively. ν_{LR} major Poisson rate in LR plane; ν_{LT} major Poisson rate in LT plane; ν_{RT} major Poisson rate in RT plane. The directions and planes that were used in this work in relation to the wood fibers are detailed in Figure 3.1.

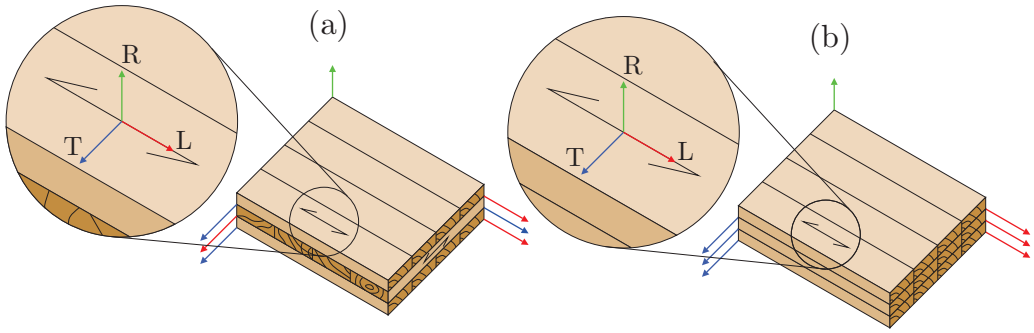

Figure 3.1: (**a**) Representation of the physical model of the CLT with an indication of the fiber and Radial, Tangential and Longitudinal directions. (**b**) Representation of the physical model of the GLULAM with an indication of the fiber and Radial, Tangential and Longitudinal directions.

To solve the TO problem, this work follows the approach proposed in the literature [84, 112–114, 133], and therefore, the following steps should be followed:

1. Discretize the design domain of the structure using a fine mesh of finite elements.
2. Define the parameters for the BESO method.
3. Analyze and solve the structure using finite elements under the imposed loadings.
4. Calculate the sensitivity number for each element according to the adopted criterion.
5. Filter the senstivity number
6. Remove the elements with the lowest sensitivity number.
7. Repeat steps 3 to 5 until the adopted stopping criterion is satisfied.

The next sections are dedicated to the solution of the BESO method for topology optimization in terms of Compliance and Displacement. The complete calculation sequence and the strategy involving the MATLAB and Ansys software will be discussed.

3.1 Compliance as an objective function

Compliance is a widely used objective function in classical optimization criteria. It is commonly defined as the inverse of stiffness, meaning that minimizing the inverse of stiffness leads to maximizing the overall stiffness of the system. In the classical compliance problem, the optimization is typically (presented in Equation 3.3) subject to constraints such as volume limitations within the working domain and the need to satisfy the equation of static equilibrium for the given structure.

$$\begin{aligned} \min_{\mathbf{x}} \quad & C = \frac{1}{2}\mathbf{F}^T\mathbf{U} \\ \text{s.t.} \quad & \mathbf{KU} = \mathbf{F} \\ & V^* - \sum_{i=1}^{nel} V_i x_i = 0, \\ & x_i \in (10^{-4}, 1) \end{aligned} \tag{3.3}$$

where C is the mean compliance of the structure. $\mathbf{F}$ and $\mathbf{U}$ represent the values of external forces and displacements in the structure domain, respectively. The equation $\mathbf{KU} = \mathbf{F}$ represents the equilibrium equation of the system. V^* denotes the prescribed volume fraction. The design domain consists of a total of *nel* structural elements, with individual elements having

volumes of V_i, and x_i representing the value of the design variable. These parameters will be presented throughout this chapter.

3.1.1 Sensitivity number calculation for compliance as an objective function

This section specifically addresses step 4 of the sequence denoted in chapter 3: "Calculate the sensitivity number for each element according to the adopted criterion". The sensitivity of the structural response due to an element change during the TO method is obtained by deriving the objective function of the design variables ($\partial C/\partial x_i$). This term can be obtained by first differentiating the equilibrium equation (Eq. 3.4):

$$\frac{\partial(\mathbf{KU})}{\partial x_i} = \frac{\partial \mathbf{F}}{\partial x_i} \tag{3.4}$$

following the chain rule equation and considering that the external forces do not change during the optimization process, therefore $\partial F/\partial x_i = 0$, it is obtained that:

$$\frac{\partial \mathbf{K}}{\partial x_i}\mathbf{U} + \frac{\partial \mathbf{U}}{\partial x_i}\mathbf{K} = 0 \tag{3.5}$$

now in Equation 3.6 we isolate the term $\partial U/\partial x_i$ from Equation 3.5:

$$\frac{\partial \mathbf{U}}{\partial x_i} = -\mathbf{K}^{-1}\frac{\partial \mathbf{K}}{\partial x_i}\mathbf{U} \tag{3.6}$$

when deriving the objective function in Equation 3.3 with respect to the design variables, the expression can be written as follows:

$$\frac{\partial \mathbf{C}}{\partial x_i} = \frac{1}{2}\frac{\partial\left(\mathbf{F}^T\mathbf{U}\right)}{\partial x_i} = \frac{1}{2}\frac{\partial\left(\mathbf{U}^T\mathbf{K}\mathbf{U}\right)}{\partial x_i} = \mathbf{U}^T\mathbf{K}\frac{\mathbf{U}}{\partial x_i} + \frac{1}{2}\mathbf{U}^T\frac{\mathbf{K}}{\partial x_i}\mathbf{U} \tag{3.7}$$

Finally, appling the Equation 3.6 in Equation 3.7, it is possible to express the sensitivity number for the topology optimization problem with respect to the compliance criterion as follows:

$$\frac{\partial \mathbf{C}}{\partial x_i} = -\mathbf{U}\mathbf{K}\mathbf{K}^{-1}\frac{\partial \mathbf{K}}{\partial x_i}\mathbf{U} + \frac{1}{2}\mathbf{U}^T\frac{\mathbf{K}}{\partial x_i}\mathbf{U} = -\frac{1}{2}\mathbf{U}^T\frac{\mathbf{K}}{\partial x_i}\mathbf{U} \tag{3.8}$$

This sequence is commonly presented in the literature, but in the majority of cases, the stiffness matrix is developed with respect to an isotropic material. However, this difference will be addressed in future sections.

3.2 Compliance as an objective function considering two solid materials

The compliance problem presented in the previous section is commonly applied and has two phases, a solid phase and a void phase. An adaptation of this method is to use two solid phases. This case still involves the same objective function of minimizing compliance, but with the addition of equations in the constraints, as presented in Equation 3.9.

$$\begin{aligned} \min_{\mathbf{x}} \quad & C = \frac{1}{2}\mathbf{FU} \\ \text{s.t.} \quad & \mathbf{KU} = \mathbf{F} \\ & V_1^* - \sum_{i=1}^{nel} V_{i1} x_i = 0, \\ & V_2^* - \sum_{i=1}^{nel} V_{i2} x_i = 0, \\ & V_1^* + V_2^* = 1 \\ & x_{ij} \in (10^{-4}, 1)\,(j = 1 \; or \; 2) \end{aligned} \tag{3.9}$$

where **U** is the displacement matrix, and **K** is the stiffness matrix; **F** is external forces applied in the structure domain. Expression $\mathbf{KU} = \mathbf{F}$ stands for the equilibrium equation of the system. **N** stands for the number of elements in design-domain, V_1^* is the fraction of the prescribed volume for the steel beam and V_2^* is the fraction of volume for the wood. x_{ij} stands for element pseudo-density of ith element for jth material ($j = 1$ for steel and $j = 2$ for wood). Given that if $j = 1$, then $x_{ij} = 1$, and if $j = 2$, $x_{ij} = 10^{-4}$.

The calculation of the sensitivity number for this particular case of TO follows the same presented in the previous section. The main difference is treated in section 3.4 entitled "Material Interpolation Scheme".

3.3 Displacement as an objective function

The optimization of the structural response is also widely used in the literature and can be described as the optimal distribution of material to minimize displacement at a given point or region.

$$\begin{aligned} \min_{\mathbf{x}} \quad & \mathbf{U}^k \\ \text{s.t.} \quad & \mathbf{KU} = \mathbf{F} \\ & V^* - \sum_{i=1}^{nel} V_i x_i = 0, \\ & x_i \in (10^{-4}, 1) \end{aligned} \tag{3.10}$$

where $\mathbf{U}^k$ is the displacement of the degree or degrees of freedom of interest. $\mathbf{F}$ and $\mathbf{U}$ are vectors of external forces and displacements in the structure domain, respectively. $\mathbf{KU} = \mathbf{F}$, stands for the equilibrium equation of the system. V^* is the fraction of the prescribed volume. The design domain includes a total of *nel* structural elements, with individual elements possessing volumes of V_i, and x_i is the value of the design variable.

3.3.1 Sensitivity analysis

The sensitivity of the structural response due to an element change is obtained by deriving the objective function of the design variables ($\partial \mathbf{U}/\partial x_i$). This term can be obtained by differentiating the equilibrium equation (Eq. 3.11):

$$\frac{\partial(\mathbf{KU})}{\partial x} = \frac{\partial \mathbf{F}}{\partial x} \tag{3.11}$$

considering that the external forces do not change during the optimization process, therefore $\partial \mathbf{F}/\partial x_i = 0$, it is obtained that:

$$\frac{\partial \mathbf{K}}{\partial x}\mathbf{U} + \frac{\partial \mathbf{U}}{\partial x}\mathbf{K} = 0 \tag{3.12}$$

isolating $\partial \mathbf{U}/\partial x_i$:

$$\frac{\partial \mathbf{U}}{\partial x_i} = -\mathbf{K}^{-1}\frac{\partial \mathbf{K}}{\partial x_i}\mathbf{U} \tag{3.13}$$

A possible approach to determine the response of the structure according to the variation in the design variable ($\partial \mathbf{U}/\partial x_i$), is apply a unit load vector to the degree (or degrees) of freedom of

interest, **Q** [94, 114].

$$\frac{\partial \mathbf{U}^P}{\partial x_i} = \mathbf{Q}^T \frac{\partial \mathbf{U}}{\partial x_i} \tag{3.14}$$

where the displacement $\mathbf{U}^P$ refers to the response of the structure to the load **Q** on the node of interest. Thus, it is possible to write the equilibrium equation of the system under load **Q** (Eq. 3.15) as:

$$\mathbf{K}\mathbf{U}_Q = \mathbf{Q} \tag{3.15}$$

where the vector $\mathbf{U}_Q$ is the response of the structure under load **Q**. It is possible to isolate the variable $\mathbf{U}_Q$ (Eq. 3.16), as:

$$\mathbf{U}_Q = \mathbf{K}^{-1}\mathbf{Q} \tag{3.16}$$

Therefore, it is possible to substitute Equation 3.16 into Equation 3.13 to obtain the elemental sensitivity of the system, α_i, as:

$$\frac{\partial \mathbf{U}}{\partial x_i} = -\mathbf{U}_{Qi}^T \frac{\partial \mathbf{K}}{\partial x_i}\mathbf{U}_i \tag{3.17}$$

3.4 Material interpolation scheme

To avoid theoretical problems during the topological optimization process, the material interpolation scheme, presented in Equation 3.18, used in this work is the same one commonly used in the topological optimization method SIMP, applied to an orthotropic nature problem. In this case, when an element is defined as empty, its modulus of elasticity is decreased [82].

$$\mathbf{E}(x_i) = \begin{Bmatrix} E_L \\ E_R \\ E_T \end{Bmatrix} (x_i)^p \; ; \; \mathbf{G}(x_i) = \begin{Bmatrix} G_{LR} \\ G_{RT} \\ G_{LT} \end{Bmatrix} (x_i)^p \tag{3.18}$$

where **E** is the Young's modulus vector and **G** is the shear modulus vector, both comprehending the orthotropic nature of the problem. p is the penalty factor.

Therefore, by applying the interpolation scheme to Equation 3.8, the sensitivity number for the compliance minimization problem is given by:

$$\frac{\partial \mathbf{C}}{\partial x_i} = -\frac{1}{2} p \mathbf{U}_i x_i^{p-1} K_i \mathbf{U}_i \tag{3.19}$$

and in Equation 3.17 for the displacement minimization problem, it is given by:

$$\frac{\partial \mathbf{U}^k}{\partial x_i} = -\frac{1}{2} p \mathbf{U}_{Qi}^T x_i^{p-1} K_i \mathbf{U}_i \tag{3.20}$$

3.4.1 Material interpolation scheme considering two solid materials

In the specific case presented in Section 3.2, it is necessary to add the second modulus of elasticity and therefore a different interpolation than the one presented in Section 3.4. For two solid phases such as steel and wood, the material interpolation can be expressed using the penalty factor p in Equations 3.21 and 3.22:

$$E(x_i) = x_i^p E_{steel} + \left(1 - x_i^p\right) E_{wood} \tag{3.21}$$

$$G(x_i) = x_i^p G_{steel} + \left(1 - x_i^p\right) G_{wood} \tag{3.22}$$

given that E_{steel} e E_{wood} are the values of the modulus of elasticity of steel and wood, respectively; G_{steel} e G_{wood} are the shear modulus vectors of steel and wood, respectively. Once Equations 3.21 and 3.22 are applied to Equation 3.8, the sensitivity number for the problem with two solid phases is given by:

$$\frac{\partial C}{\partial x_{ij}} = -\frac{1}{2} p x_i^{p-1} \left(\mathbf{U}_i^T K_i^{steel} \mathbf{U}_i - \mathbf{U}_i^T K_i^{wood} \mathbf{U}_i\right) \tag{3.23}$$

3.5 Sensitivity filtering

The sensitivity value calculated by Equation 3.19 and Equation 3.20 must be filtered to avoid checkerboard structures patterns and mesh-dependent results [134]. The filter used in this work is similar to that used by Huang and Xie [84] and defined by the Equation 3.24.

$$\overline{\alpha}_i = \frac{\sum_{j=1}^{n} W_j \alpha_j}{\sum_{j=1}^{n} W_j} \tag{3.24}$$

where $\overline{\alpha}_i$ is the filtered sensitivity number, n is the number of elements within the Ψ sub-domain defined by a radius r_{min}, according to Figure 3.2, α_j are the sensitivity numbers referring to the elements belonging to the Ψ sub-domain, and W_j is the weight parameter defined

as (Eq. 3.25).

$$W_j = \begin{cases} r_{min} - r_{ij}, \text{ when } (r_{min} - r_{ij}) > 0 \\ 0, \text{ when } (r_{min} - r_{ij}) \leq 0 \end{cases} \tag{3.25}$$

where r_{ij} is the centroid distance from element i to element j.

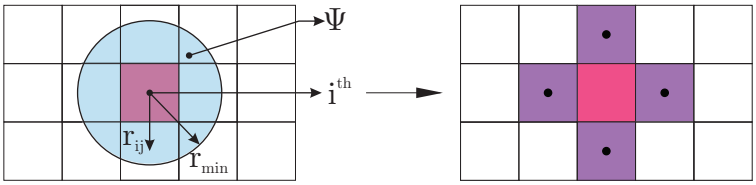

Figure 3.2: Filter radius on a particular finite element mesh and representation of the elements belonging to the sub-domain.

3.6 Sensitivity stabilization

In addition to the problem mentioned in the previous section, it is possible to improve the convergence problems by averaging with the sensitivity values from the exact previous iteration [84, 118], as per (Eq. 3.26):

$$\tilde{\alpha}_i = \frac{(\bar{\alpha}_i^k + \bar{\alpha}_i^{k-1})}{2} \tag{3.26}$$

where k is the value of the current iteration.

3.7 Optimization evolution process

The optimization process of the BESO method used in this doctoral thesis follows that proposed by Huang and Xie [118]. Initially, it is assumed that the CLT layers are completely void-free $V_{initial} = 100\%$, and the topological optimization process will reach the final volume V^* at an ER rate. This parameter indicates the percentage of material removed per iteration. In the BESO method, in addition to ER, the maximum volume changed per iteration is defined as AR. As long as the volume of the iteration does not reach the final volume, elements continue to be removed, and the value of the design variable changed to $x_i = x_{min}$. Once the volume of the current iteration reaches the final volume V^* the optimization continues, but without changing the volume, until the convergence criterion, described in (Eq. 3.27), is reached. Alternatively, it is possible to perform the simulation with constant volume, in other words, instead

of finding the optimal topology, the method redistributes the material within the workspace while maintaining the volume.

$$\frac{\left|\sum_{i=1}^{N} C_{k-i+1} - \sum_{i=1}^{N} C_{k-N+1}\right|}{\sum_{i=1}^{N} C_{k-i+1}} \leq \tau \tag{3.27}$$

In this equation, τ is the convergence error. N states the number of iterations of stable compliance set to 5.

3.8 CLT and GLULAM layers stack-up finite element method modelling

The wood layer stacking characteristic of CLT changes the fiber direction at each layer, while for GLULAM, the layers have the fibers in the same direction. The orthotropic nature of wood indicates that the mechanical properties are different along the three principal axes perpendicular to each other. The axis with the most significant mechanical properties is the longitudinal axis parallel to the direction of the wood fiber. The radial axis is perpendicular to the longitudinal axis and normal to the growth of the wood rings. The tangential axis is perpendicular to the longitudinal and radial axes and tangent to the growth of the wood rings [9]. These axes are highlighted in the physical model present in Figure 3.1.

The finite element model considering the elements of the physical model, was created using the strategy of multiple coordinate systems; for example, the elements present in the first layer have their mechanical properties tied to the coordinate system containing the longitudinal, radial, and tangential direction as Figure 3.1. As in this work, the conventional CLT structure is being evaluated. The layers are rotated by 90°, so the elements in the second layer use a coordinate system rotated by 90° around the radial axis. Successively the elements in the third layer use the same coordinate system as the first. This strategy follows until the number of layers is reached. The glue action is disregarded in this work, and the layers are rigidly joined. Furthermore, all elements used and cited in this work are 3D elements composed of 8 nodes and linear interpolation. Furthermore, for the sake of understanding, in this paper, the layers have been numbered from 1 to the total number of layers in the engineered wood, with one being the bottom layer and the last layer being the top.

3.9 Sub-design domain definition, element change criterion for two solid materials

One of the main objectives of this thesis is the positioning of reinforcement beams in wooden structures. For this, the consideration of two solid materials in the design domain is used. In addition, the sub-design domain was proposed to solve this problem. The position of the steel bars within the wood is determined by discretizing the sub-design domain according to the specific requirements and availability of each problem. In this thesis, for the 2D example, the wood beam was divided into design domains of reinforcement beam sizes Ls and Hs, as shown in Figure 3.3. To optimize the positioning of the steel bars in the sub-design domains, it is necessary to calculate and filter the sensitivity number of each element in the structure in each iteration. Next, the elements belonging to each sub-design domain are identified. This allows for the adjustment of the sensitivity number of each element belonging to the sub-design domain by the average sensitivity number of that domain. In this way, the importance of each sub-design domain can be measured by the average of its constituent elements. The quantity of bars to be used in each iteration must then be defined. Assuming that the design-domain starts completely with steel ($j = 1$ and $x_{ij} = 1$), in each iteration, a value ER is interpreted as the number of bars changed per iteration, which is used to calculate the number of bars in the next iteration. The sub-design domains with lower sensitivity numbers have their elements changed to wood $j = 2$ and $x_{ij} = x_{min}$, obeying the number of bars altered per iteration. The simulation continues until the number of steel bars/number of sub-design domains is reached and until convergence is satisfied.

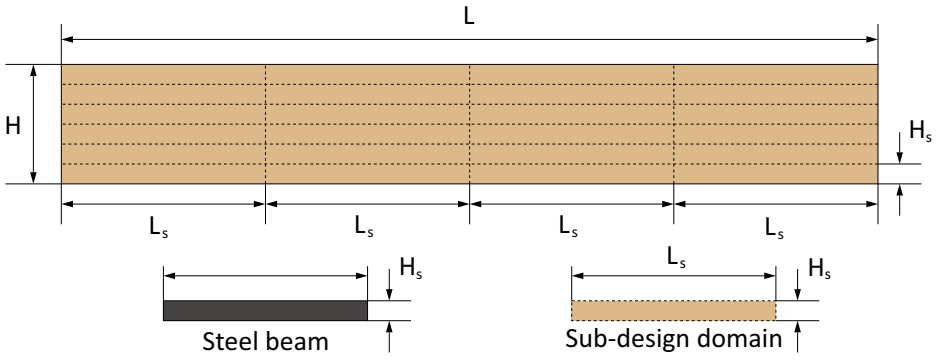

Figure 3.3: An example of the design domain and sub-design domain for 2D case.

Similarly, in 3D cases, the sub-design domain is defined by characterizing the steel bar size to be used, but with an additional dimension, Ws. In this study, steel bars with diameter d were used and positioned as shown in Figure 3.4. As with the 2D case, it is necessary to separate the elements belonging to the sub-design domain and rank the sensitivity number. However, in this case, only the elements belonging to the d diameter bar of the sub-design domain with the highest sensitivity number should be replaced with steel.

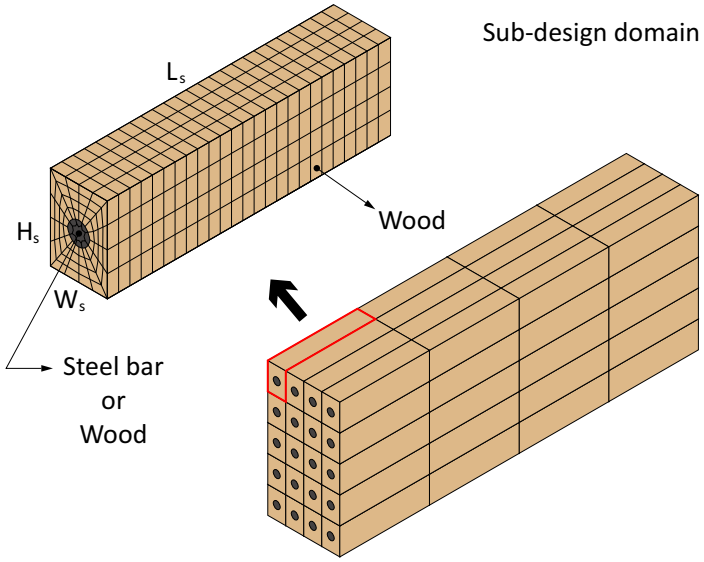

Figure 3.4: An example of the design domain and sub-design domain for 3D case.

3.10 MATLAB - Ansys framework

The selection of the commercial software Ansys for solving the proposed finite element problem in this work is primarily motivated by its extensive capability to modify the parameters of each element, particularly the ability to alter the material assigned to individual elements within the structure. Additionally, Ansys facilitates the export of various response values and model parameters, which further enhances its suitability for the study.

However, there are two main disadvantages associated with using this coupling method to solve the proposed topology optimization problem. Firstly, there is no direct communication between MATLAB and Ansys. Instead, MATLAB generates text commands that are executed by Ansys. Consequently, MATLAB does not have direct access to the results produced by Ansys and a aditional code is needed to read the output files generated by the software. Secondly, although Ansys is highly efficient in solving finite element models, it may be outperformed by simpler solutions for problems with low complexity and a small number of elements.

To provide a clearer illustration of the proposed approach utilizing MATLAB and Ansys, Figure 3.1 illustrates the workflow for each step and the involvement of the respective software components. The optimization process starts in MATLAB, where the optimization parameters of the BESO method (e.g., ER, AR, V_f, etc.) are defined. Subsequently, the model parameters, including dimensions, loadings, and boundary conditions, are specified. With this information, a logical sequence is compiled to generate a file for execution in Ansys APDL. Following by a MATLAB code that initiates the execution of Ansys APDL to create the model. Once the model is generated, the BESO algorithm is executed, and Ansys iteratively solves the model. Upon achieving convergence, the main information is plotted and analyzed.

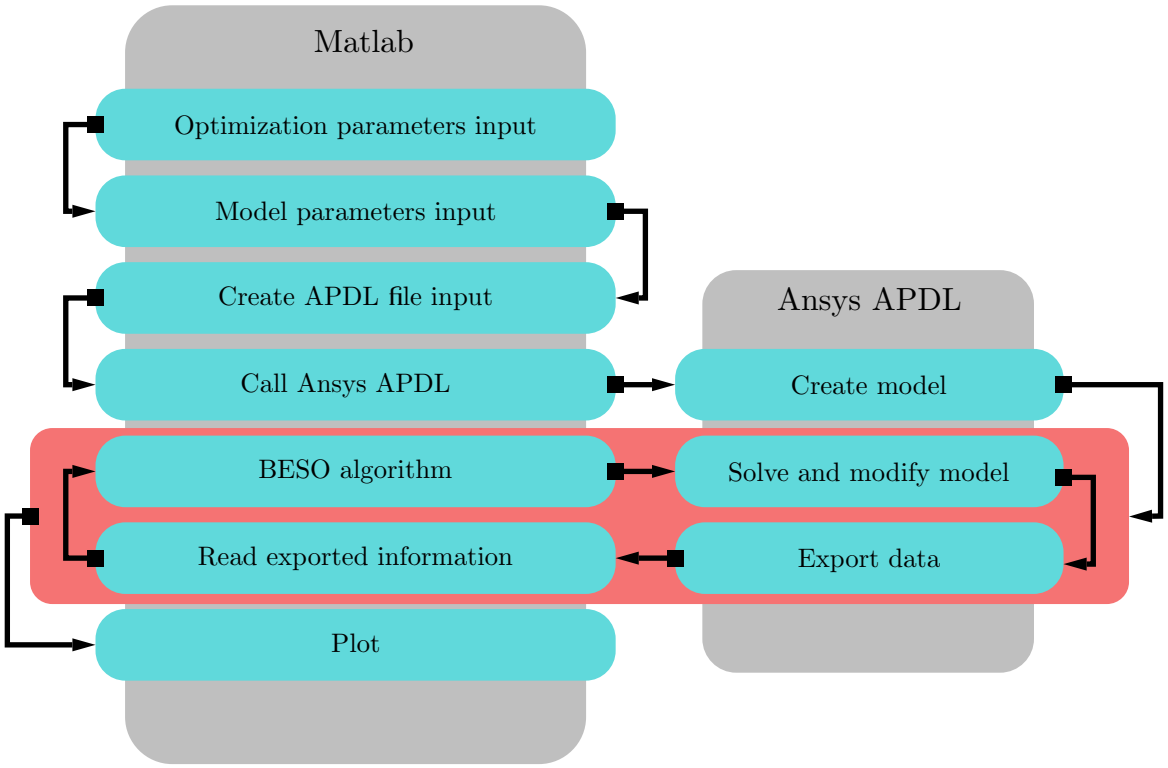

Figure 3.5: Workflow of computational tasks for the proposed methodology

As presented in the previous sections, this thesis primarily addresses two objective functions, one of which is a secondary variation. They are: "BESO Method for Compliance Optimization," "BESO Method for Compliance Optimization Considering Two Solid Materials," and "BESO Method for Displacement Optimization." For each of these cases, the number of sensitivities is calculated differently, as summarized in Table 3.1.

Table 3.1: Summary of sensitivity numbers

Type	Equation
Compliance Optimization - 1 Material	$\frac{\partial \mathbf{C}}{\partial x_i} = -\frac{1}{2} p \mathbf{U}_i x_i^{p-1} K_i \mathbf{U}_i$
Compliance Optimization - 2 Materials	$\frac{\partial C}{\partial x_{ij}} = -\frac{1}{2} p x_i^{p-1} \left(\mathbf{U}_\mathbf{i}^\mathrm{T} K_i^{\mathbf{steel}} \mathbf{U}_\mathbf{i} - \mathbf{U}_\mathbf{i}^\mathrm{T} K_i^{wood} \mathbf{U}_\mathbf{i} \right)$
Displacement Optimization	$\frac{\partial \mathbf{U}^k}{\partial x_i} = -\frac{1}{2} p \mathbf{U}_{Qi}^T x_i^{p-1} K_i \mathbf{U}_i$

The strategy used to calculate each of the sensitivity numbers is presented below. By solving the finite element method in ANSYS, it is possible to extract the value of deformation energy for each element ($SENE_i$) as follows:

$$SENE_i = \mathbf{U}_i^T K_i \mathbf{U}_i \tag{3.28}$$

therefore, in the case of compliance optimization using one material, the sensitivity value is directly extracted from the ANSYS software's response and imported into Matlab for further processing in the method. However, for compliance optimization with two materials, it is necessary to export the displacement vector of all nodes and the K_i matrix of each element. With these data in Matlab, the sensitivity number is calculated.

Finally, for displacement optimization, it is necessary to apply a unit load to the degree or degrees of freedom of interest, as described in Section 3.3.1. Therefore, it is possible to export two deformation energies: one from the finite element problem with original boundary conditions and load (as shown in Equation 3.28), and the other from the finite element problem with actual boundary conditions and a unit load Q applied to the degree or degrees of freedom of interest. These energies are given by:

$$SENE_{Qi} = \mathbf{U}_{Qi}^T K_i \mathbf{U}_{Qi} \tag{3.29}$$

To utilize the deformation energy for calculating the sensitivity number exported from ANSYS, a third finite element problem is required. This third problem encompasses exactly the same boundary conditions and loads as the original problem, along with a unit load Q. Therefore, considering a material with linear properties, the displacement of the third problem

can be expressed as follows:

$$\mathbf{W}_i = \mathbf{U}_{Qi}^T + \mathbf{U}_i \tag{3.30}$$

therefore, it is possible to express the deformation energy of the third finite element problem as follows:

$$SENE_{Wi} = (\mathbf{U}_{Qi} + \mathbf{U}_i)^T K_i (\mathbf{U}_{Qi} + \mathbf{U}_i) \tag{3.31}$$

applying the product rule to Equation 3.31, this results in:

$$SENE_{Wi} = \mathbf{U}_i^T K_i \mathbf{U}_i + \mathbf{U}_{Qi}^T K_i \mathbf{U}_{Qi} + \mathbf{U}_{Qi}^T K_i \mathbf{U}_i + \mathbf{U}_i^T K_i \mathbf{U}_{Qi} \tag{3.32}$$

rewriting Equation 3.32 using Equations 3.28 and 3.29, results in:

$$SENE_{Wi} = SENE_i + SENE_{Qi} + 2\mathbf{U}_{Qi}^T K_i \mathbf{U}_i \tag{3.33}$$

isolating the term $\mathbf{U}_{Qi}^T K_i \mathbf{U}_i$ from Equation 3.33, it is possible to express the main term of the sensitivity number in terms of deformation energies:

$$\mathbf{U}_{Qi}^T K_i \mathbf{U}_i = \frac{SENE_{Wi} - SENE_i - SENE_{Qi}}{2} \tag{3.34}$$

3.11 Numerical example

A numerical verification is carried out in this section, specifically the comparison between topology optimization using an classic isotropic material and an orthotropic material. More numerical examples are presented in Appendix A.

In this numerical example, the optimized topology of a simply supported beam with dimensions of 160 mm x 80 mm is compared under three different conditions: first, using an isotropic material; then, an orthotropic material; and finally, an orthotropic material with a 90-degree rotation. The material properties used in this example are presented in Table 3.2, where E_L stands for the Young's modulus in the longitudinal direction, E_R for the radial direction, and E_T for the tangential direction, as shown in Figure 3.1. This comparison allows for an assessment of the influence of material orthotropy on the optimized topology.

Table 3.2: Isotropics and orthotropics mechanical properties for numerical example 1.

Material Type	Parameters		
Isotropic	$E = 13400$ MPa		
	$\nu = 0.292$		
Orthotropic	E_L (MPa)	E_R (MPa)	E_T (MPa)
	13400.0	911.2	670.0
	G_{LR} (MPa)	G_{LT} (MPa)	G_{RT} (MPa)
	857.6	1045.2	93.8
	ν_{LR}	ν_{LT}	ν_{RT}
	0.292	0.449	0.39

The beam is simply supported on the left side and was discretized with 320 elements in the horizontal direction and 160 elements in the vertical direction. A concentrated force is applied at the center of the height on the right side. The filter radius is 6 mm. The objective of this optimization is the compliance subjected to a final volume of 50% ($V_f = 50\%$), the ER and AR values are both set to 1%. The schematics of the beam are shown in Figure 3.6.

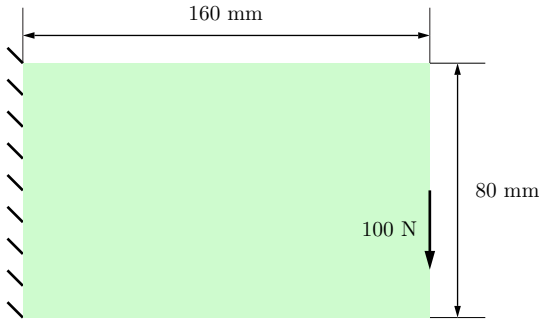

Figure 3.6: Dimensions and boundary conditions of a simply supported beam subjected to a concentrated load.

The topologies corresponding to the initial, intermediate, and final conditions of the three evaluated cases are presented in Figure 3.7. In the figure, the first column represents the classical optimization of the beam using isotropic material, as previously mentioned. In the middle and right columns, orthotropic materials are considered, with specified directions. The pri-

mary distinction between the second and third columns lies in the orientation of the elastic moduli E_L and E_R.

Regarding the clamped beam with isotropic material, the obtained result aligns with the classical response documented in the literature. However, since all three cases share the same boundary and optimization conditions, the cases displayed in the middle and right columns of Figure 3.7 highlight the significance and dependence on the utilization of orthotropic material.

The colors assigned to each topology in Figure 3.7 correspond to the values of the sensitivity number calculated using Equation 3.19 and filtered through the method described in Section 3.5. In both the isotropic material and the orthotropic material in the middle column, the sensitivity number distribution exhibits similarities, concentrated primarily in the force application and clamped regions. However, the sensitivity number distribution of the third evaluated case demonstrates notable differences, particularly in terms of the amount of crucial material identified. This discrepancy underscores the importance of considering the orthotropic material's influence on the optimization process.

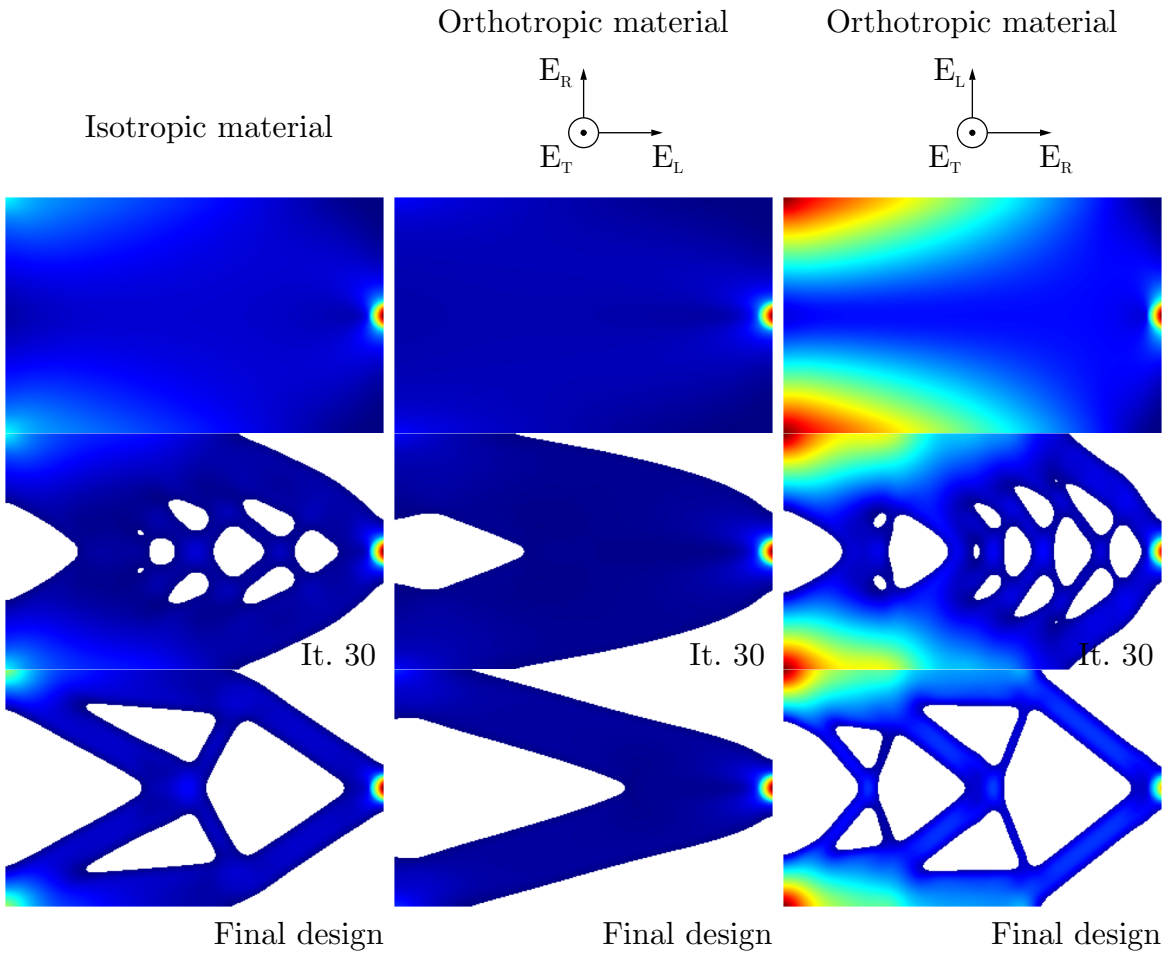

Figure 3.7: Three instants of the three evaluated conditions are shown. In the first column, three instants of the optimized topology considering the isotropic material are presented. In the middle and right columns, three instants of the optimized topology considering the orthotropic material are shown, with the main direction indicated.

Chapter 4

Topology Optimization Applied to the Core of Structural Engineered Wood Product

Within this chapter, the approach of topology optimization takes center stage, building upon the foundations laid in earlier chapters. The primary objective remains unchanged: Apply topology optimization techniques to EWP, particularly CLT and GLULAM, with the aim of optimizing material distribution. This optimization will facilitate the enhancement of structural efficiency and the reduction of the total construction mass while ensuring the integrity and satisfactory performance of the structure.

Acknowledging the inherent complexities of wood as a construction material, including its anisotropic characteristics and the distinctive layering prevalent in GLULAM and CLT, the proposed optimization method incorporates orthotropic material considerations and systematically addresses periodicity constraints. This chapter offers a practical demonstration of the potential of this approach through two illustrative numerical examples. The first example scrutinizes the core optimization of a GLULAM structure, offering a comparative analysis of results with and without periodicity constraints. Subsequently, the focus shifts to the core of a CLT structure, emphasizing the advantageous role of periodicity constraints in this specific context.

The findings presented within this chapter serve to underscore the potential of topology optimization, laying a strong foundation for a more sustainable and efficient future for engineered wood products. By peeling back the layers—both figuratively and literally—this chapter

provides essential insights into the intricate design and manufacturing aspects of engineered wood structures. Furthermore, it positions itself as a catalyst for further inquiry and future research avenues in this dynamic field.

Additionally, it's worth noting that this chapter and parts of previous chapters have been published in [17].

4.1 Topology optimization techniques to EWP

In this section two different numerical examples of the application of the method is presented. In all examples the mechanical properties as given in Table 4.1 taken from [9] is adopted.

Table 4.1: Assumed mechanical properties.

Wood species	Parameters		
Douglas fir	E_L (MPa)	E_R (MPa)	E_T (MPa)
	13400.0	911.2	670.0
	G_{LR} (MPa)	G_{LT} (MPa)	G_{RT} (MPa)
	857.6	1045.2	93.8
	ν_{LR}	ν_{LT}	ν_{RT}
	0.292	0.449	0.39

4.1.1 Numerical example 1 - 3D GLULAM

The GLULAM beam's simulated model is subjected to the three-point bending test with a 1,000 N load. In the model, the design domain is the GLULAM core wrapped by the outer layers, which are the non-design domain. As presented in the previous section, the objective function of this work is the displacement, which in this example was selected precisely at the center of the upper layer. Thus, the objective is to find the optimal topology for the chosen objective function considering the final volume as 50% of the working volume. The parameters for optimization with the BESO method are: $ER = 4\%$, $AR = 4\%$, $r_{min} = 18$ mm, $\tau = 0.001$, $N = 5$ and $p = 3$.

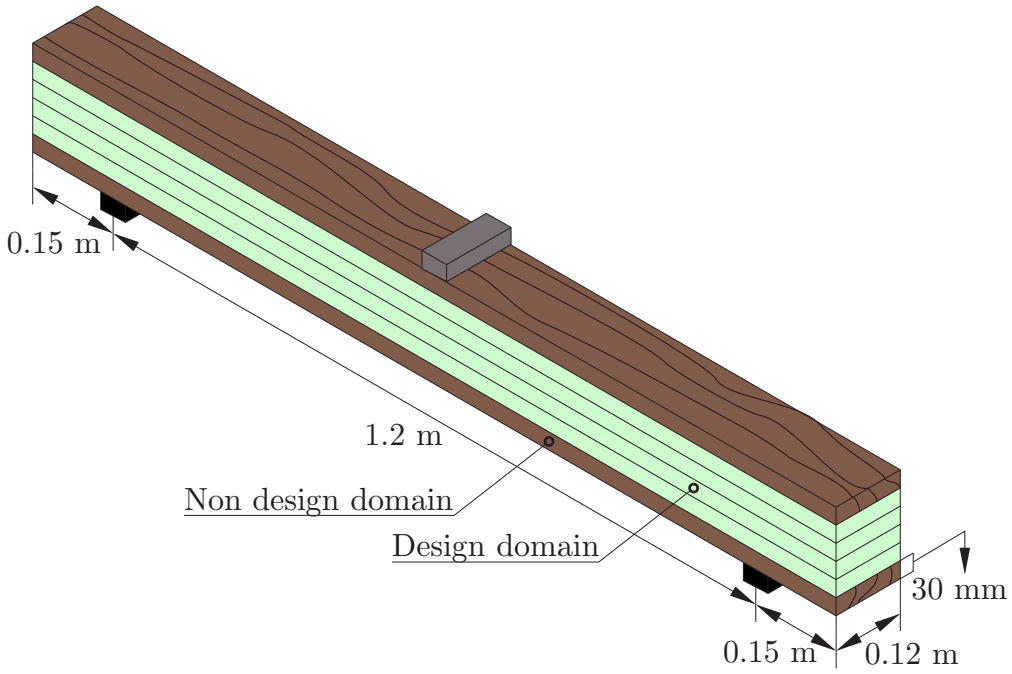

Figure 4.1: Schematic representation of numerical example 1: six-layer GLULAM with dimensions 1.5 m x 0.12 m x 0.18 m, bi-supported, and 1000 N force applied at the center. The core with four layers of the GLULAM was selected as the design domain, surrounded by two layers of the non-design domain.

Figure 4.2 shows the simulated GLULAM's initial, intermediate, and final topology. The color map represents the filtered sensitivity number presented in Equations 3.20 and 3.24, with warm colors being elements with higher sensitivity numbers and cool colors being lower values. The higher the sensitivity number, the greater the element's importance to the objective function. Therefore it is possible to evaluate that the materials positioned at the ends of the beam are less influential to the elements close to the support and application of force.

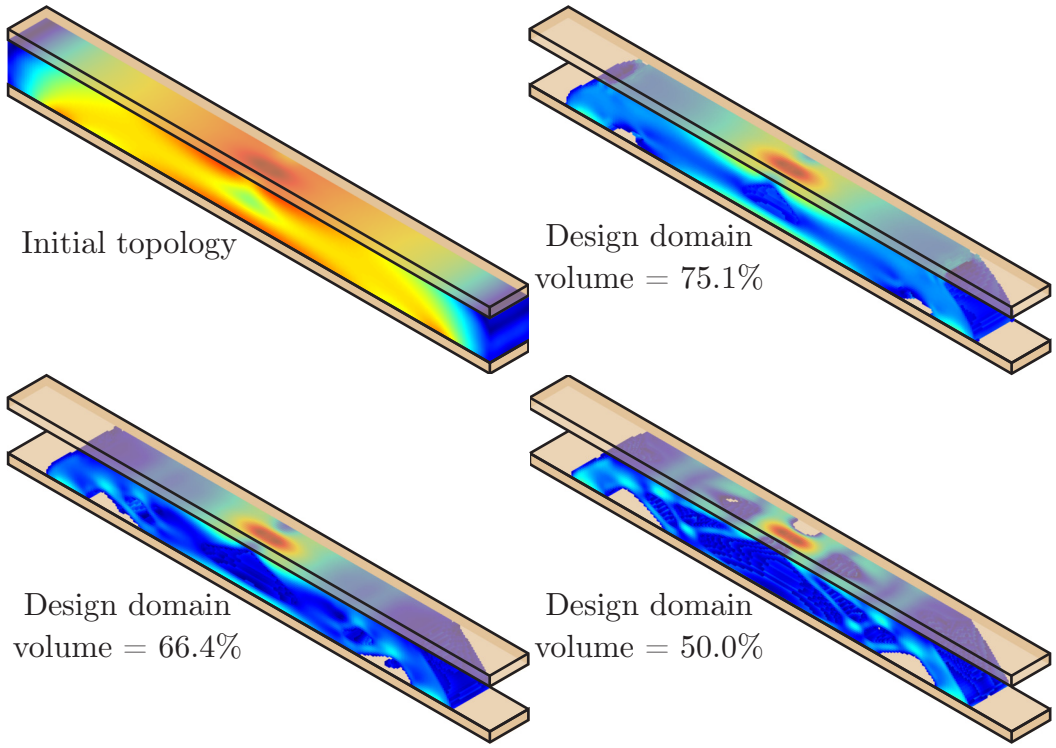

Figure 4.2: Evolution of topologies for optimization of the six-layer GLULAM core at four instants: Initial Topology, Design domain volume = 75.1%, Design domain volume = 66.4%, Design domain volume = 50.0%. The color map indicates the value of the filtered sensitivity number, as per Equations 3.20 and 3.24.

The evolution of displacement, design domain volume, and iterations are presented in Figure 4.3. As presented in the graph, removing material increases the displacement of the selected point in the structure. Furthermore, it can be seen that all material removed up to iteration 5 changes the displacement less than material removed after iteration 5. This phenomenon is explained by the low sensitivity number relative to the rest of the structure.

The initial GLULAM core shown in Figure 4.3 at iteration 0 is considerably more practical to construct than the one presented as the optimal solution, indicated by iteration 27. Due to the difficulty of manufacturing this kind of structure, a strategy that can be used is the application of periodicity constraint explored by Huang and Xie [133] and He et al. [162] to perform the topological optimization. This way, the design domain is divided into cells and then submitted to the topological optimization strategy. In summary, the periodicity constraint divides the design domain into cells with the same sensitivity number value, making it possible to create structures with repeating elements, more mathematical details and definitions in [133,

162, 163]. Thus, the periodicity constraint was applied along the length, dividing the design domain into three cells.

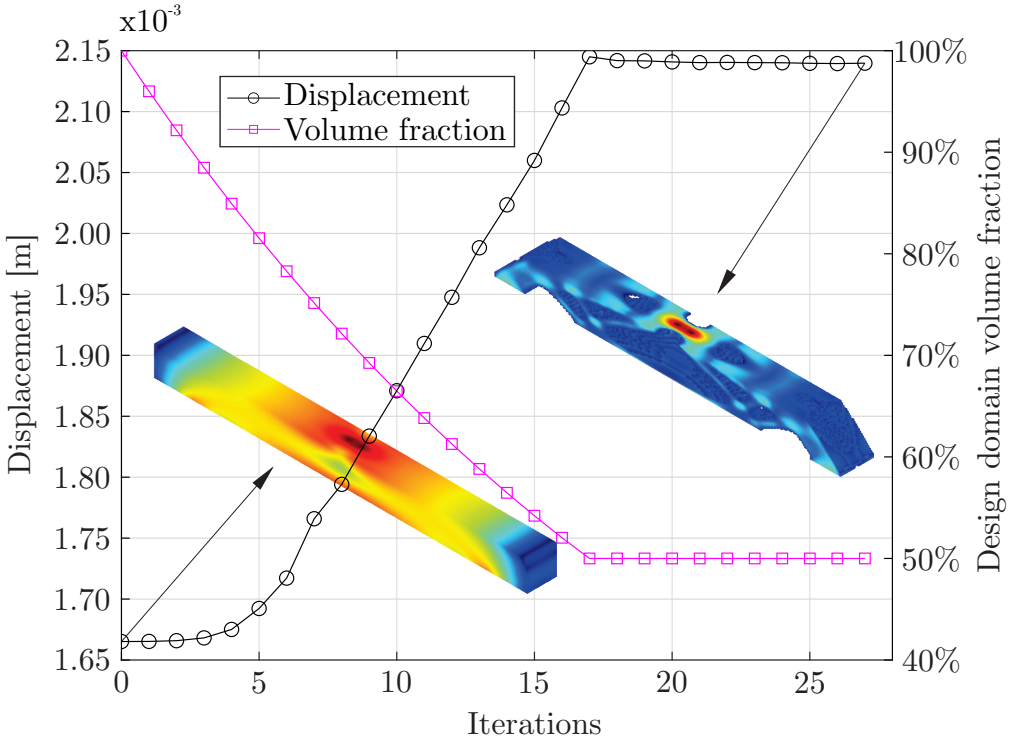

Figure 4.3: Evolution of the center point displacement of the GLULAM top layer, design domain volume, and iterations of the six-layer GLULAM core.

Figure 4.4 shows the simulated GLULAM's initial, intermediate, and final topology with periodicity constraints. Again the color map represents the filtered sensitivity number presented in Equations 3.20 and 3.24. It is possible to notice an initial removal starting from the edges of the cell towards the center of each cell.

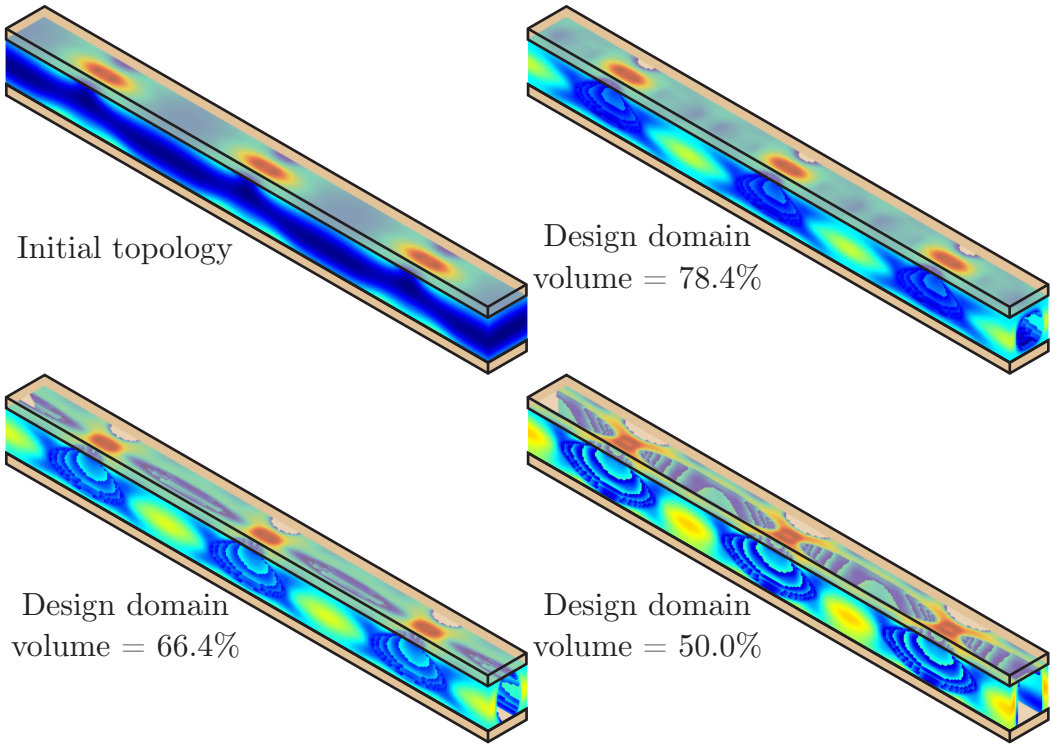

Figure 4.4: Evolution of topologies for optimization of the six-layer GLULAM core at four instants: Initial Topology, Design domain volume = 78.4%, Design domain volume = 66.4%, Design domain volume = 50.0%. The color map indicates the value of the filtered sensitivity number, as per Equations 3.20 and 3.24.

The evolution of displacement, design domain volume, and iterations of the beam with periodicity constraint is presented in Figure 4.5. As indicated in the literature [133, 162, 163], compared to the beam without periodicity constraint (Figure 4.3) it is possible to evaluate that the displacement of the optimized structure was higher compared to the optimized model with the addition of periodicity constraint. Moreover, the initial GLULAM core with and without periodicity constraints are equal, but the difference is in the optimized core with the cell presented in iteration 28 in Figure 4.5. Although the authors did not fabricate it, this cell is considerably simpler to build than the topology presented by the solution without periodicity constraints.

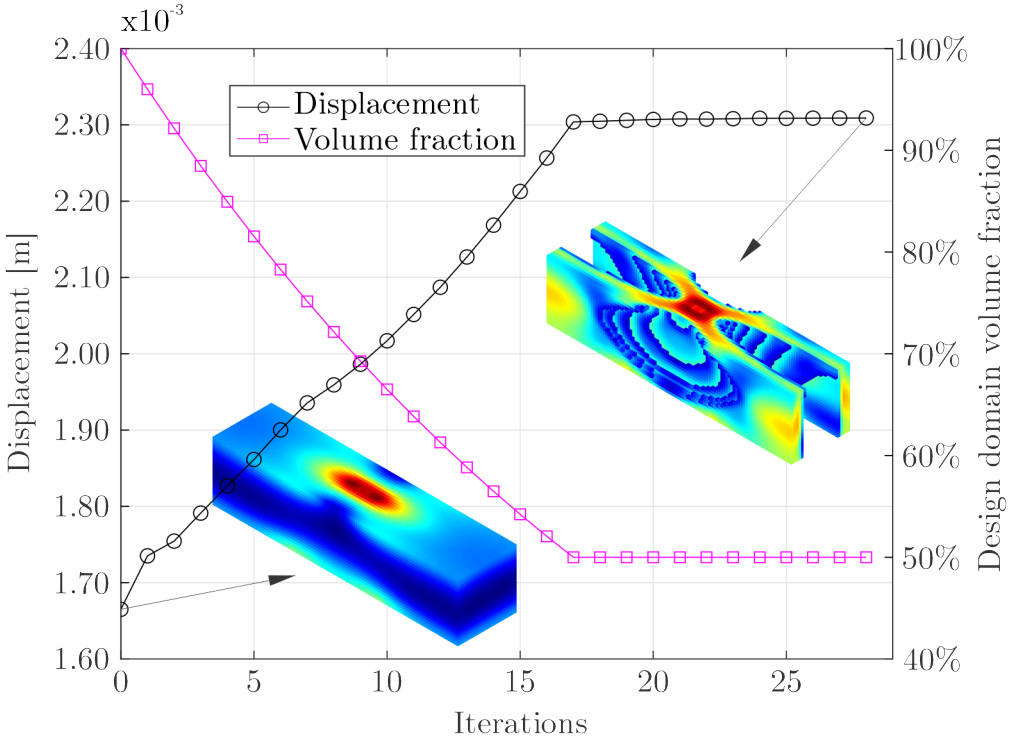

Figure 4.5: Evolution of the center point displacement of the GLULAM top layer, design domain volume, and iterations of the six-layer GLULAM core considering the model with periodicity constraint.

The layers of the optimized GLULAM core are shown in Figure 4.6. Layers two, three, four, and five of the GLULAM core are titled L2, L3, L4, and L5, respectively. The layers have different topologies and volumes. Therefore, it is possible to state that each layer has a different importance to the objective function, with layer L5 being the layer with the most significant volume of material, followed by layer L4. Layers L2 and L3 have similar topology and volume of material and are smaller than L4.

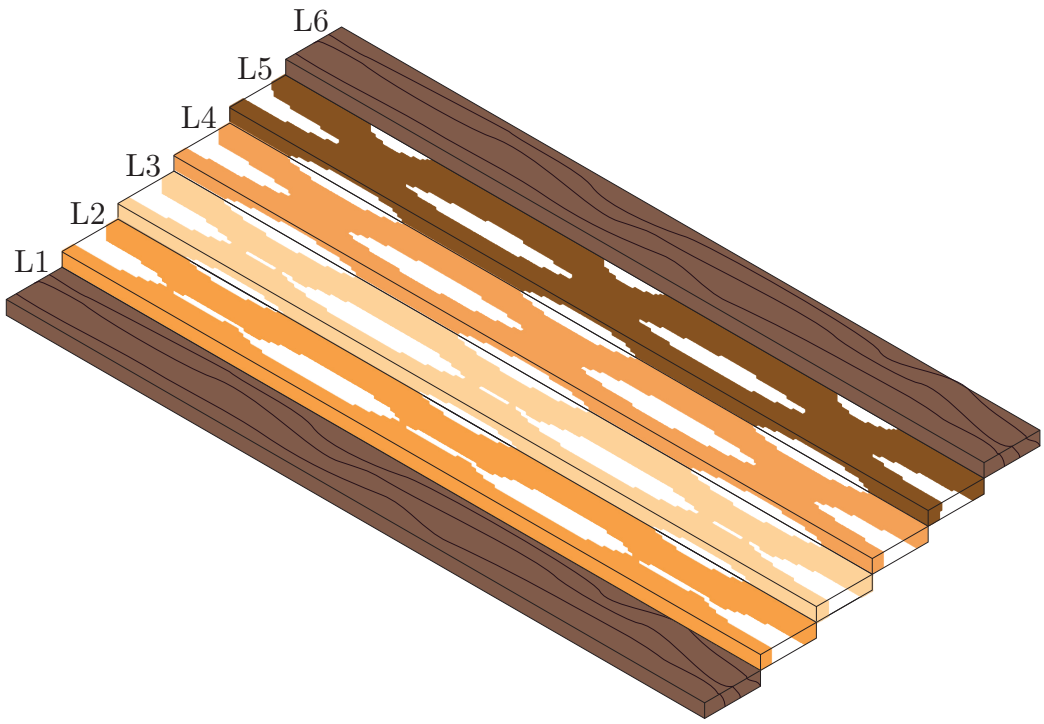

Figure 4.6: Top view of layers two, three, four and five and isometric view of stacked layers.

Considering all the approximations and restrictions in this model and simulation, it is suggested an adaptation of the approximate geometry of the cell for construction presented in Figure 4.7. This approximation seeks a reduction in the machining processes that may make it impossible to manufacture complex topologies such as those presented in Figure 4.2 and Figure 4.4. The suggested model has the exact dimensions of the initial 6-layer GLULAM but has a core composed of smaller elements.

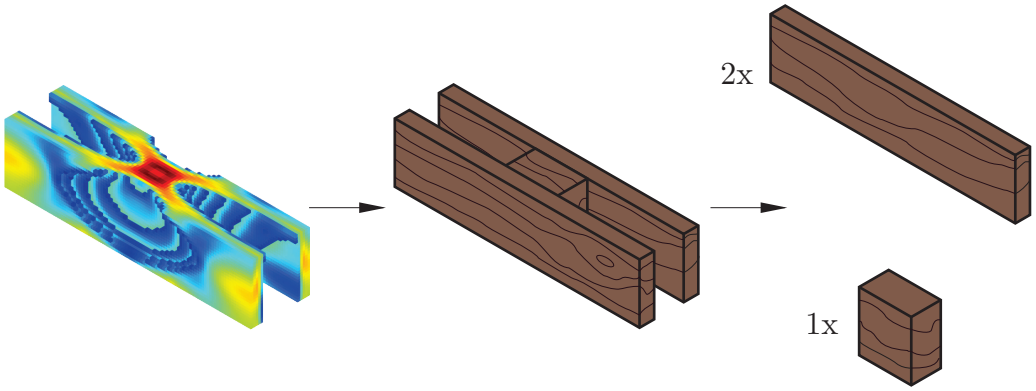

Figure 4.7: Suggested adaptation of the approximate geometry of the cell for construction.

4.1.2 Numerical example 2 - 3D CLT

In this example, the topology optimization presented in the previous section is applied to a five-layer CLT structure with dimensions 3.0 m x 1.0 m x 0.3 m, as shown in Figure 4.8. The simulated model is subjected to the three-point bending test with a 1,000 N load. In the model, the design domain are layer two and layer four of the CLT, surrounded by layers one, three, and five, which are the non-design domain. This model follows the periodicity constraint strategy presented by Huang and Xie [133] and He et al. [162] with six cells along the length. As shown in the previous section, the objective function of this work is the displacement, which in this example was selected exactly at the center of the top layer of the beam. Thus, the objective is to find the optimal topology considering 50% of the design domain volume. The parameters for optimization with the BESO method are: $ER = 4\%$, $AR = 4\%$, $r_{min} = 40$ mm, $\tau = 0.001$, $N = 5$ and $p = 3$.

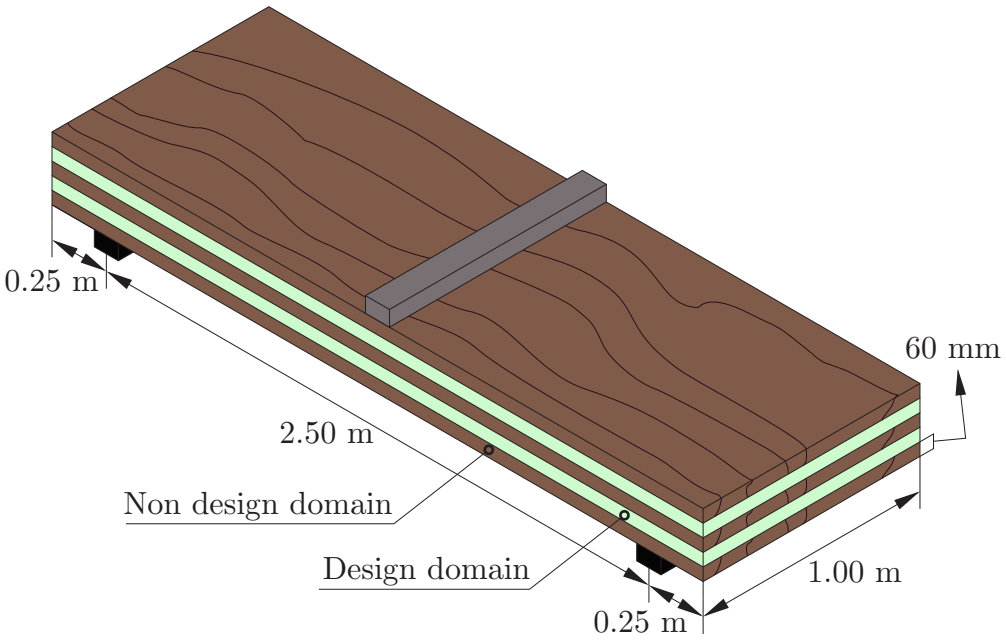

Figure 4.8: Schematic representation of numerical example 1: five-layer CLT with dimensions 3.0 m x 1.0 m x 0.3 m, bi-supported, and 1000 N force applied at the center. the design domain are layer two and layer four of the CLT, surrounded by layers one, three, and five, which are the non-design domain.

A Figure 4.9 shows the simulated CLT's initial, intermediate, and final topology with periodicity constraints. The color map represents the filtered sensitivity number presented in Equations 3.20 and 3.24. It is possible to evaluate that the removal of elements happens differ-

ently in each design domain layer, where layer one removes a more significant portion in the inner part, and layer four removes it approximately equally, forming rectangular shapes.

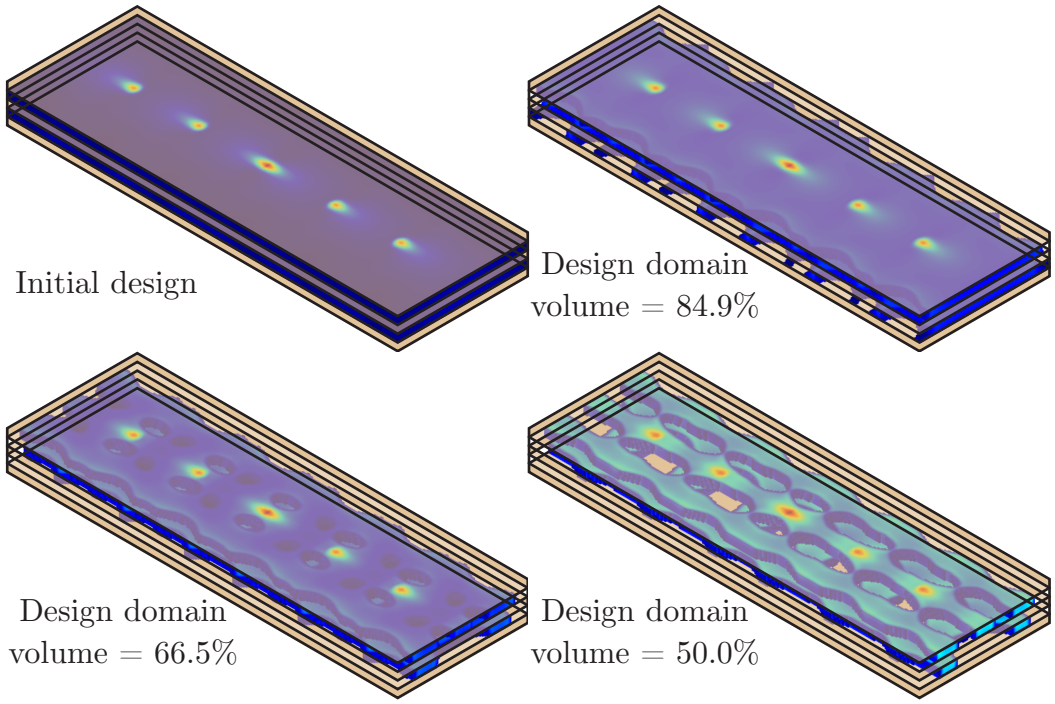

Figure 4.9: Evolution of topologies for optimization of the five-layer CLT core at four instants: Initial Topology, Design domain volume = 84.9%, Design domain volume = 66.5%, Design domain volume = 50.0%. The color map indicates the value of the filtered sensitivity number, as per Equations 3.20 and 3.24.

The evolution of displacement, design domain volume, and iterations of the beam with periodicity constraint is presented in Figure 4.10. In addition, the optimized layers are presented separately, with each layer having a different topology to ensure the best material distribution relative to the objective function.

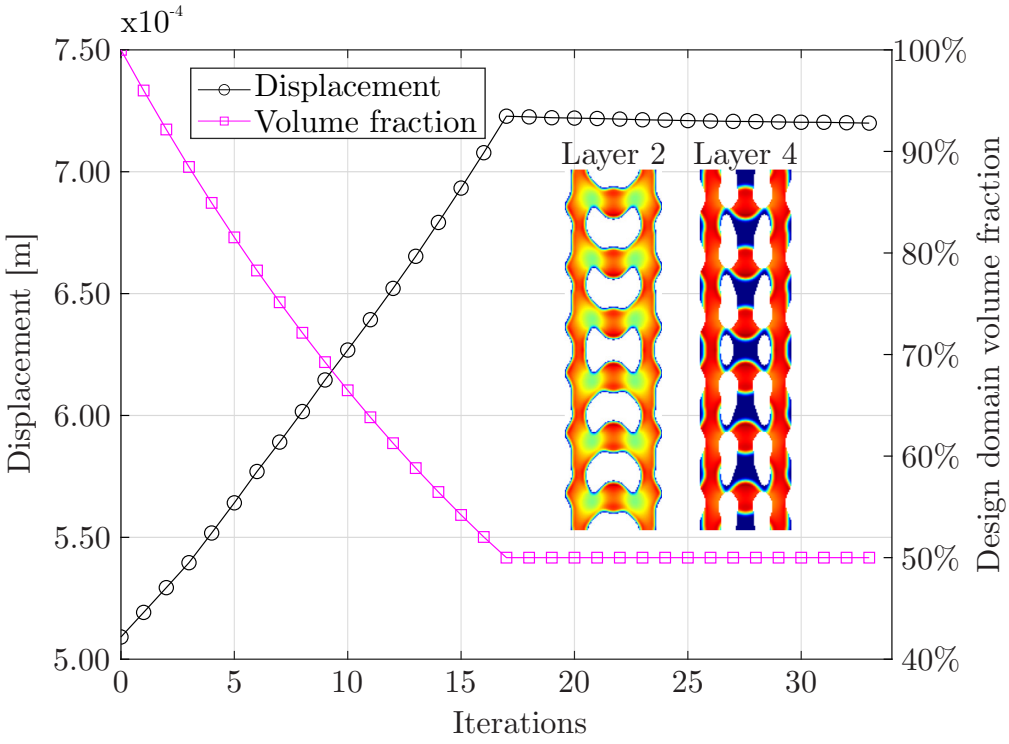

Figure 4.10: Evolution of the center point displacement of the CLT top layer, design domain volume, and iterations of the five-layer CLT core considering the model with periodicity constraint.

In both examples evaluated, including GLULAM and CLT structures, there were increases in the displacement of interest. This result occurs because, in the static case, when removing material, the global stiffness of the structure decreases. The mixture of wood and steel increases the overall strength [49] and can be explored in the methodology applied in this work.

Apart from that, due to assumptions in the procedure developed in this work, it is recommended that experiments be conducted to evaluate the mechanical response of the results presented in this paper, similar to what was reported in [4, 164].

4.2 Conclusions chapter 4

This chapter presents a topological optimization methodology applied to the core of glued-laminated timber structures, specifically GLULAM and CLT. The model considers the orthotropic characteristics of wood and the stacking nature of the layers that exist in wood products. The examples illustrate that the lack of periodicity constraint hinders the manufacture

of engineered wood products with a hollow core, whereas adding the periodicity constraint increases the manufacturability. Different optimized topologies have been found for different layers, highlighting the structural differences in the layer importance of analyzed structures.

Moreover, in the evaluated cases, an increase in displacement was observed at the points of interest, indicating a loss in the mechanical capacity of the structure. Additionally, the method demonstrates that it can create new structurally engineered wood cores with possible material reduction and a slight loss in capacity. Experiments should be conducted to confirm the relationship between mass reduction and loss of capacity. Furthermore, the methodology applied in this work can be extended to evaluate the acoustic capacity of hollow wood structure cores.

4.3 Replication of Results

The Matlab code used in this chapter is available upon request by email or for download at `https://github.com/arturvito/Hollow-Core-GLULAM`

Chapter 5

Innovative Approach for Enhancing GLULAM with Steel Bars

In this chapter, the focus is on the implementation of topology optimization, which builds upon the foundations established in earlier chapters, with a specific focus on composite GLULAM beams. The primary objective of this chapter is to employ topology optimization techniques to precisely determine the optimal placement of steel beams within GLULAM structures. The goal is to achieve maximum structural efficiency, minimize material consumption, and ensure the structural integrity and satisfactory performance of the construction.

In this chapter, we propose the use of Bi-directional Evolutionary Structural Optimization (BESO) to enhance the performance of GLULAM structures. The approach involves strategically positioning steel bars within the GLULAM structure under static loads to increase the structure's stiffness and enhance its structural integrity. To achieve this, we introduce the concept of a sub-design domain and apply optimization theory to determine the optimal placement of the steel bars. The finite element problem is solved using ANSYS software, while the topological optimization problem is addressed using MATLAB software.

The simulation results for the cases analyzed in this study demonstrate that the addition of stiffening bars can significantly increase the structure's stiffness, by up to 68%. The application of BESO to position reinforcements within GLULAM structures represents a novel approach for improving their performance. The utilization of sub-design domains and optimization theory facilitates the precise determination of the optimal reinforcement placement.

The outcomes of this study highlight the potential of this approach to enhance the structural integrity and stiffness of GLULAM structures under static loads. The proposed method

makes a valuable contribution to the field of engineering and construction, with the potential for broader applications

5.1 Topology optimization techniques to placement of steel beams

This section presents two numerical examples of the method proposed in section 3.2. The first example is a 2D model where the initial topology consists of a GLULAM beam reinforced with steel in all possible positions, and steel structures are removed iteratively according to the stipulated methodology and parameters. The second example is a 3D application with a sub design domain composed of wood and a cylindrical bar in the center. These examples are intended to demonstrate the effectiveness and versatility of the proposed method for both 2D and 3D models. In Table 5.1, the resistance parameters for the wood used and the steel are presented.

Table 5.1: Mechanical properties used in the numerical examples.

Material	Parameters		
Steel	$E = 210000$ MPa		
	$\nu = 0.30$		
Douglas fir	E_L (MPa)	E_R (MPa)	E_T (MPa)
	13400.0	911.2	670.0
	G_{LR} (MPa)	G_{LT} (MPa)	G_{RT} (MPa)
	857.6	1045.2	93.8
	ν_{LR}	ν_{LT}	ν_{RT}
	0.292	0.449	0.39

5.1.1 Numerical example 1 – 2D GLULAM beam reinforced with steel

In this example, only half of the model is simulated to decrease computational cost. The dimensions of the GLULAM are L = 2400 mm and H = 120 mm, supported at the end under a

platform and subjected to a concentrated load in the center of the beam, as shown in Figure 5.1. The steel beam in this half of the model has dimensions of $L_s = 150$ mm by $H_s = 6$ mm. Initially, all 40 sub-design domains are filled with steel bars, and at each iteration, two bars are removed until a total of 8 bar segments remain. The other parameters for the BESO method are r_{min}=65 mm, $\tau = 0.01$, and $p = 3$.

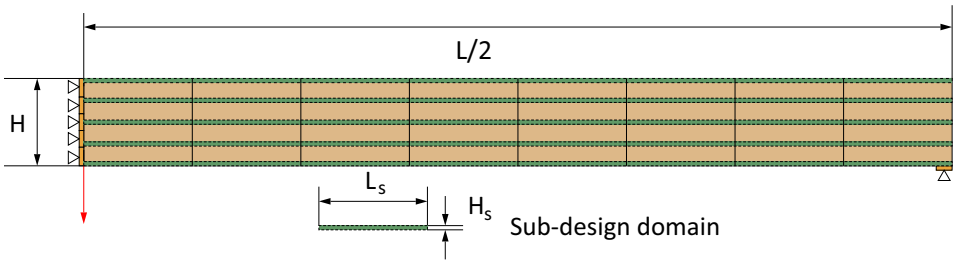

Figure 5.1: Design domain and sub-design domain of example 1 with indication of concentrated load application and boundary conditions.

Figure 5.2 provides valuable insight into the optimization process, illustrating how the objective function changes as the simulation progresses. Specifically, the graph shows the relationship between the objective function and the number of reinforcement bars used in the structure.

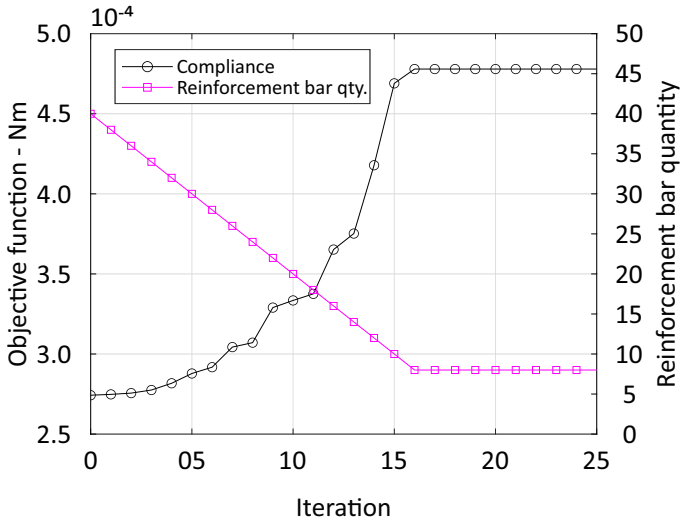

Figure 5.2: Optimization histories of the objective function and reinforcement bar quantity for example 1.

As the number of reinforcement bars decreases from 14, there is a significant increase in compliance. However, when the structure has more than 14 bars, compliance decreases at

a gradual gradient. Moreover, for comparison purposes, a simulation was carried out using completely wooden conditions and results in a compliance value of 1.43×10^{-3} Nm, which is approximately 68% lower than with the placement of 14 steel bar segments, indicating that the structure is 68% less resistant. Interestingly, this value increases to approximately 80% when 40 steel bar segments are used.

Figure 5.3 presents the distribution of steel bars obtained from four iterations of the simulation. The first iteration of the simulation represents the initial guess of the structure, which consisted of 40 steel bars. As the simulation progresses, steel bars are incrementally removed from the structure based on the filtered sensitivity number. In the eighth iteration, 16 steel bars were removed near the support and force application regions. In the 12th and 25th iterations, the bars were removed from the center, leaving steel bars at the ends of the structure near the fixed point and force application location.

Figure 5.3: Four intermediate topologies with indication of the steel bars position from numerical example 1.

5.1.2 Numerical example 2 – 3D GLULAM beam reinforced with steel

In this example, the method proposed in the paper is applied to simulate only half of the GLULAM model in order to reduce computational costs. The dimensions of the GLULAM were based on and adapted from the study by Soriano, Pellis, and Mascia [49]. Each sub-design domain has a length of $L_s = 200.0$ mm, height of $H_s = 30.0$ mm, and width of $W_s = 30.0$ mm. To create the 120mm x 120mm x 1400mm GLULAM half-beam finite element method model, four sub-design domains are required in both width and height, and seven sub-design domains in length, making a total of 112 possible locations for the bars. A 6mm diameter cylinder is

positioned in the center of each sub-design domain, where it is defined as either wood or steel, while the rest of the sub-design domain is wood. The positioning of the cylinders and the finite element mesh used, half of the beam, and the applied load is shown in Figure 5.4.

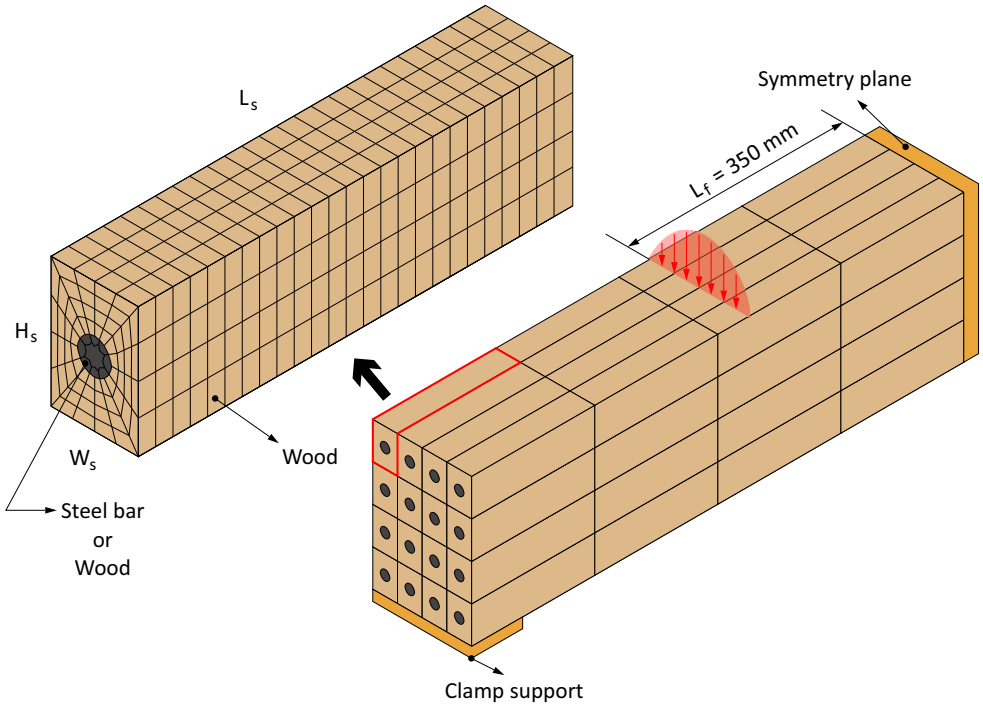

Figure 5.4: Design domain and sub-design domain of example 3D GLULAM Beam Reinforced with steel with indication of distributed load application region and boundary conditions.

Initially, 112 bars of steel are present in the structure, the steel bars are removed two-by-two until 28 bars remains. The other parameters for the BESO method were $r_{min} = 30$ mm, $\tau = 0.001$, and $p = 3$.

Figure 5.5 displays the progress of the objective function for each iteration and steel bar variation. It is worth noting that, due to the limited number of steel bars, the simulation may reach a point where no further improvement in the objective function can be achieved. At the beginning of the optimization process, the removal of bars has a smaller influence compared to the end of the simulation. This observation suggests that an excessive number of steel bars in the GLULAM beam does not necessarily lead to a proportionate increase in the structure's rigidity. However, after 34 bars, there is an abrupt change in compliance, indicating a strong correlation between this number of bars and the structural strength.

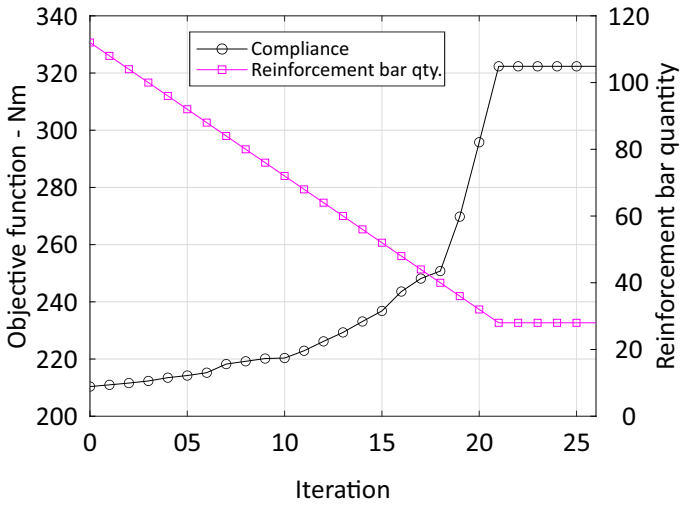

Figure 5.5: Optimization histories of the objective function and reinforcement bar quantity for example 2.

Figure 5.6 shows four possible configurations of the arrangement of 28 steel bar segments in the structure proposed in numerical example 3. The first configuration is the result of the applied method, which corresponds to a compliance of 322.35 Nm with the steel bars arranged in the central part of the beam and close to the fixed end. The next option presented is condition A, in which the 28 steel bar segments are arranged at the ends of the beam, resulting in a compliance of 346.56 Nm, approximately 6% higher than the optimized result. In condition B, the beams are arranged in the center of the width and at the ends of the height, resulting in a compliance of 346.16 Nm. Conditions A and B present similar compliance values, as there are beams positioned in the optimal regions and, therefore, are close to the best case for this condition. In condition C, the 28 steel bar segments are located in the center of both width and height, resulting in a compliance of 669.53 Nm, approximately 51% higher than the optimal condition. In this case, none of the steel bar segments are located in the optimal position.

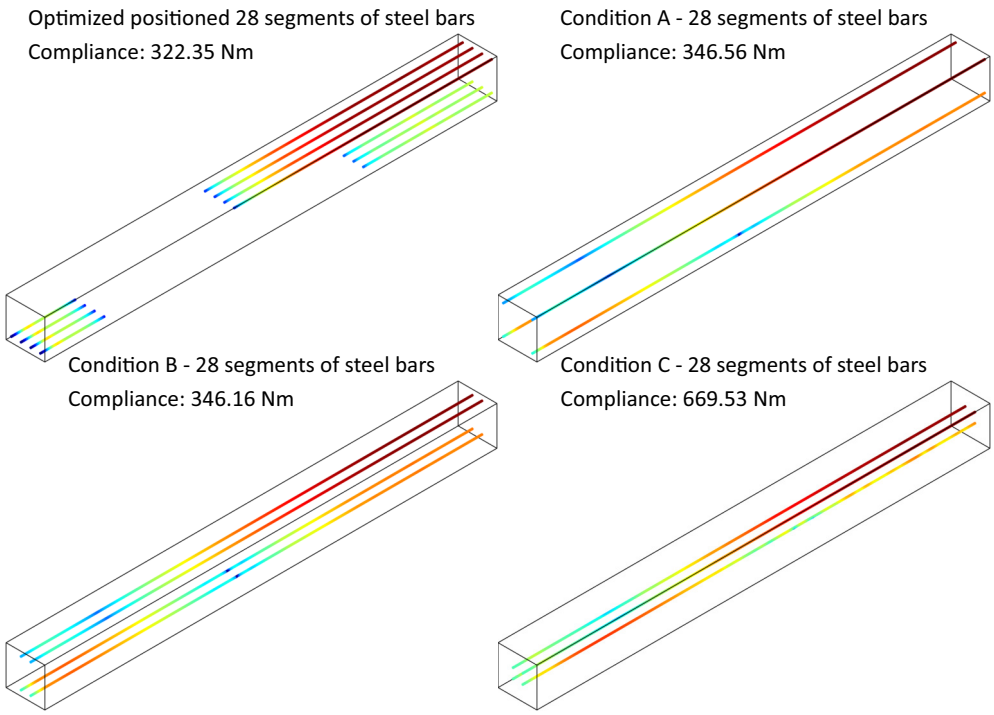

Figure 5.6: Four possible configurations for the positioning of steel bar segments in the GLULAM structure. From left to right, the first configuration is the result of topological optimization. The next configuration, condition A, has the steel bar segments located at the ends of the GLULAM beam. In condition B, the bars are positioned at the top and bottom ends of the GLULAM beam. Finally, in condition C, the bars are located in the center of the GLULAM beam.

5.2 Conclusions chapter 5

This study has demonstrated the effectiveness of utilizing the BESO method to optimize the positioning of steel reinforcing bars in GLULAM structures. By introducing the concept of sub-design domains and leveraging optimization theory, the proposed approach has enabled the determination of the optimal areas/volumes within the GLULAM structures to place the steel bars. The results of the simulations have shown that adding reinforcement bars to the wooden structure can significantly enhance its stiffness by up to 68%. However, the study also indicates that there is a threshold point at which the addition of bars reaches a plateau, highlighting the importance of carefully selecting the number and position of reinforcing bars.

The proposed method provides a valuable contribution to the field of engineering and construction by introducing a novel approach to optimizing GLULAM structures. The find-

ings have demonstrated the potential for significantly enhancing the structural integrity and stiffness of GLULAM structures under static loads, which can lead to improved safety, durability, and cost-effectiveness. Furthermore, the use of GLULAM in construction reduces carbon dioxide emissions during transportation, making it a sustainable choice for building materials.

The results presented have important implications for the design and manufacturing of composite structures and could lead to more efficient and sustainable engineering solutions. Further research into other optimization techniques and their effectiveness for different types of composite materials and structural designs could provide valuable insights for the development of more effective optimization algorithms. Despite the simplifying assumptions made in the study, the authors acknowledge the practical aspects of GLULAM fabrication and recognize the need for further investigation into these optimized structures from a manufacturing perspective in future research. The proposed methodology can be extended to other types of structures and materials, making it a valuable tool for engineers and researchers in the field of structural optimization.

5.3 Replication of results

The Matlab code used in this chapter is available upon request by email or for download at `https://github.com/arturvito/Reinforced-GLULAM`

Chapter 6

Conclusion

In conclusion, this thesis aimed to investigate the implementation of topology optimization in engineered wood products (EWP), with a specific focus on Cross-Laminated Timber (CLT) and Glued-Laminated Timber (GLULAM), to enhance structural efficiency. The study applied topology optimization techniques to optimize material distribution within CLT and GLULAM structures, considering the orthotropic characteristic of wood and the stacking nature of layers in wood products.

The results indicated that, even though this thesis did not manufacture any optimized GLULAM or CLT structures, the lack of a periodicity constraint hindered the manufacture of EWP with a hollow core. Different optimized topologies were found for different layers, emphasizing the structural differences in layer importance. It was observed that there was an increase in displacement at points of interest, suggesting a loss in the mechanical capacity of the structure under the static analysis.

Regarding the optimization of steel beam placement within GLULAM structures, the study employed the BESO method and used the concept of sub-design domains. This approach allowed for the determination of optimal areas/volumes within GLULAM structures to place steel reinforcing bars. The simulations revealed that the addition of reinforcement bars significantly enhanced the stiffness of the wooden structure. However, there was a threshold point at which the addition of bars reached a plateau, emphasizing the importance of carefully selecting the number and position of reinforcing bars.

The findings of the thesis contribute to the field of engineering and construction by providing effective approaches to optimize GLULAM structures. These optimization techniques can

enhance the structural integrity, stiffness, safety, and cost-effectiveness of GLULAM structures under static loads.

The results have important implications for the design and manufacturing of composite structures and offer insights into more efficient and sustainable engineering solutions. Overall, the proposed methodology has the potential to be extended to other types of structures and materials, serving as a valuable tool for structural optimization in the field of engineering.

6.1 Future works

- Manufacturing Considerations: Future studies should also address the practical aspects of manufacturing optimized CLT and GLULAM structures. This entails exploring the fabrication processes, production constraints, and scalability of the proposed optimization methods. It is important to investigate the manufacturability of optimized structures with hollow cores, taking into account the specific requirements and limitations of manufacturing technologies. Additionally, assessing the feasibility of integrating reinforcing bars in GLULAM structures and optimizing their placement in practical manufacturing scenarios is crucial. Considering manufacturing perspectives will ensure the practical implementation of optimized CLT and GLULAM elements on a larger scale and enable their widespread adoption in the construction industry.

- Dynamic Analysis: Future research can focus on investigating the dynamic behavior of optimized CLT and GLULAM structures. This can involve conducting dynamic tests or numerical simulations to evaluate their response to dynamic loads such as vibrations or seismic events. By analyzing the natural frequencies, mode shapes, and damping characteristics of the optimized structures, engineers can ensure their performance under dynamic conditions. Understanding the dynamic behavior will enable the design of CLT and GLULAM structures that not only excel under static loads but also exhibit satisfactory dynamic performance, enhancing their overall reliability and resilience.

- Acoustics: An important avenue for future investigation is the acoustic performance of optimized CLT and GLULAM structures. Expanding the proposed methodology to assess the acoustic capacity of hollow wood structure cores would be beneficial. This research would delve into the sound transmission properties, sound absorption characteristics, and overall acoustic efficiency of the optimized structures. By optimizing

material distribution and considering acoustic performance, designers can create CLT and GLULAM structures that provide superior sound insulation, noise reduction, and acoustic comfort, meeting the requirements of various building applications.

References

[1] M. Augustin. *Handbook 1: Timber Structures*. Graz, Austria: Leonardo Da Vinci Pilot Project, 2008, pp. 63–99.

[2] Paul Mayencourt. "Mass reduction: opportunities and structural optimization methods to reduce material use in mass timber buildings". PhD dissertation. Massachusetts Institute of Technology, 2019.

[3] Paul Mayencourt and Caitlin Mueller. "Hybrid analytical and computational optimization methodology for structural shaping: Material-efficient mass timber beams". In: *Engineering Structures* 215 (2020), p. 110532. ISSN: 0141-0296. DOI: https://doi.org/10.1016/j.engstruct.2020.110532.

[4] Paul Mayencourt and Caitlin Mueller. "Structural Optimization of Cross-laminated Timber Panels in One-way Bending". In: *Structures* 18 (2019). Advanced Manufacturing and Materials for Innovative Structural Design, pp. 48–59. ISSN: 2352-0124.

[5] Zheng Li et al. "Modern timber construction technology and engineering applications in China". In: *Proceedings of the Institution of Civil Engineers - Civil Engineering* 172 (2018), pp. 1–51. DOI: 10.1680/jcien.18.00024.

[6] Steffen Lehmann. "Low carbon construction systems using prefabricated engineered solid wood panels for urban infill to significantly reduce greenhouse gas emissions". In: *Sustainable Cities and Society* 6 (2013), pp. 57–67. ISSN: 2210-6707.

[7] B.R Hoadley. *Understanding Wood. A Craftsman's Guide to Wood Technology*. Taunton Press, 1980.

[8] M.P. Ansell. "Wood microstructure". In: ed. by Martin P. Ansell. Woodhead Publishing, 2015, pp. 3–26. DOI: https://doi.org/10.1016/B978-1-78242-454-3.00001-9.

[9] Forest Products Laboratory. *Wood Handbook. Wood as an Engineering material*. U.S. Department of Agriculture, Forest Service, Forest Products Laboratory, 2021.

[10] "Macroscopic Character of Wood". In: *Forest Products and Wood Science*. John Wiley & Sons, Ltd, 2019. ISBN: 9781119426400. DOI: https://doi.org/10.1002/9781119426400.ch2.

[11] Jaroslav Mackerle. "Finite element analyses in wood research: a bibliography". In: *Wood Science and Technology* 39.7 (2005), pp. 579–600. ISSN: 1432-5225. DOI: 10.1007/s00226-005-0026-9.

[12] MultiMedia LLC. *October 15, 1934: Glued Laminated Timber Comes to America*. 2018. URL: https://foresthistory.org/october-15-1934-glued-laminated-timber-comes-to-america/#:~:text=Otto%20Karl%20Freidrich%20Hetzer%2C%20a,curved%20glued%20laminated%20timber%20construction. (visited on 03/29/2023).

[13] Andreas J. Rhude. "Structural glued laminated timber: History of its origins and early development". In: *Forest Products Journal* 46.1 (1996). Copyright - Copyright Forest Products Society Jan 1996; Last updated - 2023-01-09; CODEN - FPJOAB; SubjectsTermNotLitGenreText - Germany; United States–US.

[14] Camille A. Issa and Ziad Kmeid. "Advanced wood engineering: glulam beams". In: *Construction and Building Materials* 19.2 (2005), pp. 99–106. ISSN: 0950-0618. DOI: https://doi.org/10.1016/j.conbuildmat.2004.05.013.

[15] Philipp Dietsch and Thomas Tannert. "Assessing the integrity of glued-laminated timber elements". In: *Construction and Building Materials* 101 (2015). Assessment of structural timber members by non- and semi-destructive methods, pp. 1259–1270. ISSN: 0950-0618. DOI: https://doi.org/10.1016/j.conbuildmat.2015.06.064.

[16] Ernest Ching and Josephine V. Carstensen. "Truss topology optimization of timber–steel structures for reduced embodied carbon design". In: *Engineering Structures* 252 (2022), p. 113540. ISSN: 0141-0296. DOI: https://doi.org/10.1016/j.engstruct.2021.113540.

[17] Artur Fernando de Vito, William Martins Vicente, and Yi Min Xie. "Topology optimization applied to the core of structural engineered wood product". In: *Structures* 48 (2023), pp. 1567–1575. ISSN: 2352-0124. DOI: https://doi.org/10.1016/j.istruc.2023.01.036.

[18] Mathieu Poulin et al. "Experimental and Analytical Investigation of Cross-Laminated Timber Panels Subjected to Out-of-Plane Blast Loads". In: *Journal of Structural Engineering* 144 (2018). DOI: 10.1061/(ASCE)ST.1943-541X.0001915.

[19] Jiale Zhou et al. "Experimental Study on Loading Capacity of Glued-Laminated Timber Arches Subjected to Vertical Concentrated Loads". In: *Advances in Civil Engineering* 2020 (2020). DOI: 10.1155/2020/7987414.

[20] Hao Li et al. "Bending and shear performance of cross-laminated timber and glued-laminated timber beams: A comparative investigation". In: *Journal of Building Engineering* 45 (2022), p. 103477. ISSN: 2352-7102. DOI: https://doi.org/10.1016/j.jobe.2021.103477.

[21] Peixing Wei et al. "A comparative study of compression behaviors of cross-laminated timber and glued-laminated timber columns". In: *Construction and Building Materials* 222 (2019), pp. 86–95. ISSN: 0950-0618. DOI: https://doi.org/10.1016/j.conbuildmat.2019.06.139.

[22] Jianhui Zhou et al. "Effective bending and shear stiffness of cross-laminated timber by modal testing: Method development and application". In: *Composites Part B: Engineer-*

ing 198 (2020), p. 108225. ISSN: 1359-8368. DOI: https://doi.org/10.1016/j.compositesb.2020.108225.

[23] Yan Xiao and Jian Ma. "Fire simulation test and analysis of laminated bamboo frame building". In: *Construction and Building Materials* 34 (2012), pp. 257–266. ISSN: 0950-0618. DOI: https://doi.org/10.1016/j.conbuildmat.2012.02.077.

[24] Joachim Schmid et al. "Simulation of the Fire Resistance of Cross-laminated Timber (CLT)". In: *Fire Technology* 54 (2018), pp. 1113–1148. ISSN: 1572-8099. DOI: 10.1007/s10694-018-0728-9.

[25] Wenliang Hu et al. "Three-Dimensional Numerical Calculation Model for Static Behavior Simulation of Cross-Laminated Timber Plates under Thermal Environment". In: *Mathematical Problems in Engineering* 2021 (2021), p. 1538928. ISSN: 1024-123X. DOI: 10.1155/2021/1538928.

[26] Yu Bai, Jin Zhang, and Hao Shen. "Experimental and numerical analysis of residual load-carrying capacity of cross-laminated timber walls after fire". In: *Structures* 30 (2021), pp. 50–61. ISSN: 2352-0124. DOI: https://doi.org/10.1016/j.istruc.2020.12.086.

[27] Zhiyan Xing et al. "Experimental study and finite element analysis on residual carrying capacity of CLT wall-floor angle bracket connections after fire". In: *Construction and Building Materials* 328 (2022), p. 127113. ISSN: 0950-0618. DOI: https://doi.org/10.1016/j.conbuildmat.2022.127113.

[28] Boris Azinović et al. "Glued-in rods in cross laminated timber – Numerical simulations and parametric studies". In: *Construction and Building Materials* 212 (2019), pp. 431–441. ISSN: 0950-0618. DOI: https://doi.org/10.1016/j.conbuildmat.2019.03.331.

[29] Till Vallée, Hossahalli Ramesh Rakesh, and Thomas Tannert. "Load-carrying capacity prediction of single rods glued into cross-laminated timber". In: *European Journal of Wood and Wood Products* 80 (2022), pp. 1041–1055. ISSN: 1436-736X. DOI: 10.1007/s00107-022-01835-1.

[30] M. Khelifa et al. "FE stress analysis and prediction of the pull-out of FRP rods glued into glulam timber". In: *Wood Material Science & Engineering* 17.2 (2022), pp. 53–62. DOI: 10.1080/17480272.2020.1776769.

[31] Viktor Hristovski et al. "Full-Scale Shaking-Table Tests of XLam Panel Systems and Numerical Verification: Specimen 1". In: *Journal of Structural Engineering* 139 (2013), pp. 2010–2018. DOI: 10.1061/(ASCE)ST.1943-541X.0000754.

[32] Motoi Yasumura et al. "Full-Scale Tests and Numerical Analysis of Low-Rise CLT Structures under Lateral Loading". In: *Journal of Structural Engineering* 142 (2016). DOI: 10.1061/(ASCE)ST.1943-541X.0001348.

[33] Ashkan Hashemi, Reza Masoudnia, and Pierre Quenneville. "Seismic performance of hybrid self-centring steel-timber rocking core walls with slip friction connections". In: *Journal of Constructional Steel Research* 126 (2016), pp. 201–213. ISSN: 0143-974X. DOI: https://doi.org/10.1016/j.jcsr.2016.07.022.

[34] G. Rinaldin and M. Fragiacomo. "Non-linear simulation of shaking-table tests on 3- and 7-storey X-Lam timber buildings". In: *Engineering Structures* 113 (2016), pp. 133–148. ISSN: 0141-0296. DOI: https://doi.org/10.1016/j.engstruct.2016.01.055.

[35] Henrik Danielsson and Erik Serrano. "Cross laminated timber at in-plane beam loading – Prediction of shear stresses in crossing areas". In: *Engineering Structures* 171 (2018), pp. 921–927. ISSN: 0141-0296. DOI: https://doi.org/10.1016/j.engstruct.2018.03.018.

[36] Henrik Danielsson et al. "Cross laminated timber at in-plane beam loading – Comparison of model predictions and FE-analyses". In: *Engineering Structures* 179 (2019), pp. 246–254. ISSN: 0141-0296. DOI: https://doi.org/10.1016/j.engstruct.2018.10.068.

[37] Henrik Danielsson and Mario Jeleč. "A unified design proposal for shear stress prediction in crossing areas for cross laminated timber at in-plane shear and beam loading conditions". In: *Construction and Building Materials* 355 (2022), p. 129167. ISSN: 0950-0618. DOI: https://doi.org/10.1016/j.conbuildmat.2022.129167.

[38] M. Khelifa and A. Celzard. "Numerical analysis of flexural strengthening of timber beams reinforced with CFRP strips". In: *Composite Structures* 111 (2014), pp. 393–400. ISSN: 0263-8223. DOI: https://doi.org/10.1016/j.compstruct.2014.01.011.

[39] B. Anshari et al. "Structural behaviour of glued laminated timber beams pre-stressed by compressed wood". In: *Construction and Building Materials* 29 (2012), pp. 24–32. ISSN: 0950-0618. DOI: https://doi.org/10.1016/j.conbuildmat.2011.10.002.

[40] Yan Xiao, Quan Zhou, and Bo Shan. "Design and Construction of Modern Bamboo Bridges". In: *Journal of Bridge Engineering* 15.5 (2010), pp. 533–541. DOI: 10.1061/(ASCE)BE.1943-5592.0000089.

[41] M. Mahdavi, P. L. Clouston, and S. R. Arwade. "Development of Laminated Bamboo Lumber: Review of Processing, Performance, and Economical Considerations". In: *JOURNAL OF MATERIALS IN CIVIL ENGINEERING* 23 (2011), pp. 1036–1042. ISSN: 0899-1561. DOI: 10.1061/(ASCE)MT.1943-5533.0000253.

[42] Y. Xiao, R.Z. Yang, and B. Shan. "Production, environmental impact and mechanical properties of glubam". In: *Construction and Building Materials* 44 (2013), pp. 765–773. ISSN: 0950-0618. DOI: https://doi.org/10.1016/j.conbuildmat.2013.03.087.

[43] Hai-tao Li et al. "Compressive performance of laminated bamboo". In: *Composites Part B: Engineering* 54 (2013), pp. 319–328. ISSN: 1359-8368. DOI: https://doi.org/10.1016/j.compositesb.2013.05.035.

[44] Bhavna Sharma et al. "Engineered bamboo for structural applications". In: *Construction and Building Materials* 81 (2015), pp. 66–73. ISSN: 0950-0618. DOI: https://doi.org/10.1016/j.conbuildmat.2015.01.077.

[45] Xiaofeng Sun, Minjuan He, and Zheng Li. "Novel engineered wood and bamboo composites for structural applications: State-of-art of manufacturing technology and mechanical performance evaluation". In: *Construction and Building Materials* 249 (2020), p. 118751. ISSN: 0950-0618. DOI: https://doi.org/10.1016/j.conbuildmat.2020.118751.

[46] Arijit Sinha, Daniel Way, and Skyler Mlasko. "Structural Performance of Glued Laminated Bamboo Beams". In: *Journal of Structural Engineering* 140.1 (2014). DOI: 10.1061/(ASCE)ST.1943-541X.0000807.

[47] Vincenzo De Luca and Cosimo Marano. "Prestressed glulam timbers reinforced with steel bars". In: *Construction and Building Materials* 30 (2012), pp. 206–217. ISSN: 0950-0618. DOI: https://doi.org/10.1016/j.conbuildmat.2011.11.016.

[48] V. De Luca and C. Marano. "A comparison of unreinforced and reinforced glulam timber with steel bars". In: *Eur J Technol Adv Eng Res* 2 (2011), pp. 45–54.

[49] Julio Soriano, Bruno Piva Pellis, and Nilson Tadeu Mascia. "Mechanical performance of glued-laminated timber beams symmetrically reinforced with steel bars". In: *Composite Structures* 150 (2016), pp. 200–207. ISSN: 0263-8223. DOI: https://doi.org/10.1016/j.compstruct.2016.05.016.

[50] Yang Wei et al. "Experimental and theoretical investigation of steel-reinforced bamboo scrimber beams". In: *Engineering Structures* 223 (2020), p. 111179. ISSN: 0141-0296. DOI: https://doi.org/10.1016/j.engstruct.2020.111179.

[51] Gary M. Raftery, Annette M. Harte, and Peter D. Rodd. "Bond quality at the FRP–wood interface using wood-laminating adhesives". In: *International Journal of Adhesion and Adhesives* 29.2 (2009), pp. 101–110. ISSN: 0143-7496. DOI: https://doi.org/10.1016/j.ijadhadh.2008.01.006.

[52] Gary M. Raftery and Annette M. Harte. "Low-grade glued laminated timber reinforced with FRP plate". In: *Composites Part B: Engineering* 42.4 (2011), pp. 724–735. ISSN: 1359-8368. DOI: https://doi.org/10.1016/j.compositesb.2011.01.029.

[53] F Micelli, V Scialpi, and A La Tegola. "Flexural reinforcement of glulam timber beams and joints with carbon fiber-reinforced polymer rods". In: *Journal of Composities for Construction* 9.4 (2005), pp. 337–347. ISSN: 1090-0268. DOI: 10.1061/(ASCE)1090-0268(2005)9:4(337).

[54] Yeou-Fong Li et al. "A study on wood beams strengthened by FRP composite materials". In: *Construction and Building Materials* 62 (2014), pp. 118–125. ISSN: 0950-0618. DOI: https://doi.org/10.1016/j.conbuildmat.2014.03.036.

[55] Tohid Ghanbari Ghazijahani, Hui Jiao, and Damien Holloway. "Composite Timber Beams Strengthened by Steel and CFRP". In: *Journal of Composites for Construction* 21 (2017), p. 04016059. DOI: 10.1061/(ASCE)CC.1943-5614.0000714.

[56] Abbas Vahedian, Rijun Shrestha, and Keith Crews. "Analysis of externally bonded Carbon Fibre Reinforced Polymers sheet to timber interface". In: *Composite Structures* 191 (2018), pp. 239–250. ISSN: 0263-8223. DOI: https://doi.org/10.1016/j.compstruct.2018.02.064.

[57] Huifeng Yang et al. "Flexural behavior of FRP and steel reinforced glulam beams: Experimental and theoretical evaluation". In: *Construction and Building Materials* 106 (2016), pp. 550–563. ISSN: 0950-0618. DOI: https://doi.org/10.1016/j.conbuildmat.2015.12.135.

[58] Abbas Vahedian, Rijun Shrestha, and Keith Crews. "Experimental and analytical investigation on CFRP strengthened glulam laminated timber beams: Full-scale experiments". In: *Composites Part B: Engineering* 164 (2019), pp. 377–389. ISSN: 1359-8368. DOI: https://doi.org/10.1016/j.compositesb.2018.12.007.

[59] Bruno F. Donadon et al. "Experimental investigation of glued-laminated timber beams with Vectran-FRP reinforcement". In: *Engineering Structures* 202 (2020), p. 109818. ISSN: 0141-0296. DOI: https://doi.org/10.1016/j.engstruct.2019.109818.

[60] Feng Shi et al. "Axial Compression Behavior of FRP Confined Laminated Timber Columns under Cyclic Loadings". In: *Buildings* 12.11 (2022). ISSN: 2075-5309. DOI: 10.3390/buildings12111841.

[61] E. Lukaszewska, H. Johnsson, and M. Fragiacomo. "Performance of connections for prefabricated timber-concrete composite floors". In: *Materials and Structures* 41.9 (2008), pp. 1533–1550. DOI: 10.1617/s11527-007-9346-6.

[62] Carlos Martins et al. "Environmentally friendly high performance timber–concrete panel". In: *Construction and Building Materials* 102 (2016). SHATIS 2013 : Research on Timber Materials and Structures, pp. 1060–1069. ISSN: 0950-0618. DOI: https://doi.org/10.1016/j.conbuildmat.2015.07.194.

[63] J. Estévez-Cimadevila et al. "Timber-concrete composite structural flooring system". In: *Journal of Building Engineering* 49 (2022), p. 104078. ISSN: 2352-7102. DOI: https://doi.org/10.1016/j.jobe.2022.104078.

[64] Osama A.B. Hassan and Christopher Johansson. "Glued laminated timber and steel beams: A comparative study of structural design, economic and environmental consequences". In: *Journal of Engineering, Design and Technology* (2018). DOI: 10.1108/JEDT-12-2017-0130.

[65] Osama A.B. Hassan, Fredrik Öberg, and Emil Gezelius. "Cross-laminated timber flooring and concrete slab flooring: A comparative study of structural design, economic and environmental consequences". In: *Journal of Building Engineering* 26 (2019), p. 100881. ISSN: 2352-7102. DOI: https://doi.org/10.1016/j.jobe.2019.100881.

[66] *Sustainability and Climate*. https://www.fs.usda.gov/managing-land/sc/carbon. Accessed on May 4, 2023. United States Department of Agriculture, Forest Service.

[67] Osama A.B. Hassan, Nour Emad A.A., and Gabriel Abdulahad. "A comparative study between glulam and concrete columns in view of design, economy and environment". In: *Case Studies in Construction Materials* 16 (2022), e00966. ISSN: 2214-5095. DOI: https://doi.org/10.1016/j.cscm.2022.e00966.

[68] Francesca Pierobon et al. "Environmental benefits of using hybrid CLT structure in midrise non-residential construction: An LCA based comparative case study in the

U.S. Pacific Northwest". In: *Journal of Building Engineering* 26 (2019), p. 100862. ISSN: 2352-7102. DOI: https://doi.org/10.1016/j.jobe.2019.100862.

[69] Sylvain Cordier et al. "Regional environmental life cycle consequences of material substitutions: The case of increasing wood structures for non-residential buildings". In: *Journal of Cleaner Production* 328 (2021), p. 129671. ISSN: 0959-6526. DOI: https://doi.org/10.1016/j.jclepro.2021.129671.

[70] Bernardino D'Amico, Francesco Pomponi, and Jim Hart. "Global potential for material substitution in building construction: The case of cross laminated timber". In: *Journal of Cleaner Production* 279 (2021), p. 123487. ISSN: 0959-6526. DOI: https://doi.org/10.1016/j.jclepro.2020.123487.

[71] Povilas Žemaitis et al. "Sustainability impact assessment of glue laminated timber and concrete-based building materials production chains – A Lithuanian case study". In: *Journal of Cleaner Production* 321 (2021), p. 129005. ISSN: 0959-6526. DOI: https://doi.org/10.1016/j.jclepro.2021.129005.

[72] K. A. Malo, R. B. Abrahamsen, and M. A. Bjertnæs. "Some structural design issues of the 14-storey timber framed building "Treet" in Norway". In: *European Journal of Wood and Wood Products* 74.3 (2016), pp. 407–424. ISSN: 1436-736X. DOI: 10.1007/s00107-016-1022-5.

[73] *Inside the Forest Service*. https://www.fs.usda.gov/inside-fs/delivering-mission/apply/worlds-tallest-timber-building-opens. Accessed on April 5, 2023. United States Department of Agriculture, Forest Service.

[74] *Ascent Building*. https://kaa-arch.com/php/page-projectLoader.php?project=135. Accessed on April 5, 2023. Korb + Associates Architects.

[75] Denis Lefebvre and Grégoire Richard. "Design and construction of a 160-Metre-Long Wood Bridge in Mistissini". In: 2015.

[76] *Mistissini Bridge*. https://www.nordic.ca/en/projects/structures/mistissini-bridge. Accessed on April 5, 2023. Nordic Structures.

[77] *The Smile / Alison Brooks Architects*. https://www.archdaily.com/869703/the-smile-alison-brooks-architects?ad_source=search&ad_medium=projects_tab. Accessed on April 5, 2023. Arch Daily.

[78] Martin Philip Bendsøe and Noboru Kikuchi. "Generating optimal topologies in structural design using a homogenization method". In: *Computer Methods in Applied Mechanics and Engineering* 71.2 (1988), pp. 197–224. ISSN: 0045-7825. DOI: https://doi.org/10.1016/0045-7825(88)90086-2.

[79] Tae Hee Lee. "Optimization of Structural and Mechanical Systems". In: chap. Shape Optimization, pp. 149–159. DOI: 10.1142/9789812779670_0005.

[80] A.G.M. Michell. "The Limits of Economy of Material in Frame Structures". In: *Philosophical Magazine*. Series 6 8 (1904), pp. 589–597.

[81] G. I. N. Rozvany, M. P. Bendsøe, and U. Kirsch. "Layout Optimization of Structures". In: *Applied Mechanics Reviews* 48.2 (1995), pp. 41–119. ISSN: 0003-6900. DOI: 10.1115/1.3005097.

[82] Martin Philip Bendsøe and Ole Sigmund. *Topology Optimization: Theory, Methods and Applications*. en. Springer, 2004. ISBN: 9783540429920.

[83] K. Zhou and J. Li. "The exact weight of discretized Michell trusses for a central point load". In: *Structural and Multidisciplinary Optimization* 28.1 (2004), pp. 69–72. ISSN: 1615-1488. DOI: 10.1007/s00158-004-0429-5.

[84] X. Huang and Yi Min Xie. "Evolutionary Topology Optimization of Continuum Structures: Methods and Applications". In: John Wiley and Sons, Ltd, 2010. ISBN: 9780470689486.

[85] George I. N. Rozvany and Tomasz Sokol. "Exact truss topology optimization: allowance for support costs and different permissible stresses in tension and compression—extensions of a classical solution by Michell". In: *Structural and Multidisciplinary Optimization* 45 (2012), pp. 367–376. ISSN: 1615-1488. DOI: 10.1007/s00158-011-0736-6.

[86] Ole Sigmund, Niels Aage, and Erik Andreassen. "On the (non-)optimality of Michell structures". In: *Structural and Multidisciplinary Optimization* 54 (2016), pp. 361–373. ISSN: 1615-1488. DOI: 10.1007/s00158-016-1420-7.

[87] José Herskovits, Evandro Goulart, and Miguel Aroztegui. "Optimization of Structural andMechanical Systems". In: chap. Optimization of Large Scale Systems, pp. 35–57. DOI: 10.1142/9789812779670_0002.

[88] E. L. Cardoso and J. S. O. Fonseca. "Complexity Control in the Topology Optimization of Continuum Structures". In: *Journal of the Brazilian Society of Mechanical Sciences and Engineering* 3 (2003). DOI: 10.1590/S1678-58782003000300012.

[89] Ole Sigmund. In: ().

[90] Matteo Bruggi and Paolo Venini. "A mixed FEM approach to stress-constrained topology optimization". In: *International Journal for Numerical Methods in Engineering* 73 (2008).

[91] Xu Guo et al. "Stress-related topology optimization via level set approach". In: *Computer Methods in Applied Mechanics and Engineering* 200.47 (2011), pp. 3439–3452. ISSN: 0045-7825. DOI: https://doi.org/10.1016/j.cma.2011.08.016.

[92] G. I. N. Rozvany. "On design-dependent constraints and singular topologies". In: *Structural and Multidisciplinary Optimization* 21.2 (2001), pp. 164–172. ISSN: 1615-1488. DOI: 10.1007/s001580050181.

[93] X. Huang et al. "Topology optimization of microstructures of cellular materials and composites for macrostructures". In: *Computational Materials Science* 67 (2013), pp. 397–407. ISSN: 0927-0256. DOI: https://doi.org/10.1016/j.commatsci.2012.09.018.

[94] William Martins Vicente et al. "Concurrent topology optimization for minimizing frequency responses of two-level hierarchical structures". In: *Computer Methods in Ap-*

plied Mechanics and Engineering 301 (2016), pp. 116–136. ISSN: 0045-7825. DOI: https://doi.org/10.1016/j.cma.2015.12.012.

[95] A. Gersborg-Hansen, M. P. Bendsøe, and O. Sigmund. "Topology optimization of heat conduction problems using the finite volume method". In: *Structural and Multidisciplinary Optimization* 31.4 (2006), pp. 251–259. ISSN: 1615-1488. DOI: 10.1007/s00158-005-0584-3. URL: https://doi.org/10.1007/s00158-005-0584-3.

[96] X. Huang et al. "Computational Design of Microstructural Composites with Tailored Thermal Conductivity, Numerical Heat Transfer, Part A: Applications". In: *An International Journal of Computation and Methodology* 54 (2008), pp. 686–708. DOI: 10.1080/10407780802339031.

[97] Jiadong Deng, Jun Yan, and Gengdong Cheng. "Multi-objective concurrent topology optimization of thermoelastic structures composed of homogeneous porous material". In: *Structural and Multidisciplinary Optimization* 47.4 (2013), pp. 583–597. ISSN: 1615-1488. DOI: 10.1007/s00158-012-0849-6. URL: https://doi.org/10.1007/s00158-012-0849-6.

[98] Ole Sigmund and Kurt Maute. "Topology optimization approaches". In: *Structural and Multidisciplinary Optimization* 48.6 (2013), pp. 1031–1055. ISSN: 1615-1488. DOI: 10.1007/s00158-013-0978-6.

[99] M. P. Bendsøe. "Optimal shape design as a material distribution problem". In: *Structural optimization* 1 (1989), pp. 193–202. ISSN: 1615-1488. DOI: 10.1007/BF01650949. URL: https://doi.org/10.1007/BF01650949.

[100] M. Zhou and G.I.N. Rozvany. "The COC algorithm, Part II: Topological, geometrical and generalized shape optimization". In: *Computer Methods in Applied Mechanics and Engineering* 89.1 (1991). Second World Congress on Computational Mechanics, pp. 309–336. ISSN: 0045-7825. DOI: https://doi.org/10.1016/0045-7825(91)90046-9.

[101] H. P. Mlejnek. "Some aspects of the genesis of structures". In: *Structural optimization* 5.1 (Mar. 1992), pp. 64–69. ISSN: 1615-1488. DOI: 10.1007/BF01744697. URL: https://doi.org/10.1007/BF01744697.

[102] Grégoire Allaire, François Jouve, and Anca-Maria Toader. "A level-set method for shape optimization". In: *Comptes Rendus Mathematique* 334.12 (2002), pp. 1125–1130. ISSN: 1631-073X. DOI: https://doi.org/10.1016/S1631-073X(02)02412-3.

[103] Grégoire Allaire, François Jouve, and Anca-Maria Toader. "Structural optimization using sensitivity analysis and a level-set method". In: *Journal of Computational Physics* 194.1 (2004), pp. 363–393. ISSN: 0021-9991. DOI: https://doi.org/10.1016/j.jcp.2003.09.032.

[104] Michael Yu Wang, Xiaoming Wang, and Dongming Guo. "A level set method for structural topology optimization". In: *Computer Methods in Applied Mechanics and Engineering* 192.1 (2003), pp. 227–246. ISSN: 0045-7825. DOI: https://doi.org/10.1016/S0045-7825(02)00559-5.

[105] Antonio André Novotny and Jan Sokołowski. *Topological Derivatives in Shape Optimization*. 1st ed. Berlin, Heidelberg: Springer, 2013, pp. XII, 324. ISBN: 978-3-642-35244-7. DOI: 10.1007/978-3-642-35245-4.

[106] Yi Min Xie and G.P. Steven. "A simple evolutionary procedure for structural optimization". In: *Computers & Structures* 49.5 (1993), pp. 885–896. ISSN: 0045-7949. DOI: https://doi.org/10.1016/0045-7949(93)90035-C.

[107] William Martins Vicente. "Otimização topológica evolucionária aplicada a sistemas elasto-acústicos". PhD dissertation. Universidade Estadual de Campinas, Faculdade de Engenharia Mecânica, 2013.

[108] R. Picelli et al. "Evolutionary topology optimization for natural frequency maximization problems considering acoustic–structure interaction". In: *Finite Elements in Analysis and Design* 106 (2015), pp. 56–64. ISSN: 0168-874X. DOI: https://doi.org/10.1016/j.finel.2015.07.010.

[109] R. Picelli, William Martins Vicente, and R. Pavanello. "Bi-directional evolutionary structural optimization for design-dependent fluid pressure loading problems". In: *Engineering Optimization* 47.10 (2015), pp. 1324–1342. DOI: 10.1080/0305215X.2014.963069.

[110] William Martins Vicente et al. "Topology optimization of frequency responses of fluid–structure interaction systems". In: *Finite Elements in Analysis and Design* 98 (2015), pp. 1–13. ISSN: 0168-874X. DOI: https://doi.org/10.1016/j.finel.2015.01.009.

[111] William Martins Vicente et al. "Topology Optimization of Periodic Structures for Coupled Acoustic-Structure Systems". In: 2016.

[112] Yi Min Xie and G.P. Steven. *Evolutionary Structural Optimization*. Springer London, 1997.

[113] Y.M. Xie and G.P. Steven. "Evolutionary structural optimization for dynamic problems". In: *Computers & Structures* 58.6 (1996), pp. 1067–1073. ISSN: 0045-7949. DOI: https://doi.org/10.1016/0045-7949(95)00235-9.

[114] D.Nha Chu et al. "Evolutionary structural optimization for problems with stiffness constraints". In: *Finite Elements in Analysis and Design* 21.4 (1996), pp. 239–251. ISSN: 0168-874X. DOI: https://doi.org/10.1016/0168-874X(95)00043-S.

[115] O. M. Querin, G. P. Steven, and Y. M. Xie. "Evolutionary structural optimisation (ESO) using a bidirectional algorithm". In: *Engineering Computations* 15.8 (1998), pp. 1031–1048. ISSN: 0264-4401. DOI: 10.1108/02644409810244129.

[116] O.M. Querin et al. "Computational efficiency and validation of bi-directional evolutionary structural optimisation". In: *Computer Methods in Applied Mechanics and Engineering* 189.2 (2000), pp. 559–573. ISSN: 0045-7825. DOI: https://doi.org/10.1016/S0045-7825(99)00309-6.

[117] X. Y. Yang et al. "Bidirectional Evolutionary Method for Stiffness Optimization". In: *AIAA Journal* 37.11 (1999), pp. 1483–1488. DOI: 10.2514/2.626.

[118] X. Huang and Yi Min Xie. "Convergent and mesh-independent solutions for the bi-directional evolutionary structural optimization method". In: *Finite Elements in Analysis and Design* 43.14 (2007), pp. 1039–1049. ISSN: 0168-874X. DOI: https://doi.org/10.1016/j.finel.2007.06.006.

[119] Xiaodong Huang and Yi-Min Xie. "A further review of ESO type methods for topology optimization". In: *Structural and Multidisciplinary Optimization* 41.5 (2010), pp. 671–683. ISSN: 1615-1488. DOI: 10.1007/s00158-010-0487-9. URL: https://doi.org/10.1007/s00158-010-0487-9.

[120] M. Zhou and G. I. N. Rozvany. "On the validity of ESO type methods in topology optimization". In: *Structural and Multidisciplinary Optimization* 21.1 (2001), pp. 80–83. ISSN: 1615-1488. DOI: 10.1007/s001580050170. URL: https://doi.org/10.1007/s001580050170.

[121] G. I. N. Rozvany. "A critical review of established methods of structural topology optimization". In: *Structural and Multidisciplinary Optimization* 37.3 (2009), pp. 217–237. ISSN: 1615-1488. DOI: 10.1007/s00158-007-0217-0. URL: https://doi.org/10.1007/s00158-007-0217-0.

[122] Haidong Lin et al. "An ANSYS APDL code for topology optimization of structures with multi-constraints using the BESO method with dynamic evolution rate (DER-BESO)". In: *Structural and Multidisciplinary Optimization* 62.4 (2020), pp. 2229–2254. ISSN: 1615-1488. DOI: 10.1007/s00158-020-02588-2.

[123] Rodrigo L. Pereira, Heitor N. Lopes, and Renato Pavanello. "Topology optimization of acoustic systems with a multiconstrained BESO approach". In: *Finite Elements in Analysis and Design* 201 (2022), p. 103701. ISSN: 0168-874X. DOI: https://doi.org/10.1016/j.finel.2021.103701.

[124] Ning Gan and Qianxuan Wang. "Topology optimization of multiphase materials with dynamic and static characteristics by BESO method". In: *Advances in Engineering Software* 151 (2021), p. 102928. ISSN: 0965-9978. DOI: https://doi.org/10.1016/j.advengsoft.2020.102928.

[125] Xiaojie Tian et al. "Jack-up platform leg optimization by topology optimization algorithm-BESO". In: *Ocean Engineering* 257 (2022), p. 111633. ISSN: 0029-8018. DOI: https://doi.org/10.1016/j.oceaneng.2022.111633.

[126] M. Bruyneel and C. Fleury. "Composite structures optimization using sequential convex programming". In: *Advances in Engineering Software* 33.7 (2002). Engineering Computational Technology & Computational Structures Technology, pp. 697–711. ISSN: 0965-9978. DOI: https://doi.org/10.1016/S0965-9978(02)00053-4.

[127] Xinxing Tong, Wenjie Ge, and Yonghong Zhang. "Optimal fiber orientation and topology design for compliant mechanisms with fiber-reinforced composites". In: *Proceedings of the Institution of Mechanical Engineers, Part C: Journal of Mechanical Engineering Science* 231.12 (2017), pp. 2302–2312. DOI: 10.1177/0954406216631783.

[128] J. Stegmann and E. Lund. "Discrete material optimization of general composite shell structures". In: *International Journal for Numerical Methods in Engineering* 62.14 (2005), pp. 2009–2027. DOI: https://doi.org/10.1002/nme.1259.

[129] Xingjun Gao and Haitao Ma. "A modified model for concurrent topology optimization of structures and materials". In: *Acta Mechanica Sinica* 31.6 (2015). ISSN: 1614-3116. DOI: 10.1007/s10409-015-0502-x.

[130] Xiaolei Yan et al. "Concurrent topology design of structures and materials with optimal material orientation". In: *Composite Structures* 220 (2019), pp. 473–480. ISSN: 0263-8223. DOI: https://doi.org/10.1016/j.compstruct.2019.04.028.

[131] Xiaolei Yan et al. "Concurrent optimization of macrostructures and material microstructures and orientations for maximizing natural frequency". In: *Engineering Structures* 209 (2020), p. 109997. ISSN: 0141-0296. DOI: https://doi.org/10.1016/j.engstruct.2019.109997.

[132] Robert D. Cook et al. *Concepts and Applications of Finite Element Analysis, 4th Edition.* 4th ed. Wiley, Oct. 2001. ISBN: 0471356050.

[133] X. Huang and Y. M. Xie. "Optimal design of periodic structures using evolutionary topology optimization". In: *Structural and Multidisciplinary Optimization* 36.6 (2008), pp. 597–606. ISSN: 1615-1488.

[134] Ole Sigmund and J. Petersson. "Numerical instabilities in topology optimization: A survey on procedures dealing with checkerboards, mesh-dependencies and local minima". In: *Structural Optimization* 16 (1998), pp. 68–75.

[135] Central City Association. *White Paper: Mass Timber A Faster, More Affordable, And More Sustainable Way To Build Housing.* Tech. rep. Los Angeles, California: Central City Association, 2019.

[136] P. D. Kremer and M. A. Symmons. "Mass timber construction as an alternative to concrete and steel in the Australia building industry: a PESTEL evaluation of the potential". In: *International Wood Products Journal* 6.3 (2015), pp. 138–147. DOI: 10.1179/2042645315Y.0000000010.

[137] Xue Jianyang et al. "Experimental study on lateral performance of glued-laminated timber frame infilled with cross-laminated timber shear walls". In: *Engineering Structures* 239 (2021), p. 112354. ISSN: 0141-0296. DOI: https://doi.org/10.1016/j.engstruct.2021.112354.

[138] Wei Li et al. "A review of formwork systems for modern concrete construction". In: *Structures* 38 (2022), pp. 52–63. DOI: https://doi.org/10.1016/j.istruc.2022.01.089.

[139] Leif Gustavsson, Kim Pingoud, and Roger Sathre. "Carbon Dioxide Balance of Wood Substitution: Comparing Concrete- and Wood-Framed Buildings". In: *Mitigation and Adaptation Strategies for Global Change* 11.3 (2006), pp. 667–691. ISSN: 1573-1596. DOI: 10.1007/s11027-006-7207-1.

[140] Chadwick Dearing Oliver et al. “Carbon, Fossil Fuel, and Biodiversity Mitigation With Wood and Forests”. In: *Journal of Sustainable Forestry* 33.3 (2014), pp. 248–275. DOI: 10.1080/10549811.2013.839386.

[141] R. Gutkowski et al. “Laboratory tests of composite wood–concrete beams”. In: *Construction and Building Materials* 22.6 (2008), pp. 1059–1066. ISSN: 0950-0618. DOI: https://doi.org/10.1016/j.conbuildmat.2007.03.013.

[142] A. Hassanieh, H.R. Valipour, and M.A. Bradford. “Experimental and numerical study of steel-timber composite (STC) beams”. In: *Journal of Constructional Steel Research* 122 (2016), pp. 367–378. ISSN: 0143-974X. DOI: https://doi.org/10.1016/j.jcsr.2016.04.005.

[143] W.M. Sebastian et al. “Experimental evidence for effective flexural-only stiffnesses to account for nonlinear flexural-slip behaviour of timber-concrete composite sections”. In: *Construction and Building Materials* 149 (2017), pp. 481–496. ISSN: 0950-0618. DOI: https://doi.org/10.1016/j.conbuildmat.2017.04.082.

[144] Marcin Chybiński and Lukasz Polus. “Theoretical, experimental and numerical study of aluminium-timber composite beams with screwed connections”. In: *Construction and Building Materials* 226 (2019), pp. 317–330. ISSN: 0950-0618. DOI: https://doi.org/10.1016/j.conbuildmat.2019.07.101.

[145] A. Hassanieh, H.R. Valipour, and M.A. Bradford. “Experimental and analytical behaviour of steel-timber composite connections”. In: *Construction and Building Materials* 118 (2016), pp. 63–75. ISSN: 0950-0618. DOI: https://doi.org/10.1016/j.conbuildmat.2016.05.052.

[146] Alireza A. Chiniforush et al. “Energy implications of using steel-timber composite (STC) elements in buildings”. In: *Energy and Buildings* 176 (2018), pp. 203–215. ISSN: 0378-7788. DOI: https://doi.org/10.1016/j.enbuild.2018.07.038.

[147] Lorenzo Franzoni et al. “Influence of orientation and number of layers on the elastic response and failure modes on CLT floors: modeling and parameter studies”. In: *European Journal of Wood and Wood Products* 74 (2016), pp. 671–684.

[148] L. Franzoni et al. “Elastic behavior of Cross Laminated Timber and timber panels with regular gaps: Thick-plate modeling and experimental validation”. In: *Engineering Structures* 141 (2017), pp. 402–416. ISSN: 0141-0296. DOI: https://doi.org/10.1016/j.engstruct.2017.03.010.

[149] L. Franzoni et al. “Closed-form solutions for predicting the thick elastic plate behavior of CLT and timber panels with gaps”. In: *Engineering Structures* 164 (2018), pp. 290–304. ISSN: 0141-0296.

[150] J.A. Sethian and Andreas Wiegmann. “Structural Boundary Design via Level Set and Immersed Interface Methods”. In: *Journal of Computational Physics* 163.2 (2000), pp. 489–528. ISSN: 0021-9991. DOI: https://doi.org/10.1006/jcph.2000.6581.

[151] Lei Wang et al. “Evidence theory-based reliability optimization for cross-scale topological structures with global stress, local displacement, and micro-manufacturing constraints”. In: *Structural and Multidisciplinary Optimization* 65.1 (2021), p. 23.

[152] Rubens Bohrer and Il Yong Kim. "Multi-material topology optimization considering isotropic and anisotropic materials combination". In: *Structural and Multidisciplinary Optimization* 64.3 (2021), pp. 1567–1583. ISSN: 1615-1488. DOI: 10.1007/s00158-021-02941-z.

[153] H. Rahami, A. Kaveh, and Y. Gholipour. "Sizing, geometry and topology optimization of trusses via force method and genetic algorithm". In: *Engineering Structures* 30.9 (2008), pp. 2360–2369. ISSN: 0141-0296.

[154] A. Kaveh and A. Zolghadr. "Topology optimization of trusses considering static and dynamic constraints using the CSS". In: *Applied Soft Computing* 13.5 (2013), pp. 2727–2734. ISSN: 1568-4946.

[155] A. Kaveh and A. Zolghadr. "Sizing, geometry and topology optimization of trusses using force method and supervised charged system search". In: *Structural Engineering and Mechanics* 50.3 (2014). ISSN: 365–382.

[156] Lei Wang, Yaru Liu, and Min Li. "Time-dependent reliability-based optimization for structural-topological configuration design under convex-bounded uncertain modeling". In: *Reliability Engineering & System Safety* 221 (2022), p. 108361. ISSN: 0951-8320. DOI: https://doi.org/10.1016/j.ress.2022.108361.

[157] Zeshang Li, Lei Wang, and Zhenxian Luo. "A feature-driven robust topology optimization strategy considering movable non-design domain and complex uncertainty". In: *Computer Methods in Applied Mechanics and Engineering* 401 (2022), p. 115658. ISSN: 0045-7825. DOI: https://doi.org/10.1016/j.cma.2022.115658.

[158] Ji-Hong Zhu, Wei-Hong Zhang, and Liang Xia. "Topology Optimization in Aircraft and Aerospace Structures Design". In: *Archives of Computational Methods in Engineering* 23.4 (2016), pp. 595–622. ISSN: 1886-1784. DOI: 10.1007/s11831-015-9151-2.

[159] Stephen W. K. Roper et al. "Simultaneous isotropic and anisotropic multi-material topology optimization for conceptual-level design of aerospace components". In: *Structural and Multidisciplinary Optimization* (2021). DOI: 10.1007/s00158-021-02893-4.

[160] Haoyu Huang et al. "Performance of the hollow-core cross-laminated timber (HC-CLT) floor under human-induced vibration". In: *Structures* 32 (2021), pp. 1481–1491. ISSN: 2352-0124. DOI: https://doi.org/10.1016/j.istruc.2021.03.101.

[161] Nikola Perković, Vlatka Rajčić, and Monika Pranjić. "Behavioral Assessment and Evaluation of Innovative Hollow Glue-Laminated Timber Elements". In: *Materials* 14.22 (2021). ISSN: 1996-1944.

[162] Guanqiang He et al. "Topology optimization of periodic structures using BESO based on unstructured design points". In: *Structural and Multidisciplinary Optimization* 2 (2016), pp. 271–275. ISSN: 1615-1488. DOI: 10.1007/s00158-015-1342-9.

[163] Simon Thomas, Qing Li, and Grant Steven. "Finite periodic topology optimization with oriented unit-cells". In: *Structural and Multidisciplinary Optimization* (2021). ISSN: 1615-1488.

[164] Z.-D. Ma et al. “Experimental validation and prototyping of optimum designs obtained from topology optimization”. In: *Structural and Multidisciplinary Optimization* 31.5 (2006), pp. 333–343. ISSN: 1615-1488.

[165] Jim Hart, Bernardino D’Amico, and Francesco Pomponi. “Whole-life embodied carbon in multistory buildings: Steel, concrete and timber structures”. In: *Journal of Industrial Ecology* 25.2 (2021), pp. 403–418. DOI: https://doi.org/10.1111/jiec.13139.

[166] Lucas Sacramoni Peixoto et al. “Bending behavior of steel bars reinforced Glulam beams considering the homogenized cross section”. In: *Wood Material Science & Engineering* 17.6 (2022), pp. 533–539. DOI: 10.1080/17480272.2021.1900392.

Appendix A

Numerical Examples

A.1 Example 1

In this example a 3-layer CLT of dimensions L = 400 mm, w = 150 mm and each layer with a height of 6 mm with both ends clamped and a distributed force on the top surface of the CLT for a total of 100 N with both shown in Figure A.1. The design and non-design domain have 75 elements in width, 200 elements in length and 3 elements in layer height, totaling 90,000 elements. Thus, the complete model of the 3-layer CLT structure contains a total of 270,000 elements. The optimization aims to decrease the initial design domain volume by 35% ($V_f = 65\%$) while the non-design domain regions remain unchanged during the whole process. The parameters for optimization with the BESO method are: $ER = 2\%$, $AR = 2\%$, $r_{min} = 10$ mm, $\tau = 0.001$, $N = 5$ and $p = 3$. In this example, the supports are in steel with Young's modulus of 210 GPa, and a Poisson ratio of 0.30. The frame highlighted in Figure 4.1 is aluminum with Young's modulus of 70 GPa and a Poisson ratio of 0.31. Both the supports and the frame are not part of the design domain.

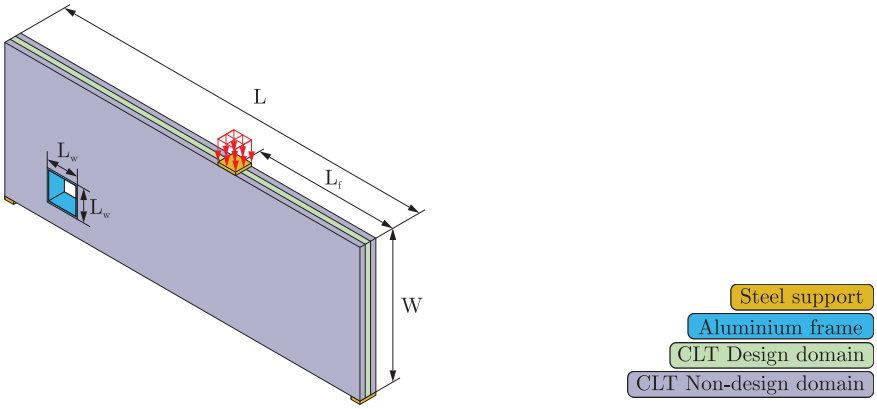

Figure A.1: Representation of first example: 3-layer CLT beam clamped in both ends with distributed force along the length.

At the beginning of the simulation, the design domain is considered full volume (V_i = 100%), and at each iteration, this volume approaches the final volume stipulated. In Figure A.2 it is possible to understand this evolution process with emphasis on the design domain. The colors represent the value of the sensitivity number of the elements that compose the structure, being cold colors have a lower sensitivity number while warm colors a higher sensitivity number.

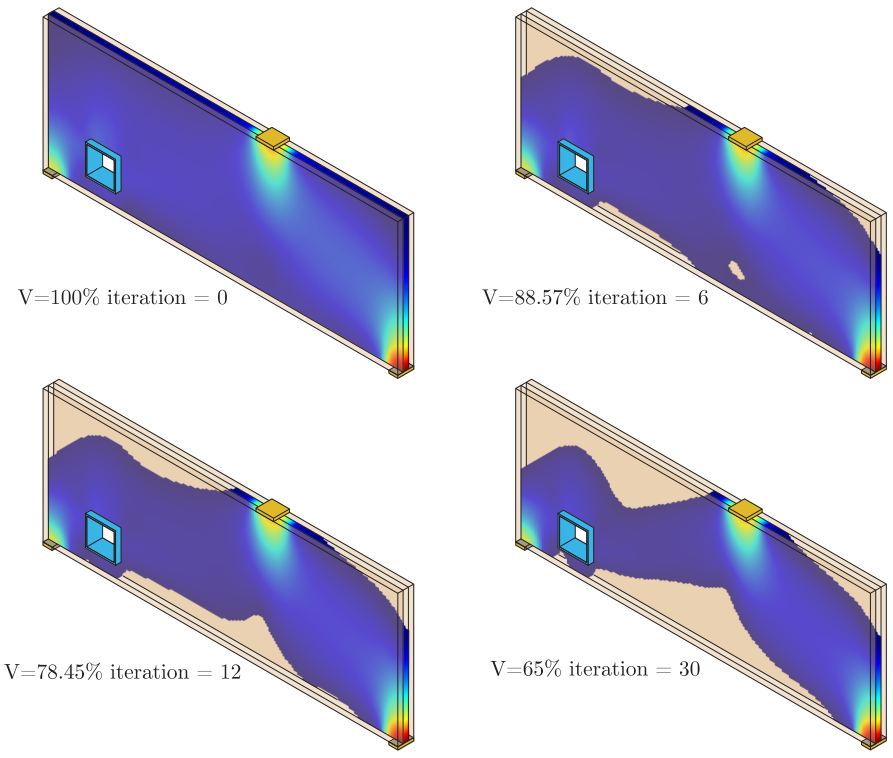

Figure A.2: Distribution of the three-layer CLT intermediate layer sensitivity number in four different iterations: V_0 = 100%, V_{06} = 88.57%, V_{12} = 78.45%, V_{30} = 65.00%.

The evolution of the simulation is seen in detail in Figure A.3. In this graph, it is possible to notice that the objective function value increases throughout the simulation, which means that the structure loses stiffness at each iteration. However, it should be pointed out that there was a loss of approximately 3.5% in stiffness for a 35% reduction in design-domain for this example and exact conditions.

As soon as the structure reaches the final volume, in iteration number 30, the value of the objective function suffers a slight reduction. As soon as the final volume is reached, the methodology changes the existing elements to increase the structure's stiffness.

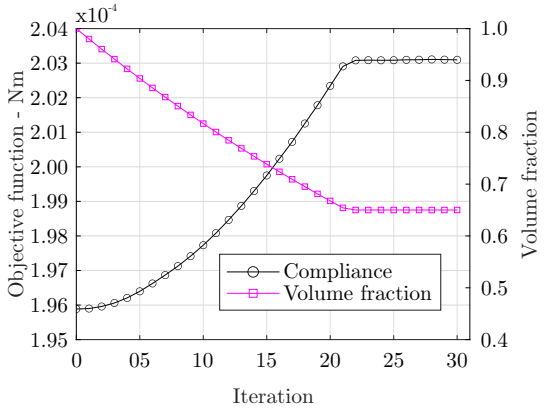

Figure A.3: Optimization histories of the objective function for the and the evolution histories of the volume fraction for the 3-layer CLT structures with both ends clamped.

Figure A.4 shows the final result of this simulation, highlighting the optimized layer while the first and third layer remained unchanged.

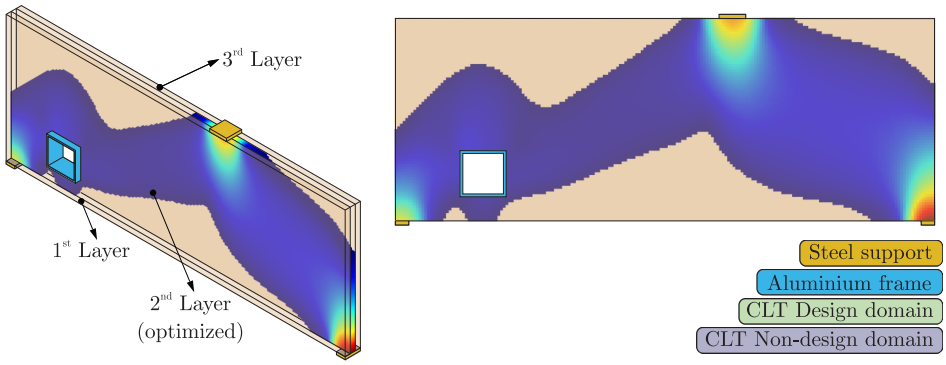

Figure A.4: Final topology for final design-domain prescribed volume of $V_{30} = 65\%$

A.2 Example 2

In this example a five-layer CLT of dimensions L = 500 mm, W = 150 mm and each layer with a height of 10 mm with both ends clamped and distributed force on the top surface of the CLT for a total of 100 N as shown in Figure A.5. In this example, the strategy of double symmetry in length and width was used to perform the simulation at a lower computational cost. Therefore, only a quarter of the model was solved in the finite element problem. Furthermore, in this example, the design domain is located on layers two and four. The design domain has 250 elements in width, 75 elements in length, and ten elements in layer height, totaling 375,500 elements in a quarter of the model and the regions of the design domain. In contrast, in the non-design domain region, five elements are in the height of each layer, for a total of 93,750 elements in the three CLT layers. Thus, a quarter of the model of the five-layer CLT structure contains a total of 656,250 elements. The parameters for optimization with the BESO method are: $ER = 5\%$, $AR = 5\%$, $r_{min} = 8$ mm, $\tau = 0.001$, $N = 5$ and $p = 3$.

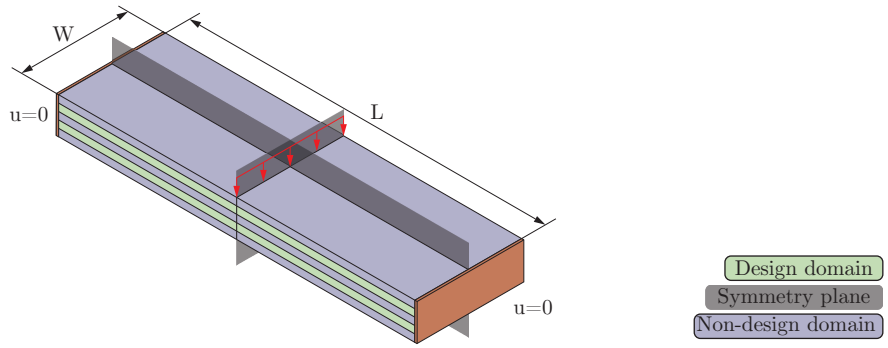

Figure A.5: Representation of second example: five-layer CLT beam clamped in both ends with distributed force along the length and representation of the symmetry planes considered.

In this example, the initial volume (V_i) is 50% of the design domain, the same value for the final volume ($V_f = 50\%$). The initial volume of the design domain was distributed symmetrically to the corners of the structure as Figure A.6. Throughout the simulation, the elements changed to achieve the structure with the highest possible stiffness. As the iterations progress, the material arranges itself from the edges towards the center in this example. In addition, there is a larger number of elements in layer number 4 than layer 2 in detail in Figure A.8.

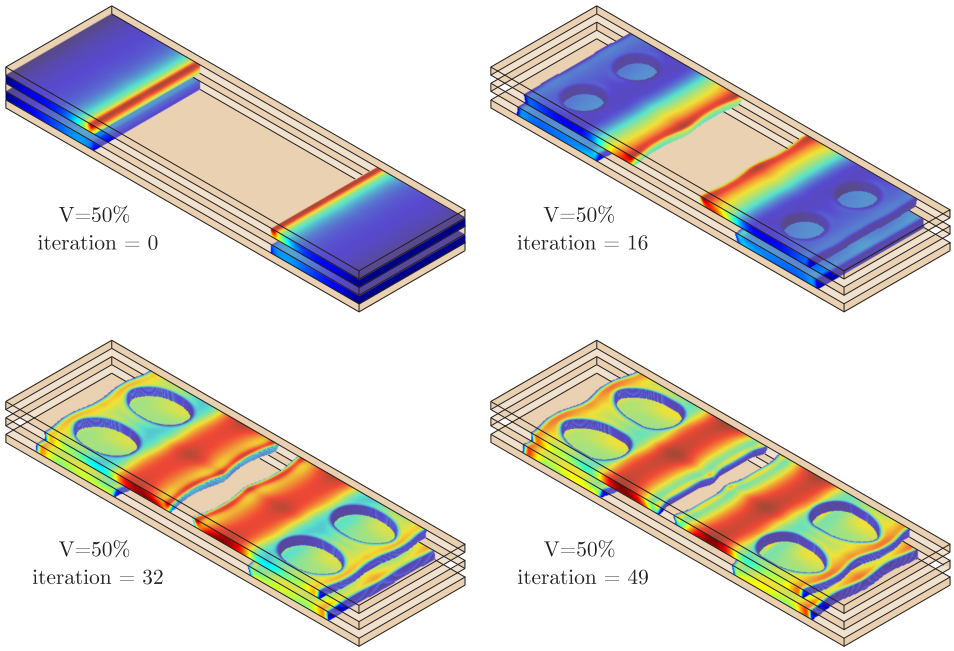

Figure A.6: Distribution of the sensitivity number of the CLT layers that are part of the design domain (second and fourth layer) in four different iterations: $V_0 = 50\%$, $V_{16} = 50\%$, $V_{32} = 50\%$, $V_{49} = 50\%$.

Figure A.7 presents the evolution graph, Objective Function *vs* Iteration. The first iteration acts as an initial guess since the material distribution was chosen symmetrically in the structure's corners. The simulation seeks to change the minor elements to ensure the stiffest possible structure within the limits and tolerances imposed in the method.

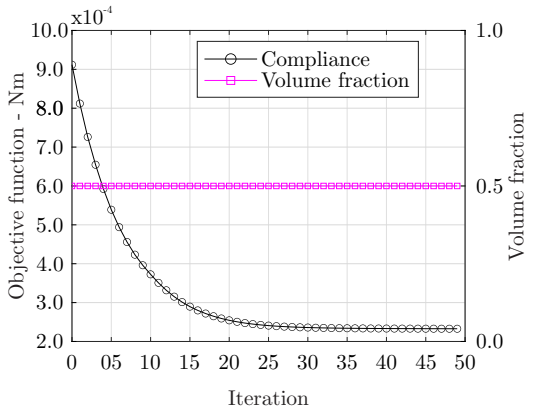

Figure A.7: Optimization histories of the objective function for the and the evolution histories of the volume fraction for the five-layer CLT structures with both ends clamped.

The increase in the number of layers shows that, for these conditions, layers two and four have different levels of importance (Figure A.8), and from an optimization point of view,

should be treated in different ways. In comparing the layers present in the design domain, layer four has higher importance for the structure than layer two since 103,625 solid elements are arranged in this layer. In comparison, 83,875 solid elements are arranged in layer two. This is intuitive since the applied load is closer to layer four than layer two. However, in layer two, there are hot collar regions (higher number of sensitivities) with a high level of importance to ensure the structure with higher stiffness possible.

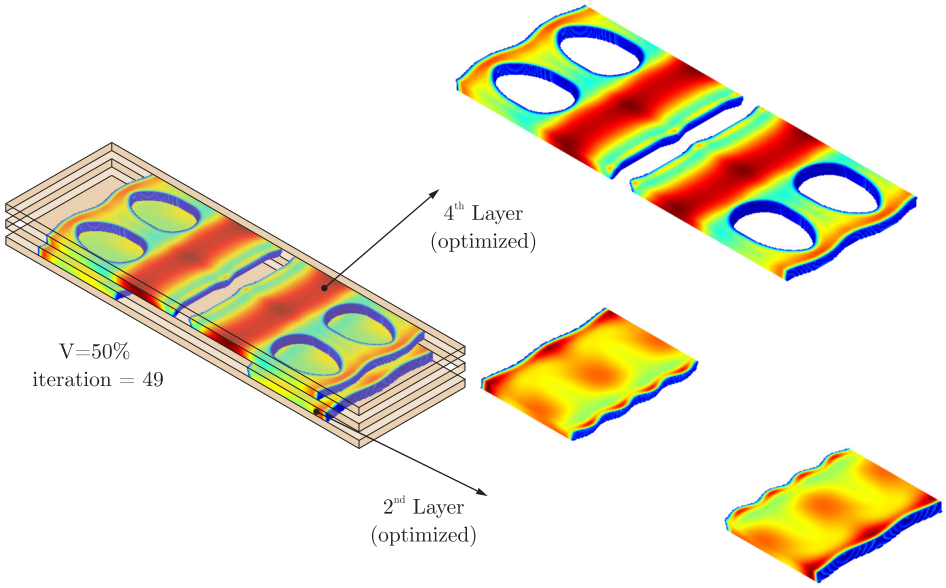

Figure A.8: Final topology for final design-domain prescribed volume of $V_{49} = 50.00\%$.

A.3 Example 3

In this example a three-layer CLT of dimensions L = 400 mm, W = 120 mm and each layer with a height of ten mm supported at a distance $L_s = 20$ mm from the end and two distributed force on the top surface of the CLT at a distance $L_f = 105$ mm from the corner for a total of 50 N each, as shown in Figure A.9. The design domain has 400 elements in length, 400 elements in width and ten elements in layer height, totaling 480,000. In contrast, in the non-design domain region five elements are in the in layer height of each layer, for a total of 240,000 elements in both layers. Thus, the three-layer CLT structure model contains a total of 270,000 elements. The parameters for optimization with the BESO method are: $ER = 2\%$, $AR = 2\%$, $V_f = 75\%$,$r_{min} = 10$ mm, $\tau = 0.001$, $N = 5$ and $p = 3$. Aiming to achieve a structure with greater ease of fabrication, periodicity constraints were applied, dividing the model into four cells along the length L. The strategy used follows the guidelines of Huang and Xie [133] and He et al. [162].

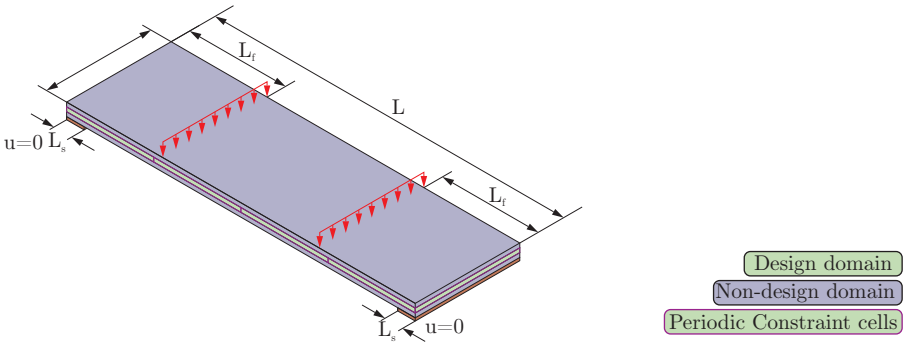

Figure A.9: Representation of third example: three-layer CLT beam supported in both ends with distributed force along the length and representation of the periodic constraint.

Figure A.10 shows four iterations of the topological optimization, for example 3, highlighting the design domain (second layer). It highlights the symmetry of the importance of the elements inside each cell until the final volume ($V_f = 75\%$) is reached at iteration number 38.

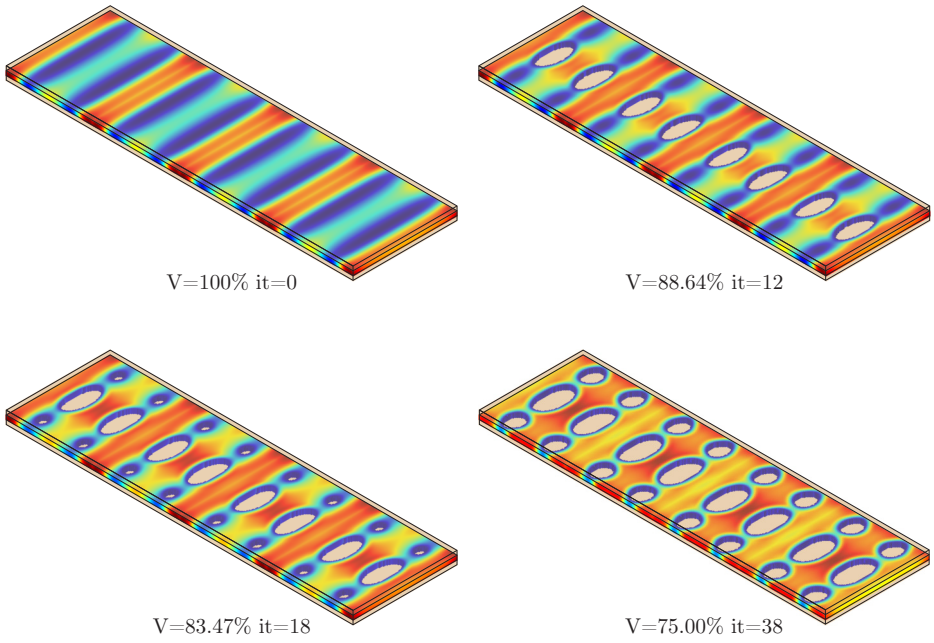

Figure A.10: Distribution of the three-layer CLT intermediate layer sensitivity number in four different iterations: $V_0 = 100\%$, $V_{12} = 88.64\%$, $V_{18} = 83.47\%$, $V_{38} = 75.00\%$.

In this example, the evolution of the simulation is represented by Figure A.11. There was a reduction of approximately 11% in the stiffness of the overall structure for a 25% reduction in the volume of the design domain.

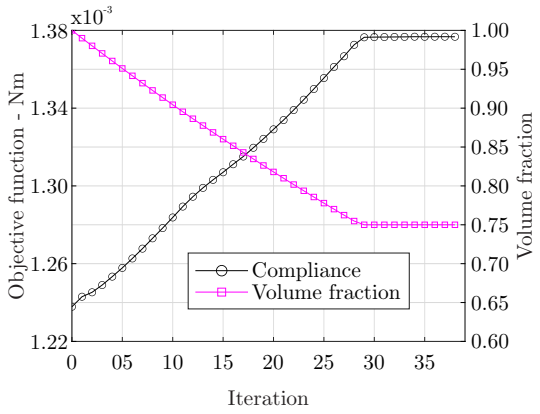

Figure A.11: Optimization histories of the objective function for the and the evolution histories of the volume fraction for the three-layer CLT structures with both ends supported.

Figure A.12 demonstrates in detail the optimal topology considering the applied periodicity constraint and boundary condition.

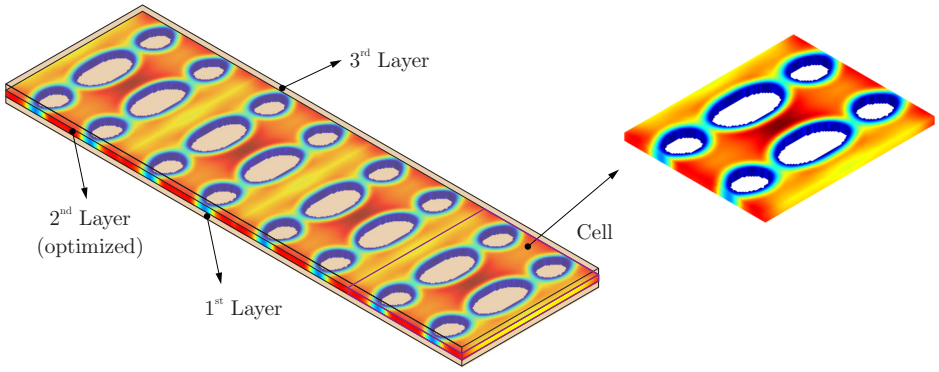

Figure A.12: Final topology for final design-domain prescribed volume of $V_{39} = 75.00\%$.